Study of Mangrove Biomass, Net Primary Production & Species Distribution using Optical & Microwave Remote Sensing Data.

Thesis submitted to Andhra University

In partial fulfillment of the requirements for the award of

Master of Technology in Remote Sensing and Geographical Information System

ANDHRA UNIVERSITY

Submitted by

Sandipan Karmaker

Supervised by

Dr. D. Mitra
Marine Sciences Division
Indian Institute of Remote Sensing
&
Dr. P. Sanyal
School of Oceanographic Study
Jadavpur University, Kolkata

iirs

Indian Institute of Remote Sensing
National Remote Sensing Agency
Dept. of Space, Govt. of India
Dehradun – 248 001
February, 2006

ACKNOWLEDGEMENTS

This report is the output of the essence of blessings and good wishes of almighty and my elders as well as support, love and co-operation of my and near and dear ones. It gives me immense pleasure to express my appreciation of the assistance rendered to me by all those who helped me in completion of this project. In the course of acknowledgement it may not be possible to mention all the names, who had supported me all the way in fulfillment of this project. Hope they will forgive me for this injustice.

I am highly indebted to my project supervisor, **Dr. D. Mitra**, Scientist & In-Charge, Marine Science Division, IIRS, for his active co-operation, valuable instructions, thoughtful advice, constructive criticism and efficient guidance and moral support to carry out this project work. I express my sincere thanks and gratitude to him.

My special thanks to my Co-guide, **Dr.Pranabes Sanyal**, visiting Scientist, School of Oceanography, Jadavpur University, Kolkata, who came across a very polite, helpful and accessible person. I am very lucky to be close to him in whole of my project duration and working under his valuable guidance.

IIRS will never be the same again. The new thrust in research activity and emphasis on quality work has become a reality because of the activity involvement of **Dr. V.K. Dadhwal**, Dean, IIRS. I sincerely thank him for his keenness and support to the students. I also thank him for the excellent lab facilities and services that are unparallel in academic institutions.

I express my sincere thanks to **Dr. P. S. Roy**, Deputy Director (RS and GIS, NRSA and former – Dean, IIRS), for not only giving me the opportunity to become a part of IIRS family but also for being very supportive in extending facilities.

I am happy to express my sincere gratitude to **Dr. T.K.Jana**, Head Of The Department, Department Of Marine Science, University Of Calcutta and **Dr.U.K.Basu**, Registrar, University of Calcutta for giving me the opportunity to attend this course on Remote Sensing and GIS organized by Indian Institute Of Remote Sensing (IIRS), Dehradun, Uttaranchal.

My sincere thanks go to **Dr. A. K. Mishra**, Scientist, Marine Science Division and course Coordinator, IIRS for giving me the opportunity to continue this course and for his support to carry out the project work successfully.

I would like to thank **DFO**, South 24 Parganas Sundarban, West Bengal and all the forest guards of Lothian island, Sundarban for providing me necessary permission related to carry out the fieldwork. Without their co-operation this work could not be completed.

My sincere thanks go to **Dr. Rita Saha**, Scientist, CPCB, regional office, Kolkata for her immense support and cooperation in carrying out the analysis of soil samples.

I record my deep gratitude to my senior **Miss. Sanhita Banerjee** (M.Tech. trainee of Marine Science division, IIRS, 2004-06) and **Mr. Dillip Das Mahapatra** M.Tech. trainee of Geo-Science division, IIRS, 2004-06) for strong mental, technical support in the periods of stress and help in the time of need all through, in spite of his busy schedule.

For some People I have to put their name in the acknowledgement. They are my juniors who have helped me so much in some way or the other. I really thank **Anirban Mukhopadhyay** and **Rahul Krishna Pandey** with all my heart and wish them all the best for their future.

It was a great atmosphere in our campus, thanks to my colleagues **Rajiv joshi**, **Rahul Jain, Biren Baishya** and **Vivek kumar Singh**. We shared so much among ourselves. Though we worked in different projects but each one of us was helping others throughout the course duration. I can never thank them enough for their cooperation.

The support of the staff members of IIRS was exemplary. My special thanks goes to **Sri M.L. Batra** and **Sri A.B. Singh** of TSO who were extremely helpful in the administrative affairs.

How can I forget the people who ensured smooth running of the softwares and hardwares throughout my study duration! It required only a phone call to them to solve the system related problems. I express my sincere thanks to all the staff members of computer Maintenance Division and specially **Mr. Bhaskar Bahuguna** with whom we share a great rapport and friendship.

My stay at IIRS hostel was one of the best experiences of career. I am grateful to the support staff of the hostel especially **Anand, Gayan, Laxman, Subhas** for their excellent service and care.

It is beyond me to express my feelings for my **parents** and **family members**, without the support of whom it would have been simply impossible to complete the project and work. During this long absence from home they were of constant moral support and encouragement. I missed them a lot during my stay at Dehradun, but it is their emotional support that simulated me throughout and propelled me to excel.

Dehradun **Sandipan Karmaker**
17.08.06

ABSTRACT

Mangrove is one of the most significant ecosystem of the coastal wetland from both ecological and biodiversity point of view. This ecosystem mainly exists on the muddy substratum at the confluence of river and ocean. Many physico- chemical parameters like tidal fluctuation, salinity, pH etc. controls this ecosystem dynamics. This ecosystem is being threatened by the over growing coastal populations. Understanding the mangrove ecosystem dynamics is very important for coastal environmental study. The present study aims to address three main objectives 1) Mapping mangrove species distribution along the soil salinity gradient, using Remote sensing and GIS approach, 2) Observing radar interactions with the mangrove community and also extracting information on mangrove biomass and other forest stand parameters from radar backscatter, 3) Mapping mangrove Net primary productivity (NPP) from satellite remote sensing data. Study was carried on Lothian island of Indian Sundarban region, having latitudinal extent from 21° 36′ 30″ N to 21° 42′ 30″ N and longitudinal extent from 88° 18′ 00″E to 88° 21′ 00″E. ENVISAT ASAR radar data is used for biomass study and IRS P6 LISS IV (optical) data is used for species distribution and NPP study. For ENVISAT ASAR, having only C- band frequency, the correlation between radar backscattering coefficient (σ°) of different polarization (VV, HH and HV) and mangrove above ground biomass is not significant, though C-VV backscattering coefficient (σ°) is significantly correlated with the canopy biomass. This observation reveals the poor penetration capability of C band wavelength.

In species distribution study – a relation has been established between the IVI (Important Value index) and soil salinity for three *Avicennia* species. Then the IVI maps of different Avicennia species were generated using surface soil salinity of the study area.
In NPP (Net Primary production) study community wise LAI (Leaf area index) maps has been generated from optical remote sensing data – IRS P6 LISS IV. NPP maps of three mangrove- communities are also generated as an output of the study. These LAI maps were used as the base map for generating NPP map of different mangrove community.

TABLE OF CONTENTS

LIST OF FIGURES

LIST OF TABLES

CHAPTER 1.

Introduction

In tropical regions, monitoring the dynamics of mangrove forest is of particular interest owing to their considerable ecological and economic importance. In particular, mangrove forest plays a major role in supplying organic nutrients to coastal marine ecosystem (e.g. Hutching and Saenger 1987). The trophic relationships between mangroves and coastal ecosystem can be characterized by the biomass and productivity of the mangrove forests. For the regions under consideration, biomass and productivity data are scarce, mainly because of the difficulties associated with field measurements. In this context, data delivered by space- borne radars and optical sensors present numerous advantages since they can provide information of the extent of mangrove surfaces as well as on their structural parameters (Hess et al, 1990).

1.1. Importance of mangrove Ecosystem.

Mangrove is the most significant ecosystem from both ecological and economical point of view. The importance issues are listed below.

- ✓ Stabilizes shoreline and prevent coastal erosion.
- ✓ Acts as wind breakers and protects the shoreline from storms.
- ✓ Supports high level of biodiversity.
- ✓ Provides food, breeding and nursery grounds for many commercially important species of fish, crabs, crustaceans and molluscs.
- ✓ Mangrove areas have high biological productivity & helps nutrients enrichment in coastal water through recycling.
- ✓ Mangroves are the source of wood (e.g. fuel wood, charcoal, building poles, fishing gears etc.).
- ✓ Provide non-wood products (e.g. Food item, medicinal products, Tannin, fodder for cattle etc.).
- ✓ Secondary products (Fish, edible fauna, wax, honey, shells, salt etc.).

1.2. Remote sensing resources and application

1.2.1. History and Development

Reconnaissance from hot air balloons, the first aerial platform, was one of the earliest applications of Remote Sensing. From its crude beginning in the 1850s (Estes, 2001) this new technology took advantage of rapid, parallel advances in photography and human flight.

By the early 1900s, when color film was introduced, many people began to realize the great potential of Remote Sensing (i.e. aerial photography at that time) for mapping natural and man-made features, and the demand for such information escalated quickly. Since the development of orbital launch capabilities, satellite platforms have given us new opportunities to study natural processes and human activity. It was quickly apparent in the early days of the space program that monitoring atmospheric conditions from space could lead to better weather forecasting and undoubtedly save lives and property, especially in coastal areas. Today, weather satellite images are used routinely in weather reports and are the most widely distributed form of remote sensing data for the public.

Remote sensing from satellites is economically competitive with other forms of data collection, such as aerial photography, especially where low or moderate resolutions are adequate. Broad swath widths and the advent of high-resolution systems enable frequent repeat coverage of targets. Systems can also collect data over denied or hazardous areas without interruption. While optical sensors have been successfully exploited for such studies, their use in tropical areas is severely limited by weather conditions. Indeed, cloud cover poses the greatest restriction to the acquisition of data that may be required at different intervals. This limitation has been somewhat alleviated by the use of Synthetic Aperture Radars (SARs) which are essentially all-weather systems. Typically such systems provide information of the ground reflectivity, in a manner which is phase preserving. The utility of the phase information was first demonstrated by Graham, 1974 where he used two vertically separated airborne antennas to receive simultaneously backscattered signals from the terrain. The coherent addition of the signals received by two spatially separated antennas, which forms the basis of what is now called SAR Interferometry, provides useful information about the topography of the terrain. This technique has also been employed in space borne systems where the ‘displacement of antennas’ is achieved by a single antenna in two separate passes of the satellite.

Satellite sensors today not only observe the earth in visible light, but also in the infrared region and with microwaves. Spatial resolution ranges from more than one kilometer to less than one meter. At the turn of the new century we are witnessing a host of low-cost derived products that monitor the dynamic nature of the earth’s land, oceans and atmosphere for the public good. These products include cloud properties, land cover, snow and ice cover, fire occurrences, vegetation properties, surface temperatures and evapotranspiration. When combined with the historical record that has been accumulated by remote sensing satellites over the last three decades, these observations can help us understand long-term trends at local and global levels.

1.2.2. Radar return and image signature

Energy reflected from the terrain to radar antenna is called radar return.

Following parameters strongly affect the radar return-

a) System properties -
- ✓ Wavelength / frequency,
- ✓ Polarization,
- ✓ Incidence angle.

b) Terrain properties -
- ✓ Dielectric constant,
- ✓ Surface roughness,
- ✓ Feature orientation.

1.2.3. Radar wavelength and frequency

Standard bandwidths used and their letter codes are –

Table 1-1 Representing Radar band code, wavelength and frequency

Band code	Wavelength (λ) in cm	Frequency(ν) GHz
Ka	0.8 – 1.1	40 – 26.5
K	1.1 – 1.7	26.5 – 18.0
X	2.4 – 3.8	12.5 – 8.0
C	3.8 – 7.5	8.0 – 4.0
S	7.5 – 15.0	4.0 – 2.0
L	15.0 – 30.0	2.0 – 1.0
P	30.0 – 100.0	1.0 – 0.3

Radar return mainly depends on the wavelength or the frequency used. Terrain features have a unique interaction in a particular wave band and hence the return is also unique for the wave band used. Shorter wave bands have atmospheric effects because of the interaction with the atmospheric water vapour. Longer wave bands comparatively penetrate through the skin of the earth surface.

1.2.4. Polarization

HH image and VV image - like polarized images. VH image and HV image - cross-polarized images.

Radar system containing single antenna can receive only one image type i.e. either of the like-polarized or cross-polarized. If Radar system contains two antennas it can receive two image types simultaneously i.e. either both like polarized or both cross-polarized or one like polarized and one cross-polarized.

Comparison of like and cross-polarized returns might reveal differences leading to terrain identification. Water and trees appear same in like and cross-polarized images while swamps appear brighter in like polarized and darker in cross-polarized imagery. Grasslands appear darker in like polarized image and brighter in cross-polarized image.

1.2.5 Advantage of using SAR data

Multi-spectral optical remote sensing data such as Landsat and SPOT have been widely used in the management, monitoring and mapping of natural resources. However, the use of such data in tropical regions faces a major hurdle due to the inability of the spectral bands of the optical sensors to penetrate through cloud cover. One of the methods to overcome this problem is to use a combination data of different sources (Shafiee *et al*., 1998). By combining data of different sources, areas under cloud-cover in one of the image sets are derived by the other (Shafiee *et al*., 1998). SAR systems operate within the microwave range of the electromagnetic band, which is able to penetrate through cloud covers. Thus, data acquisition of SAR system is more reliable especially in tropical zone than optical system as it is not affected by weather conditions and acquisition can also be carried out during nigh. SAR system therefore provides more frequent repetitive coverage than optical system.

A wide range of approaches have been developed to exploit remote sensing data collected in the visible, near infra red and thermal infra red region of the electromagnetic spectrum to study tropical ecosystems. However, imaging radar data have received less attention than data acquired by optical systems. Hindrances to use of SAR data have included – 1) Difficulty to understand the information content of the complex phase and amplitude information recorded in multifrequency, polarimetric SAR data; 2) The lack of available, calibrated data over sites of interest 3) Lack of accessible computer software to exploit the information present in the data; 4) Unique characteristics of SAR data, including topographic effects and image speckle (Kasischke, 1997). In recent years computer software and hardware have been developed to the point where most of the technological constraints of using SAR data have dissipated. In addition, much calibrated SAR imagery now exists and is being collected by significant number of air borne and satellite systems (Kasischke, 1997).

Sundarbans being a tropical coastal region, the cloud-free optical remote sensing data for the area is not very often available. Synthetic aperture radar, which has the ability to penetrate cloud, permits regular and repetitive observation of the study area.
In short the advantages of using Synthetic Aperture Radar data can be summarized as –

- ✓ Time independent.
- ✓ Weather independent.
- ✓ Sensitive to moisture in soil, vegetation and snow.
- ✓ Enhancement of surface roughness / relief.
- ✓ Penetration of soil and vegetation cover.
- ✓ Ability to collect data, which are far away from flight path.

1.3. Remote sensing data used in the whole study

The data used in the whole study are:
SATELLITE DATA:

OPTICAL DATA: Multispectral optical data.
SATELLITE NAME - IRS P6 (Resourcesat 1)

Sensor Name	Path	Row	Date
LISS-III	108	56	06.03.04

MICROWAVE SAR DATA:
SATELLITE NAME - ENVISAT

Sensor Name	Orbit	Track	Frame	Date	Polarization	Swath
ASAR	11646	2069	0441	22.05.04	VV	IS2
	12147	2069	0441	26.06.04	HH	IS2
	12147	2069	0441	26.06.04	HV	IS2

OTHER DATA:

- ✓ TOPOGRAPHIC BASE MAP ON 1: 50,000 SCALE.
- ✓ MAPS OBTAINED FROM THE NATIONAL ATLAS AND THEMATIC MAPPING ORGANISATION (NATMO).
- ✓ MAPS PRESENT IN THE BOOK ENTITLED ‘COMMUNITY ZONATION OF SELECTED MANGROVE HABITATS OF INDIA USING SATELLITE DATA, SAC, 2003.
- ✓ GROUND DATA FROM FIELD SURVEY IN MAY 2004 and APRIL 2005.

1.4. Brief introduction to Satellite and Sensors

1.4.1. Optical Satellite and sensors

Indian Remote Sensing Satellite - IRS-P6 (Resourcesat 1)

IRS P6 (ResourceSat1) has been launched into polar orbit in 2004. The LISS-IV camera can be operated either in panchromatic or multi spectral mode with a resolution of 5.8 m. LISS-III has a resolution of 23.5 m. AWiFS has a resolution of 60 m.

1.4.2. Radar Satellite and Sensors

ENVISAT:

ENVISAT is an advanced polar-orbiting, earth observation satellite, which provides measurements of the atmosphere, ocean, land and ice since 2002. Envisat is the most powerful European Earth observation satellite. It makes the most complete set of observations of our planet that any satellite has ever made. The satellite has an ambitious and innovative payload that is ensuring the continuity of the data measurements of the ERS Satellites. The payload consists of the following:

- ✓ ASAR : Advanced Synthetic Aperture Radar
- ✓ MERIS: Medium Resolution Imaging Spectrometer
- ✓ AATSR: Advanced Along Track Scanning Radiometer
- ✓ RA-2: Radar Altimeter
- ✓ MWR: Microwave Radiometer
- ✓ GOMOS: Global Ozone Monitoring by Occultation of Stars
- ✓ MIPAS: Michelson Interferometer for Passive Atmospheric Sounding
- ✓ SCIAMACHY: Scanning Imaging Absorption Spectrometer for Atmospheric Chartography.
- ✓ DORIS: Doppler Orbitography and Radio positioning Integrated by Satellite.
- ✓ LRR: Laser Retro-Reflector.

The ENVISAT images used in this study were taken by the ASAR sensor, which provides all weather, day or night radar imaging. The ASAR, also operating at C-band, ensures continuity with the image mode (SAR) and the wave mode of the ERS-1/2 AMI. It features enhanced capability in terms of coverage, range of incidence angles, polarization, and modes of operation. This enhanced capability is provided by significant differences in the instrument design: a full active array antenna equipped with distributed transmit/receive modules which provides distinct transmit and receive beams, a digital waveform generation for pulse “chirp” generation, a block adaptive quantization scheme and a Scan SAR mode of operation by beam scanning in elevation.

Recently, the development of SAR interferometry has proved that not only the amplitude of the radar echo but also phase carries important information for remote sensing applications. Particularly the interferometric correlation, which is a measure for the variance of the interferometric phase, provides useful information about the properties of a 'scene', which often complements measurements of the intensity of backscattering. SAR interferometry, data collected by ERS satellites can now be widely used for land surveillance.

1.5. Scientific objectives and outline of the thesis.

There are three scientific objectives of the present studies –

- ✓ Study of Mangrove biomass and Radar backscattering response.
- ✓ Studying effect of soil salinity on mangrove distribution from remote sensing and GIS approach.
- ✓ Mapping mangrove primary productivity from Remotesensing and GIS approach.

The entire thesis is comprised of total 9 chapters. After the brief introduction of the thesis in Chapter – 1 the details about the study area is described in Chapter – 2. A review of literatures consulted in the whole study is summarized in Chapter – 3. Chapter – 4 highlights the basic principles of microwave remote sensing. Chapter – 5 describes the microwave interaction with mangrove. Chapter – 6 deals with the study of radar ENVISAT ASAR backscatter in relation to mangrove forest biomass and other stand parameters. A remote sensing and GIS approach to study mangrove distribution along the soil salinity gradient is described in Chapter – 7. Chapter – 8 is associated with mapping Net Primary productivity (NPP) from remote sensing and GIS aspect.

CHAPTER 2.

Area of study

2.1. Introduction

The present study was undertaken at Lothian Island of the western Sundarban from April 2004 to December 2005. It is a small island of approximately 38 km^2 area which extends from 88°18′10″ E to 88°20′30″ E longitude and 21°32′50″ N to 21°42′30″ N latitude. It is located at the confluence of the Saptamukhi estuary and Bay of Bengal. The island resembles the shape of an inverted mango with the protruded end in the northwest and a broader southern region. This island was notified as a wildlife Sanctuary in 1948 and re-notified in June 1976. The island is regularly inundated by diurnal tide up to a certain distance form the northern coast. A north – south spinal road approaches from northern coast up to nearly middle of the island.

As stated in the Coastal Regulation Zone (CRZ) Notification of Ministry of Environment and Forest, Govt. of India, the coastal stretch of West Bengal has been demarcated into three categories i.e. CRZ-I, CRZ-II and CRZ-III under the management plan of West Bengal. A total of 4571.49 km^2 has been identified under CRZ, of which CRZ-I alone constitute 4164.84 km^2, CRZ-II 14.25 km^2 and CRZ-III 392.40 km^2.

CRZ-I - This includes the ecologically sensitive and important areas like National Marine Parks (proposed marine park at Sagar Island), sanctuaries (Sajnekhali, Lothian and Halliday islands), reserve forest, wild life habitats, mangroves (Sundarbans, Nijkasba, Khejuri), areas close to breeding and spawning grounds of fish and other marine life (Sagar, Newmoor, Sand heads islands), areas of natural beauty (lower long sand) and historical heritage (Sagar temple and Ganga Sagar). It also includes the areas between Low Tide Line (LTL) and High Tide Line (HTL).

CRZ-II - It encompasses the developed areas upto or close to shoreline. Haldia town and eastern part of Digha have been included in this zone.

CRZ-III - The areas which are not particularly developed and does not fall under category CRZ-IV (Coastal stretches in the Andaman and Nicobar, Lakshadweep and small islands), comes under this zone. The zone includes coastal zone in rural areas (developed and under-developed) and areas within municipal limits or in other legally designated urban areas, which are not substantially built up. Sankarpur area and western Digha fall within this category (COPOCS, 00-01).

2.2. Geomorphology.

From the geographical investigation it was ascertained that only 7000 B.P. the lower Gangetic Delta region were under Bay of Bengal. The largest inter-tidal mangrove deltaic region of undivided Sundarbans was formed gradually by the Ganges Brahmaputra river

system. The two major rivers collected fine silt and clay particles from the Himalayas and pour it down to the mouth of Bay of Bengal through two great channels namely river Bhagirathi and Padma. The sub-aerial delta is typically sub-divided into a saline lower delta plain colonized by salt marsh and/or mangroves grading landward with increased elevation into freshwater wetland of the upper delta plain (Wright, 1973). The lower delta plain is sensitive to change in the balance between hydrodynamics and riverine input and to change in relative sea level. The Geomorphology map (Fig. 2-1) showing important geomorphic units of the study area.

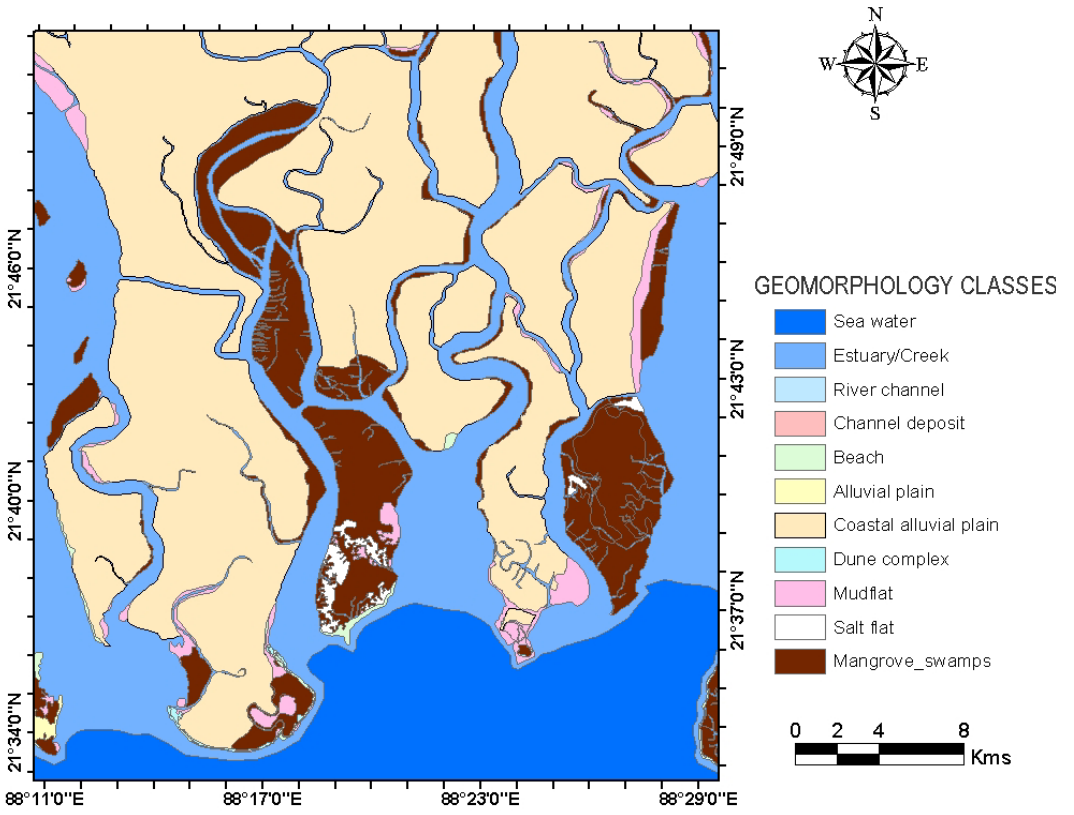

Figure 2-1 Geomorphology of the study area.

2.3. Drainage.

Most of the rivers at the sundarban biosphere region flow north to south are influenced by tides from the Bay of Bengal. The channels connecting these rivers generally flow east or west. Innumerable silt laden rivers, rivulets and creeks cover the entire area. The main estuaries from west to east are Hooghly (Hugli), Saptamukhi, Thakuran, Matla, Bidya, Ajmalmari, Bidyadhari, Gosaba, Kalindi and Raimangal. These rivers, apart from the Hooghly, have no connection with the headwater channel of the upland river system

The Lothian Island is situated at the confluence of saptamukhi and Bay of Bengal. The island itself is bifurcated by a no of large and small creeks. The river water varies

seasonally as well as with the distance from the sea. Insignificant variations in salinity with in the outer and middle estuaries were recorded although a significant variation was found to exist in the inner estuaries (Banerjee, 2002).

2.4. Topography.

The northern part of Lothian is newly formed and shallow, which is inundated twice a day regularly. Where as southern part of the island is gradually elevated and inundated only during spring tide.

2.5. Seasonality and Climate.

Whole Sundarban area belongs to tropics and as the study area is a part of Sundarban so the tropical climate prevails here. It is humid tropical with pronounced hot and wet season. Because of its location adjacent to the Bay of Bengal as well as due to regular tidal flushing in the estuaries the winter is cool but never cold, summer is warm but the day temperature rarely goes beyond 38^0 C in May-June. The seasonal climate in Sundarban may be conveniently categorized into pre-monsoon (March to June), monsoon (July to October), post-monsoon (November to February). High humidity prevails all through the year with a pleasant winter from Nov-Jan. The average maximum temperature is 31.2^0 C and average minimum temperature is 13.7^0 C. Rainfall is of monsoon type, the monsoon generally starts from July and continues till Oct. Humidity goes up to 82 %. Total annual rainfall is about 1500-2000 mm mostly receive during July-Oct. The south- west wind triggers the precipitation in the monsoon period with an average rainfall of about 165 cm (Mitra *et al.,* 2002). Rough weather lasts from 15^{th} March to 15^{th} Sept. Cyclonic storms occur sometimes in April but frequently associated with monsoon rainfall in July-Aug. Coastal processes are very dynamic and are accelerated by tropical cyclones which is locally called "Kal Baisakhi"(Nor'Westers). The oscillation of different physical variables are discussed below –

Wind - The direction and velocity of the wind system in the Indian Sundarbans are mainly controlled by the north-east and south-west monsoons. The month of January and February are relatively calm with an average wind speed around 3.5 km / hr. Violent wind speed recommences from the south-west around the middle of March and continues till September (Mitra *et al.,* 2002).

Waves and tides - Sea waves in this region rarely become destructive except during cyclone storms. During Nor'Westers, the wind speed rises above 100 km / hr. and is usually accompanied by huge tidal waves (Mitra *et al.,* 2002).

Water temperature – The mean surface water temperature in pre monsoon is around 34^0C, whereas the monsoon period shows it around 32^0C and in post monsoon period surface water temperature is around 23^0C (Mitra *et al.,* 2002).

Turbidity – Turbidity of water in Indian Sundarbans is mainly attributed to runoff process that contributes considerable amount of colloidal and finely divided suspended matter (Satyanarayana *et al.,* 2001). Max aquatic turbidity, witnessed during the monsoon season.

Water salinity – Variation of water salinity of the river Ganges depends upon the amount of fresh water flow, tidal amplitude and amount rainfall.

2.6. Soil.

The deltaic soil of SBR comprises mainly with saline alluvial soil consisting of clay, silt, fine sand and coarse sand particles. Soil of upper deltaic plain are fine loamy in texture and neutral to slightly alkaline (pH 7-7.8), in lower delta region is fine texture and acidic to alkaline (pH 5.0-8.0), while soils of marshes area also fine in texture and show acidic to neutral reaction (pH 5.6-7.5). All the three types of soil show gradual increase in pH with the increasing soil depth. The soil of the Sundarbans proper is devoid of humous (0.98%) and supports tangled mass of mangrove. It shows that towards the outer estuarine region percentage of sand is higher and towards the middle and inner regions the percentage of silt and clay is more (Banerjee, 1987). The soil analysis data are presented in Table 2-2 and the soil map is shown in Fig. 2-2.

Table 2-1 Soil analysis data.(10 samples from each type)

Areas	Particle size distribution (depth 30cm)				pH	Organic matter%	Salinity EC(ds m^{-1})
Sundarbans delta	Clay %	Silt %	Fine Sand %	Coarse sand %			
Outer estuaries	24.5	48.5	18	9	7.8	0.79	38.4
Inner estuaries (creeks & canals)	46.5	23.5	20	10	8.02	1.04	33.5
Hinter land	23.5	12.5	33.5	30.5	8.01	1.50	22.8

(Source Banerjee, 2002)

According to National Bureau of Soil Survey, Nagpur the following types of soil are found in Sundarbans area (Table 2-2).

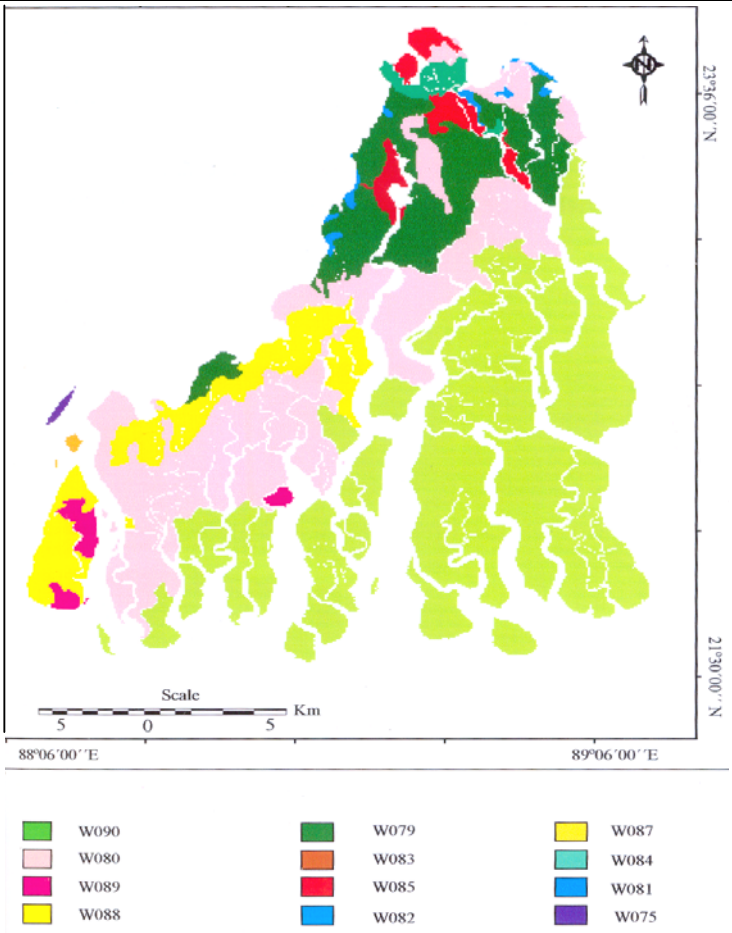

Figure 2-2 Soil map of Sundarbans (Source: NSSB & LUP).

Table 2-2 Soil type of Sudarban Biosphere Reserve.

Serial No.	Soil type code	Taxonomic name	Description
1	W075	Fine Aeric Halaquepts	Very deep, poorly imperfectly drained, fine soils occurring on level to nearly level marshes in coastal plain with clayey surface, moderate flooding and salinity.
2	W079	Fine loamy, Typic Halaquepts	Very deep, poorly drained, fine loamy soils occurring on nearly level upper delta interdistributory sediments with loamy surface. Severe flooding and moderate salinity (limited extent).
3	W080	Fine, Typic Halaquepts	Very deep, poorly drained, fine soil occuring on nearly level upper delta interdistributory sediments with loamy surface. Severe flooding and moderate salinity (limited extent).
4	W081	Fine Arctic Halaquepts Fine loamy typic ustorthents	Very deep, poorly drained, fine soils occuring on level to nearly upper delta plain with clayey surface with, moderate flooding associated with very deep, imperfectly drained, fine loamy soils.
5	W082	Fine loamy Arctic Halaquepts	Very deep, poorly drained, fine loamy soils occuring on level to nearly level upper delta plain with loamy surface and subject to severe flooding associated with very deep, poorly drained, fine loamy soils.
6	W083	Fine Arctic Halaquepts Fine loamy Arctic Halaquepts	Very deep, poorly drained, fine soils occuring on level to nearly level upper delta plain with clayey surface and subject to severe flooding associated with very deep, poorly drained, fine loamy soils.
7	W084	Fine Arctic Halaquepts Fine typic Halaquepts	Very deep, poorly drained, fine soils occuring on level to nearly level upper delta plain with clayey surface and subject to severe flooding associated with very deep, poorly drained, fine soils.
8	W085	Fine Arctic Halaquepts Fine typic Ustorthents	Very deep, poorly drained, fine soils occuring on level to nearly levelmarshes with clayey surface and subject to severe flooding, associated with very deep, imperfectly drained, fine soils with severe flooding.
9	W087	Fine Arctic Halaquepts Fine typic Halaquepts	Very deep, poorly drained, fine soils occuring on level to nearly level upper delta inter distributory sediments with clayey surface and moderate flooding, associated with very deep, well drained sandy soils.
10	W088	Fine Arctic Halaquepts Fine, typic Halaquepts	Very deep, poorly drained, fine soils occuring on level to nearly level lower delta with clayey surface with severe flooding and moderate salinity (moderate extent) associated with very deep, poorly drained, fine soils.
11	W089	Fine Arctic Halaquepts	Very deep, poorly drained, fine soils occuring on level to nearly level lower delta with clayey surface severe flooding annnd moderate salinity.
12	W090	Fine loamy, typic Halaquepts Fine Loamy typic Fluvaquents	Very deep, poorly drained, fine soils occuring on level to nearly level lower delta with loamy surface severe flooding and very strong salinity (extensive extent). Associated with very deep, very poorly drained, fine loamy soils.

From the soil map of sundarban Biosphere Reserve and soil type chart it has been found that the soil type (W090) of the Lothian Island is Fine loamy, typic Halaquepts Fine Loamy typic Fluvaquents. It is describes as very deep, poorly drained, fine soils occurring on level to nearly level lower delta with loamy surface, severe flooding and very strong salinity (extensive extent) associated with very deep, very poorly drained, fine loamy soil.

CHAPTER 3.

Review of Literature

3.1. Mapping and Monitoring of Mangroves Using Optical Remote Sensing Data.

In many still undisturbed mangrove ecosystems, gradients in salinity, tide action and drainage often cause major differentiation in species composition and their structure across relatively short (10–100 m) transects. High diversity mangrove systems, such as those found in tropical coastal areas of northern Australia, Papua New Guinea and Irian Jaya, can contain up to 30 different species, broadly segmented into 'mangrove zones'. Although broad separation of mangroves from surrounding rain forests or other ecosystems is feasible with traditional sensors, studies using remote sensing techniques to assess in more detail the diversity within mangrove forests are still uncommon (Jensen *et al.,* 1991; Green *et al.,* 1998b, Rasolofoharinoro *et al.,* 1998). Due to the often-narrow extent along coastlines, detailed mangrove ecosystem characterization is difficult with moderate-resolution (30 m) satellite data (Green *et al.,* 1998b). A number of authors have investigated differentiation of mangroves into broad classes based on density / age using moderate-resolution optical sensors, such as SPOT (Jensen *et al.*, 1991, Gao, 1998, Green *et al.,* 1998b) and Landsat TM (Rasolofoharinoro *et al.,* 1998). Ramsey and Jensen (1996) found that vegetation indices from satellite optical sensors could be well correlated to mangrove Leaf Area Index (LAI) and canopy height, but that species composition mapping was still difficult with this type of low-resolution data. While air photography offers the high spatial resolution needed to distinguish different types and zones, it often requires experience in its interpretation. Green *et al.,* (1998a) and Mumby *et al.,* (1999), have suggested that high-resolution, multi-band optical sensors are not only well suited technologies for detailed coastal ecosystem mapping, such as coral reefs, submerged macrophytes and mangroves, but that they are also cost-effective, when compared to traditional air photo interpretation and selective ground sampling costs. In order to describe these ecosystems more accurately and objectively in terms of their zonation, productivity and diversity patterns, the combination of high spatial (3 m pixels or less) and spectral resolutions are thus needed.

Murray *et al*. in 2003 worked on the distribution, composition and classification of Belize mangroves. Between the late 1980s and early 1990s, Belizean coast came under escalating pressure from development resulted habitat loss which need for assessment of the extent, characteristics and use of remaining mangrove. Authors confirmed the presence of three true mangroves—*Rhizophora* mangle, *Avicennia germinans* and

Laguncularia racemosa, and one mangrove associate *Conocarpus erectus*. Twenty different sub-communities were distinguished on the basis of physiographic setting, GIS analysis of 1990 remote sensing (Landsat TM) data revealed that Belize's mangroves covers 3.4% of the country's land. Through the examination of early aerial photos, historical records and ground conditions, it was estimated that a 0.7% reduction in the national total in just two years. The main factors controlling the distribution of mangroves in Belize are the presence of the barrier reef, the coastline's shallow gradient and the narrow tidal range. Though mangrove distribution is further influenced by local subsidence, geomorphology, drainage, hinterland soils and past hurricane tracks but its existence largely depend on two factors—hurricane activity and human influence.

Satyanarayana *et al*., 2001, tried to find the relationship between vegetation indices and dendrometric parameters in Coringa mangrove. The purpose of the study was to map the mangrove formations and its surroundings based on a supervised classification of remote sensing data (IRS 1C LISS3) and to analyze the potential relationship between mangrove dendrometric parameters and spectral indices. During field survey mangrove vegetation parameters like basal area and tree density have been estimated using Point Centered Quarter Methods (PCQM) on transects lines of at least 100m of 128 points. The satellite data was classified using supervised classification resulted in 14 classes among which 3 corresponds to different mangrove signatures. Vegetation indices (VI) were calculated at locations for which mangrove parameters were obtained from field survey. Scatter-plots and analysis of variance (ANOVA) have been used in order to explore the relationship between VI and mangrove parameters. It was concluded that there is a relationship between the VI and basal area, but not with density. When spectral indices and mangrove parameters are considered altogether, it appears that only two classes of mangrove were possible to discriminate.

3.2. Effect of soil salinity on Mangrove distribution

Hema Joshi and M Ghose, 2003 have done an analysis in sundarban mangrove to relate the community structure and distribution of species with soil salinity and pH gradients. Soil salinity (13.0 to 31.2 ppt) decreases with increasing distance from the tidal coast but no such trend was noticed in soil pH (7.0 – 7.9). They predicted that frequency of tidal inundation to affect soil salinity. They reported that *Acanthus ilicifolius*, *Avicennia alba* and A. marina dominates the site having regular diurnal tidal inundation. Maximum complexity index was noted in least salinity zone. They also ecologically grouped the mangrove species. Ecological group classification indicates that *Avicennia marina* and *A. officinalis* can tolerate wide range of soil salinity, while *Aegiceras corniculatum*, *Ceriops decandra*, *Dalbergia spinosa*, *Derris trifoliata* and *Excoecaria agallocha* are restricted to low salinity areas. Most species had an optimum pH range except *Avicennia marina*,

which occurred in varied pH conditions. *Acanthus ilicifolius* was relatively insensitive to pH and salinity gradient due to its wide ecological amplitudes.

3.4. Mangrove Leaf area index (LAI)

E. Green, C. Clark (The Remote Sensing Handbook for Tropical Coastal Management) correlates *in situ* LAI values against the NDVI information derived from the SPOT XS data for 29 field sites surveyed in 1995. A linear regression was fitted to these data and a good coefficient of determination obtained ($r^2 = 0.74$, $P < 0.001$, $n = 29$). The F-test for the model and *t*-test for the slope estimate were both significant at the 0.001 level of confidence, indicating a strong relationship, which can be used to convert NDVI values to LAI. The NDVI model was then used to estimate values of mangrove LAI for the entire image. LAI ranged from 0.83 to 8.51, with a mean value of 3.96. Thus they produced a thematic image of LAI for the mangrove areas of the Caicos Bank.

Peng Gong, Ruiliang Pu, Greg S. Biging, and Mirta Rosa Larrieu, 2003 estimates Leaf area index of conifer forest in semiarid Patagonia region of southern Argentina using vegetation indices derived from Hyperion Hyperspectral data. They construct 12 two-band Vegetation indices using all available 168 hyperian bands. Finally they evaluated the correlation of each possible vegetation index with LAI measurements to determine the most effective bands for forest LAI estimation. Their experimental result indicates that most of the important hyperspectral bands with high R^2 are related to bands in the short-wave infrared (SWIR) region and some in the near- infrared (NIR) region. It has been noted that the originally defined Vegetation indices that use red and NIR bands did not produce higher correlation with LAI than Vegetation indices constructed with bands in SWIR and NIR region.

3.5. Mangrove Above Ground Biomass and Radar remote sensing

C Proisy, E Mougin. F Fromard, V Trichon, M.A. Karam, 2002 evaluated the effect of canopy structure on polarimetric radar response of mangrove forest at French Guiana coast (52° 19′ W, 4° 52′N). They reported that two different mangrove stands of equal biomass but different, greatly in their structure differently responses differently with radar. For the three considered frequencies (C-, L- and P- bands), experimental observations show that the back scattering form open declining stand is higher that of the closed forest they suggested for using backscattering coefficient values specially P-H, P-HV or the HH-VV phase difference at P band.

Proisy *et al.* (2000) interpreted the polarimetric radar signature of mangrove forests, using NASA / JPL AIRSAR full polarimetric data at P (0.44 GHz), L (1.25 GHz), and C (5.3 GHz) band at a mean incidence angle of 35^0 of South American campaign. Polarimetric scattering model is based on an iterative solution of the vector radiative transfer equations up to the second order (Karam *et al*., 1995). On the whole, it was concluded the P band provides the most pronounced polarimetric signatures. The polarization ratio was found to be useful for analyzing scattering mechanisms and for discriminating between various forest stages. Comparison between AIRSAR data and simulations showed that the model is able to describe the overall radar signature of mangrove forests at P, L and C band.

Hashim (1999) has reviewed comparison of classification of mangrove forest at species-level, and estimation of mangrove biomass using JERS-1 SAR and Radarsat SAR (standard mode) data, carried out in test site Sungai Pulai, Malaysia. Unsupervised-supervised approach with maximum likelihood classifier was performed on JERS-1 and Radarsat image. More classes could be identified from JERS-1 than from Radarsat. Results showed Radarsat (5.6 cm wavelength) is less sensitive compare with JERS-1 (23.5 cm). The mangrove biomass estimation was found related to JERS-1 and Radarsat backscatter coefficient at $r^2 = 0.5$ and 0.31. Lower accuracy was observed as biomass increases – two reasons that might contribute to this accuracy trend are: (1) non-representative regression model due to limited samples used in generating the biomass-backscatter relationship, (2) mixed species in area of larger biomass but only dominating pioneering species were accounted in derived biomass. The results demonstrate the utility of SAR data as potential source in mapping classes and indicator for biomass.

Peter N. Tiangco and Bruce C. Forester 2000 works on extraction of information of forest crown and trunk component from radar data according to them at C- band the backscattering energy is correlated mainly with canopy constituents such as leaves, twigs and small brunches. Information on the other components beneath the canopy can be sensed through the use of bands with longer wavelengths such as the L-or P-band. The sensitivity of co-polarized and cross-polarized waves to the shapes and orientation of different tree constituents provide an added advantage in the information extraction procedure. The Trunk-Canopy Biomass Index (TCBI), which is the sum of the L-HH and C-HV backscatter, can be a measure of the total aboveground biomass as both the crown and trunk layers are taken into consideration. Owing to possible morphological variation, the relationship between TCBI and biomass is however not expected to be unique for a whole forest vegetation. It is important therefore that stand structure be first considered to allow a more accurate biomass assessment by the TCBI. An index of the relative proportions of the crown and trunk may be indicative of the approximate tree

morphology. It is believed that the Trunk-Canopy Morphology Index (TCMI), which is the ratio of the L-HH to C-HV backscatter, provides a measure of tree structure.

Hema Joshi and M. Ghose, 2001 reported on the mangrove community structure and above ground biomass of Lothian island. They recorded the all stand parameters like DBH, density, species diversity of different plots located at both sides of central rods starting from the northern tidal coast of island to wards the south with gradually increasing distance.

CHAPTER 4.
SAR Basics and Imagine Principle

This chapter gives a brief overview about the SAR technique and system inherent properties, which are important for an understanding of the interactions between the imaging system and an object. The focus lies hereby on the properties of an active SAR system in the microwave region of the electromagnetic spectrum, as it is realized by the ENVISAT ASAR sensor used within this work. An amount of good introductions to SAR imaging techniques can be found in the literature (e.g. BAMLERand SCHÄTTLER, 1993; KLAUSING and HOLPP, 2000; OLMSTED, 1993; LEWIS and HENDERSON, 1998). The introduction therefore concentrates on important features for the presented investigation.

4.1. SAR principle

An air- or space borne synthetic aperture radar system scans the Earth surface in a side looking manner as depicted in Figure 4-1. While the sensor is moving on its orbit it transmits and receives electromagnetic pulses at the rate of the pulse repetition frequency. The flight direction provides the azimuth and the perpendicular direction the range coordinate. From each object, illuminated within the systems footprint, it receives information at different times and from different pulses. By measuring the travel time of a pulse between transmission and reception, the range distance of an object can be determined.

Contrary to real aperture radar (RAR), the received echoes from various pulses are used within a SAR system to generate a synthetic antenna length (synthetic aperture). By time integrating over different sub apertures, the systems spatial resolution can be significantly improved.

Hence a SAR system is an active system, which illuminates the Earths surface with an own source of electromagnetic waves. Being independent from external sources of illumination makes it possible to operate the system day and night.

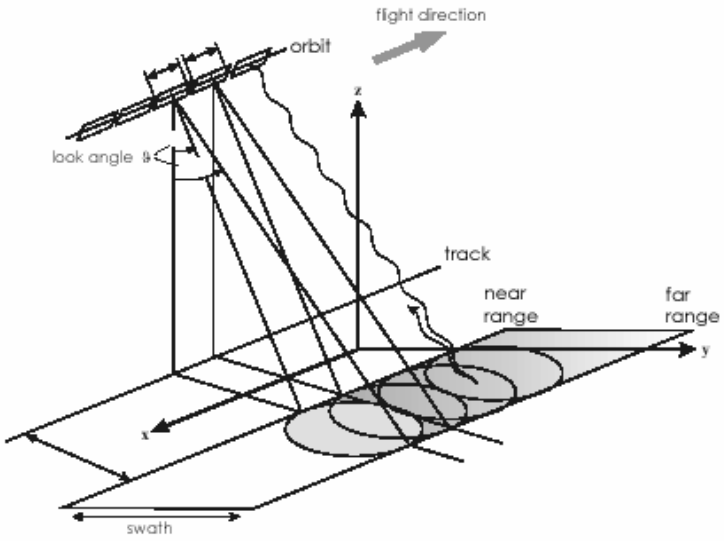

Figure 4-1 SAR imagine principle

The atmosphere is almost transparent for microwaves. Contrary to the optical part of the electromagnetic spectrum the influence of the atmosphere on the signal is negligible. This should not mislead to the assumption that there is no influence of the atmosphere. For several applications, e.g. weather radar, short microwaves are used to detect heavy rain or hail. The phase of the electromagnetic wave is also influenced by the atmospheric water content, which can even be used for inversion approaches (HANSSEN et al., 1999).
The commonly used frequency bands in the microwave region are given in Table 4-1. Dependant on the sensor configuration of a SAR system, different interactions of the electromagnetic wave with an object can be observed.

Table 4-1 Microwave Frequency Band

Frequency Band	Wave length (cm)	**Frequency**
K	0.8 – 2.4	40. – 12.5
X	2.4 – 3.8	12.5 – 8.0
C	3.8 – 7.5	8.0 – 4.0
S	7.5 – 15.0	4.0 – 2.0
L	15.0 – 30.0	2.0 – 1.0
P	30.0 – 100.0	1.0 – 0.3

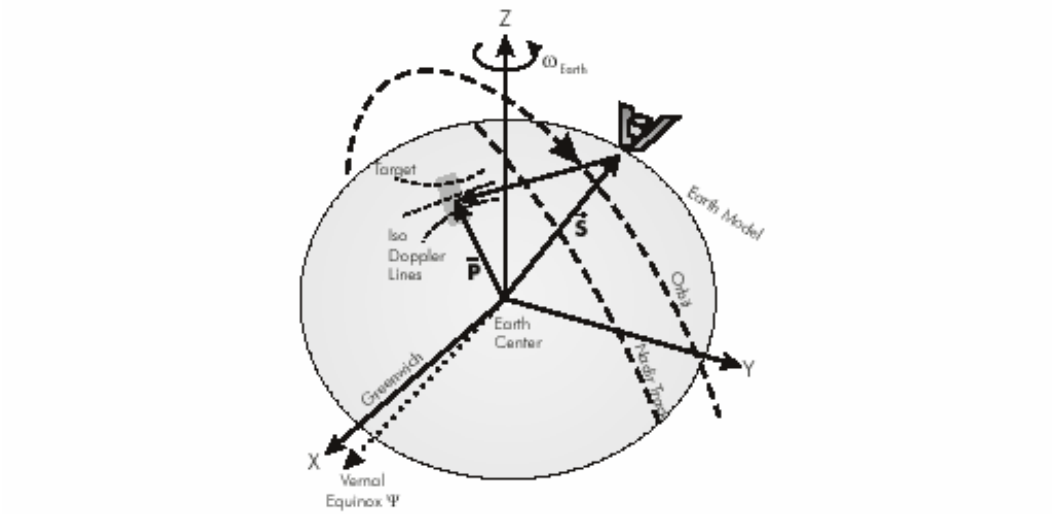

Figure 4-2 General SAR imagine geometry

4.2. SAR imaging model

4.2.1. Imaging model

The position of a SAR system on an orbit at time t is given by its Earth centred state vector *S*(t).Assuming the imaging geometry given in Figure 4-2, the range distance $R_s(t)$ to a target *P* can be calculated by

$R_s = \sqrt{(S-P).(S-P)}$ ……..4.1

As already mentioned, a SAR system receives the echoes of an object within multiple pulses. The footprint of a system with a small beam width of 0.3 ° (e.g. ERS) gives a footprint on the Earth's surface of about 5 km. At a pulse repetition frequency of 1680 Hz, the beams footprint moves only ~4 m between the pulses. This means that each object is seen more than 1000 times by the radar (OLMSTEDT, 1993).

The coherently recorded echoes of an object have to be integrated during the image formation process to estimate the objects position within the image plane. For that the Doppler frequency shift f_D can be calculated for each orbit position by

$$f_D = \frac{2 f_0}{c} \frac{(\vec{v}_P - \vec{v}_S)\vec{R}_S}{|R_S|} \quad \text{……4.2}$$

with the carrier frequency f_0 and the target and sensor velocities *Vp* and *Vs*.

The Doppler frequency is higher for objects approaching the sensor, than for objects the sensor is moving away from. The point, where the object is perpendicular to the sensors position, corresponds to the Zero-Doppler position. For any given object the corresponding Zero-Doppler position can be calculated iteratively using (4.1) and (4.2) (e.g. MEIER, FREI and NÜESCH, 1993; LÖW and MAUSER, 2003).

4.2.2. SAR Imaging properties

4.2.2.1. Local imaging geometry

The angle between the incident wave and the normal vector on the geoid is defined as the incidence angle θ. It has a major influence on the radar backscatter. While θ is defined for a flat Earth the local incidence angle θ_i takes the local terrain slope into account. It is defined as the angle between the incident ray and the local surface normal. This is illustrated in Figure 4-3.

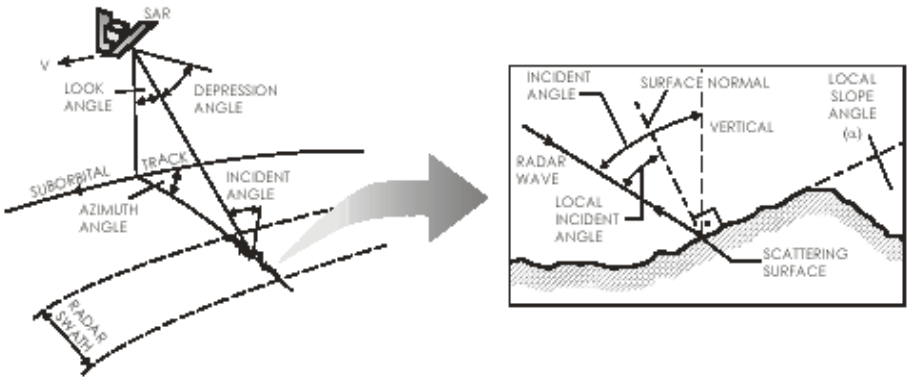

Figure 4-3 Global and local imagine geometries

4.2.2.2. Azimuth resolution

The geometric resolution of an imaging system determines the spatial extent of a resolution cell on the Earth surface. The azimuth resolution $_a\rho$ of a SAR system is the resolution of the system in flight direction, given as

$$\rho_a = \frac{L}{2} \quad \text{.....4.3}$$

where L is the length of the physical antenna. Note, that $_a\rho$ is independent from range distance. Theoretically the azimuth resolution is therefore not influenced by the targets distance to the sensor.

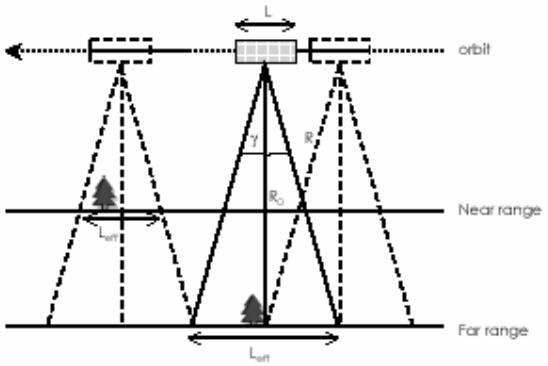

Figure 4-4 SAR Azimuth resolution

This can be explained by the concept of the SAR, which integrates information gathered within a certain time interval. For a physical antenna, the angular beam width γ is directly proportional to the antenna size L and the wavelength λ f_n as (OLMSTED, 1993).

$$\gamma = \frac{\lambda}{L} \quad \text{.....4.4}$$

The corresponding footprint L_{eff} is a function of the range distance R as

$$L_{eff} = \gamma R = \frac{\lambda R}{L} \quad \text{.....4.5}$$

For synthetic aperture radar, L_{eff} corresponds to the distance; the target is within the beam. For targets in near range this integration time is shorter than for targets in far range, as can be seen from Figure 2.4. The effective angular beam width of a SAR system is then given by

$$\gamma_{eff} = \frac{\lambda}{2L_{eff}} \quad \text{.....4.6}$$

which is similar to (2.4), except for the factor 2, which is caused by the different collecting of phase shifts (MOREIRA, 1992). Using (2.5) the azimuth resolution can then be calculated as

$$\rho_a = \gamma_{eff} R = \frac{\lambda R}{2L_{eff}} = \frac{\lambda R}{2\frac{\lambda R}{L}} = \frac{L}{2} \quad \text{.....4.7}$$

Which is equal to (4.3).

4.2.2.3. Range resolution

The range resolution of a SAR system depends on the pulse length τ of the transmitted signal. Two objects, illuminated by the same pulse, cannot be distinguished, whereas objects with a distance larger than the resolution cell can be separated (Figure 4-5). The slant range resolution ρ_r is given by

$$\rho_r = \frac{c\tau}{2} \quad \text{.....4.8}$$

Where c is the speed of light. Assuming a flat Earth surface, the corresponding ground range resolution $_G\rho$ for an incidence angle θ is given by

$$\rho_G = \frac{c\tau}{2\sin(\theta)} \quad \text{.....4.9}$$

Thus, the geometric ground resolution is dependant on the incidence angle. In the Far Range region, the resolution is better than in the Near Range of the footprint. This is shown in Figure 4-5, where the points P_1 and P_2 can not be separated by the SAR system whereas P_3 and P_4, which have the same ground distance, can be separated due to the better spatial resolution.

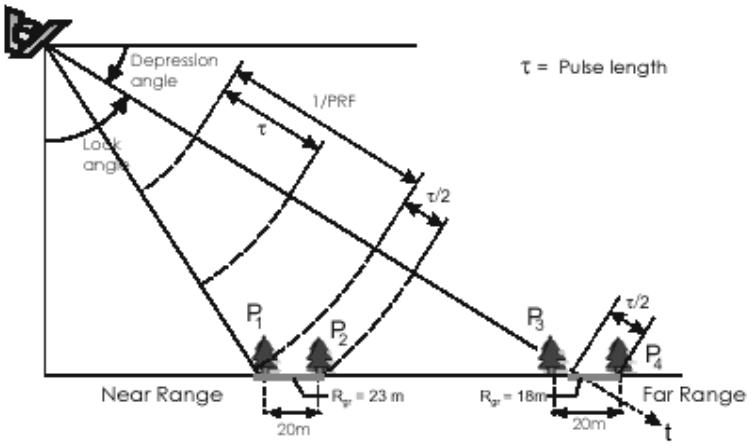

Figure 4-5 Range resolution of SAR system: The ground range resolution is increasing from Near to Far Range

4.2.2.4. Relief distortion

Due to the side looking geometry of a SAR, the relief can induce significant geometric and radiometric distortions to the image product. Scattering occurs from sloping and faceted surfaces, which create local distortions that depend on the surface to beam orientation. These distortions can be corrected using rigorous image processing techniques.

Figure 2.6 shows the slant and ground range planes for rugged terrain as seen by a SAR system. Slopes, facing towards the sensor cause a displacement of the elevated parts of the terrain towards the sensor. This foreshortening is the reason why surfaces, directing towards the sensor, appear bright in SAR images. The energy of many scatters is compressed within few image pixels. The extreme foreshortening, where the signal from the top of a mountain reaches the sensor before that of the base is named layover. Areas aspecting away from the sensor or lying behind the top of a mountain are not illuminated. No backscatter return is therefore received from that shadow region.

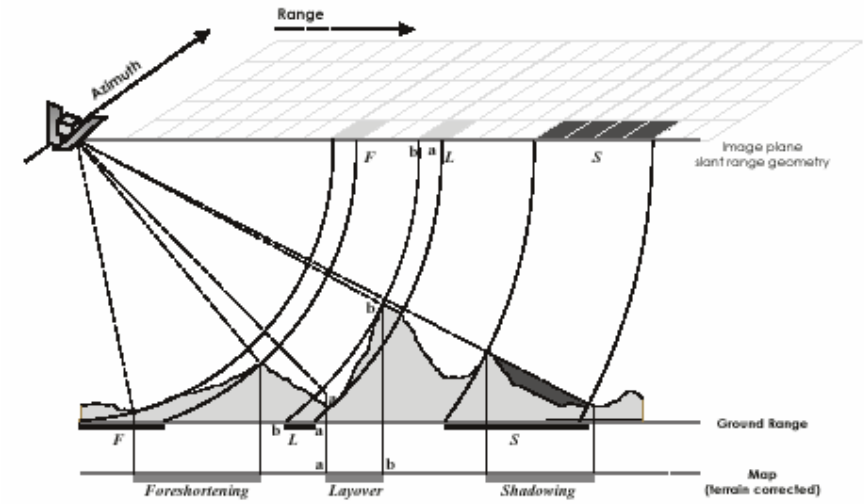

Figure 4-6 Geometric and Radiometric relief distortion.

In along track direction, the radial velocity between the sensor and the target changes with changing terrain height, which introduces an additional Doppler frequency shift. For the ERS configuration, this terrain introduced shift causes a misalignment of 110 m or 9 azimuth pixels for a height difference of 1000 m and targets in the mid-latitudes (MEIER, FREI and NÜESCH, 1993).

For slopes, facing the incident wave front, a larger ground area contributes to the returned signal of a slant range resolution cell, than for slopes lying in the opposite direction. The slope and aspect of the scattering surface produces significant changes of the scattering area among neighboring resolution cells. The correction of this effect is crucial. It is shown in Chapter 4 that it can be compensated in a rigorous way.

4.3. Radar equation and backscattering coefficient

The power, received at the antenna of a SAR system, is recorded and can be processed to a two-dimensional image (e.g. BAMLER and SCHÄTTLER, 1993; CURLANDER and MCDONOUGH, 1991; MOREIRA, 1992).

The received power is given by (ULABY et al., 1982; KLAUSING and HOLPP, 2000):

$$\overline{P}_R = \frac{\lambda^2}{(4\pi)^3} \int \frac{P_T G^2}{R^4} \cdot \sigma^0 dA \qquad \text{.....4.10}$$

$\overline{P}_R$, P_T = Average received power, transmitted power.

G = Antenna gain.

A = Illuminated area.

R = Range distance.

λ = Wavelength.

σ° = Backscattering coefficient.

Equation (4.10) is known as the radar equation. A derivation of the formula is given in Appendix A. The target scattering characteristics are comprised by the backscattering coefficient σ_0. It describes the ratio of the energy scattered by the target compared to the energy scattered by a lambertian isotropical surface. For distributed targets, σ_0 is the normalized radar cross section (RCS) of the scatterers within a resolution cell:

$$\sigma^0 = \frac{\sigma}{A}\left[\frac{m^2}{m^2}\right] \quad \text{.....4.11}$$

Thus for the derivation of σ_0, the scattering area must be known. As will be seen in Chapter 4, the scattering area is strongly influenced by terrain undulations. During the image generation procedure, the local terrain slopes are not known. Therefore image products are not normalized to the ground surface. The normalization of the gray values is done in the slant range geometry, which means that the unit area is given by the azimuth and slant range resolution of the imaging system. Thus, the image is directly proportional to the received power and is called a brightness image. Contrary to the backscattering coefficient on the ground σ_0, it is abbreviated by β_0. A third possibility exists, where the image is normalized to the area perpendicular to the incident ray. In Figure 4-7 the three different possible normalization methods are shown. The only backscattering coefficient, being independent from the local imaging geometry is β_0. This is the reason why SAR image products are always delivered as β_0 images (LAUR et al., 1998; SHEPARD, 2000; ROSICH and MEADOWS, 2004).

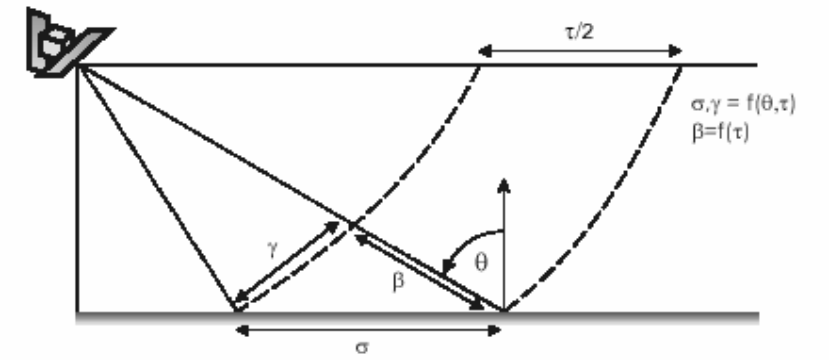

Figure 4-7 Definition of the backscattering coefficients σ 0 , β 0 , γ 0.

ENVISAT ASAR

The Advanced Synthetic Aperture Radar (ASAR) is the biggest instrument of the payload, boarded on the ENVISAT platform. It was built to continue and extend Earth observation using SAR. Figure 4-8 shows the ASAR antenna on board of the satellite and in the laboratory. The deployed antenna has a size of about 10 meters.

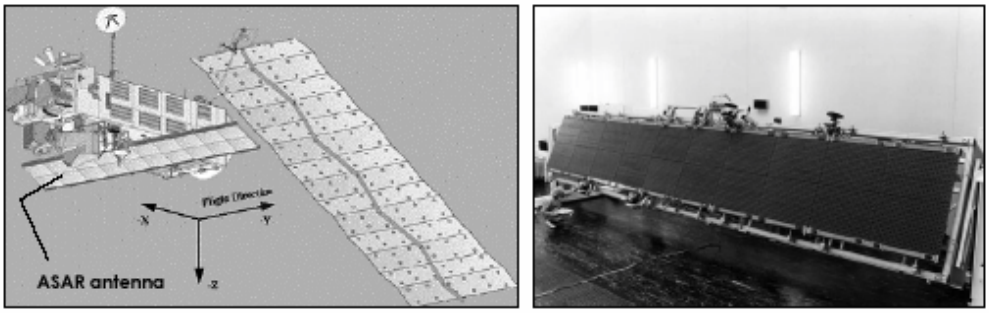

Figure 4-8 ASAR sensor onboard (left) and antenna in the laboratory (right); Microwave Interaction with Mangrove

Based on the experience with ERS-1/2, several enhancements have been made for ASAR. Most important is the replacement of a central power amplifier for the antenna, by an active phase array antenna system with distributed elements. The whole antenna consists of 320 independent Transmit/Receive (T/R) modules, organized in 32 rows of 10 modules, which can be adjusted each individually (ROSICH et al., 2003). As a result, the instrument can be used in a very flexible manner. It allows different polarization combinations, incidence angles and imaging modes. Table 4-2 summarizes the main characteristics of the sensor. More detailed technical information can be found in ESA (2002).

The innovative concept of the sensor allows for new acquisition modes with different image content. The major improvements are presented next.

Table 4-2 Main ASAR configuration parameter.

Parameter	ASAR configuration
Orbit altitude.	~799km
Orbit inclination angle [°]	98.55
Incidence angle range [x]	14 - 45°
Swath width [x]	58 – 109 km
Frequency / wavelength	5.331GHz /5.6224 cm (C-band)
Polarization	HH / VV / VH / HV
Calibration Accuracy	± 0.5 dB
Range sampling rate [MHz]	19.21
Pulse repetition frequency [Hz] [x]	1709 –2067

[X] dependent on the selected configuration.

4.4.1. Selectable imaging mode and incidence angle

ENVISAT ASAR has different selectable imaging modes, which can be chosen by the user prior to the acquisition. Additionally the possibility to control the direction of the antenna lobe allows for the acquisition of images with different incidence angles.

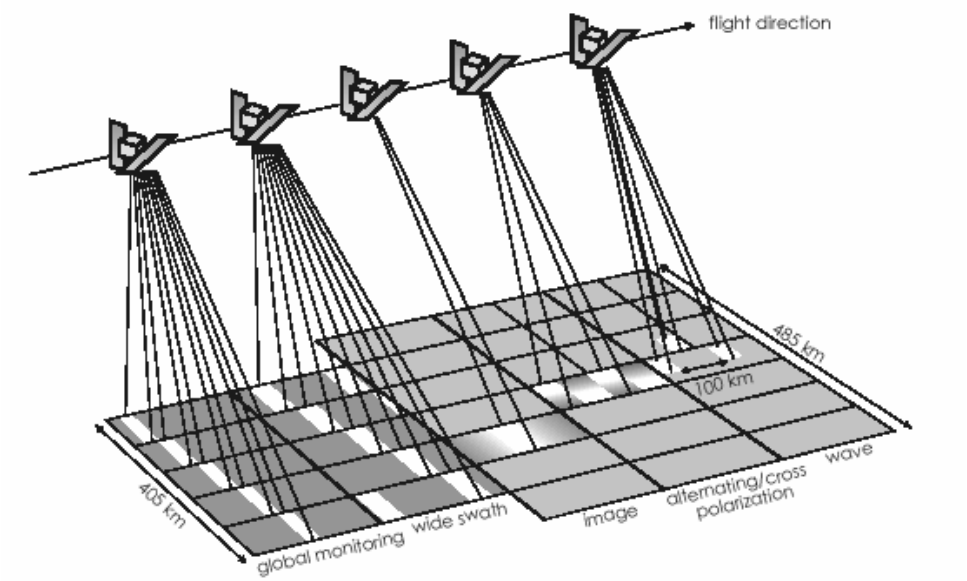

Figure 4-9 ASAR imaging modes (modified after ESA, 2002)

The different imaging modes of ASAR, shown in Figure 4-9, are (ESA, 2002):

Image Mode (IM)

VV or HH polarisation images from any of 7 selectable swaths. Swath widthbetween approximately 56 km (swath 7) and 100 km (swath 1) across track.Spatial resolution of about 30 m (for precision product).

Alternating Polarisation (AP)

Two co-registered images per acquisition, from any of 7 selectable swaths. HH/VV, HH/HV or VV/VH polarisation pairs possible. Spatial resolution of approximately 30 m (for precision product).

Wide Swath (WM)

400 x 400 km² wide swath image. Spatial resolution of approximately 150 m. VV or HH polarisation. The image is acquired using the ScanSAR technique where 5 subswaths form the whole image.

Global Monitoring Mode (GM)

Same acquisition technique as for the wide swath mode, but with reduced spatial resolution. Spatial resolution of approximately 1 km. HH or VV polarisation

Wave Mode (WV)
A small imagette is acquired at regular intervals of 100 km along track. The imagette can be positioned anywhere in an image mode swath. HH or VV polarisation may be chosen. Imagettes are converted to wave spectra for ocean monitoring.

The different imaging modes allow using the sensor in a very flexible manner. It can switch between the different modes within a few seconds. The main achievements of these new imaging capabilities are:
Frequent observations - the different swaths allow to observe an area of interest from different orbit paths, which increases the observation frequency. For areas in the mid-latitudes, coverages from two up to four times a week are possible. The different ENVISAT ASAR swathes and their properties are summarized in Appendix A.

Multi-incidence observations - The radar backscatter has an angular dependency. The programmable incidence angles allow choosing the best incidence angle for a certain application
Wide area coverage - For many applications it is important to cover a wide area with an acceptable spatial resolution. In hydrological applications it can be of interest to retrieve surface parameters (e.g. soil moisture, snow covered area) for a whole watershed. The wide swath mode with an area extent of 400 x 400 km² is well suited for these needs, when the corresponding loss in spatial resolution remains acceptable. It provides homogeneous, temporal consistent datasets for large areas. Figure 2.10 shows an example of a WSM image in southern Germany.

4.4.2. Dual polarization

Imaging radars can transmit and receive differently polarised electromagnetic waves. The electric field can be polarised horizontally (H) or vertically (V) with respect to the incident wave on the surface. Each possible combination of transmit/receive configuration is abbreviated by the H and V characters. The first character corresponds to the transmit, the second to the receive polarization (e.g. VH stands for vertical transmit and horizontal receive). A SAR system with the same transmit/receive combination (VV or HH) is a copolarised system, contrary to the crosspolarised case (VH or HV).

ENVISAT ASAR is the first operational space borne sensor which provides a dual polarization channel. In its alternating polarization mode (AP mode), one of three different channel combinations is possible:
VV and HH
HH and HV

VV and VH

The different polarization combinations contain different information about the scattering processes and therefore allow inverting land surface parameters with less degree of freedom, which might simplify inversion strategies (ESA, 2002).

CHAPTER 5.

Microwave interaction with Mangrove

There has been much recent interest in using Synthetic Aperture Radar (SAR) Remote Sensing to retrieve biophysical characteristics from forest targets (Richards, 1990). Microwave radiation interacts differently with distinct plant communities of the floodplain and surrounding areas (Costa, 2000). The characteristics of the plant (density, distribution, orientation, shape of the foliage, dielectric constant, height, and branches), the ground (dry, moist, and flooded), and the sensor (polarization, incidence angle, and wavelength) are important in determining the radiation backscattered towards the radar antenna (Dobson *et al*., 1996). Because of their high moisture content, individual components of forest canopies and other vegetation (e.g., leaves, branches, trunks etc.) represent discrete scattering and attenuation elements to the microwave energy transmitted by the imaging radars. Variation of the microwave dielectric constant of vegetative elements or ground surface play a central role in the determining the intensity and the phase of the microwave energy scattered from a vegetated surface and recorded and processed into a SAR image. Factor influencing the dielectric constant of vegetated surfaces include temperature of the scattering medium, relative moisture content of the vegetation and soil and the presence of water on vegetation (Kasischke, 1997). The frequency and polarization of microwave scattering from land surfaces is strongly dependent on the size and orientation of the different elements comprising the vegetation. In wetlands, where there is water beneath vegetation canopies, the SAR response is often very bright resulting from a combination of the smooth horizontal surface of the water and the vertical orientation of stems or branches of the vegetation. This is often called a "double bounce" return and allows for a very good mapping of wetlands as they are brighter than non-flooded vegetation. There are some conditions, however, that need to be met for the double bounce signal to be strong enough to stand out in the image (Fig. 5-1): (1) if the vegetation canopy is closed, the overall total biomass of the vegetation stand has to be low enough to allow penetration, and (2) in heavier biomass stands the inundated surface could also be identified if the openings in the canopy are substantial enough to allow the radar waves to reach the water surface. For better penetration, a microwave sensor with near vertical incidence angle, and improved spatial resolution and signal-to-noise ratio, is required (Dwivedi *et al.,* 1999).

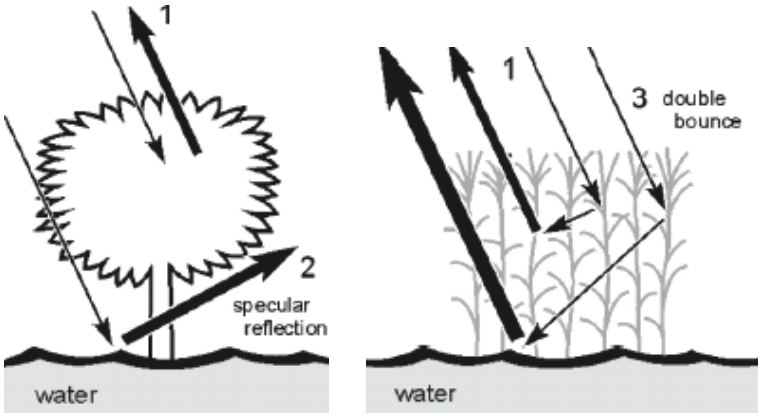

Figure 5-1 Schematic representation of the scattering mechanisms at C band for (a) Flooded forest and (b) Aquatic vegetation. The thickness of the returning arrows (1, 2, and 3) represents relative magnitude of scattered radiation.

Wetlands with standing water without vegetation appear as a dark to very dark-grey tone and fine texture. rivers and estuaries with calm water also exhibit a similar response (Dwivedi *et al.,* 1999). Amongst vegetation, mangroves exhibit a characteristic response and are seen in the SAR image as light-grey in tone and have a very coarse texture. Although radar backscattering from forest is influenced by their structural properties (Imhoff, 1995a), many studies have demonstrated useful relationship between backscattering coefficients and the aerial density of the above ground biomass within particular type of forest (Baker *et al.,* 1994; Le *et al.,* 1992; Dobson *et al.,* 1992; Imhoff, 1995b). These relationships may provide a method of monitoring forest ecosystems which play such a vital role in carbon storage and CO2 flux between the land surface vegetation and the atmosphere (Luckman, 1997). Radar-forest interactions are complex and a particular combination of frequency and polarization may generate markedly different signatures for the various growth forms of a species as well as different species (Fig. 5-2).

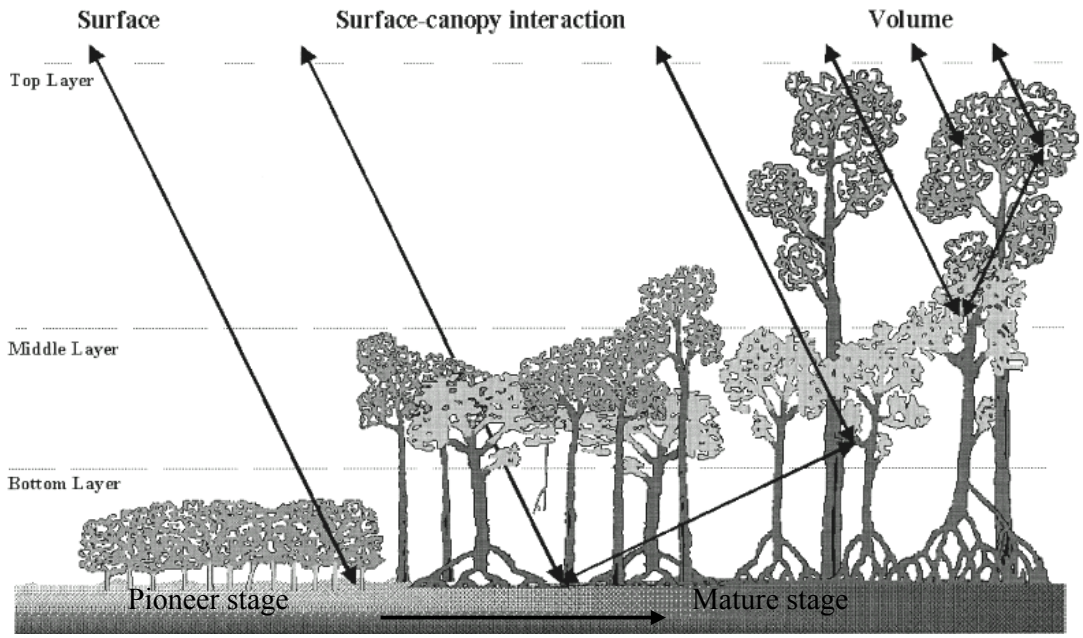

Figure 5-2 Geometry of the mangrove forest model.

Mangrove forests and flooded vegetation generally exhibit well pronounced microwave signatures (Mc-Donald *et al.,* 1980; Imhoff *et al.,* 1986). This occurs when the incident wave propagates through the entire canopy and reaches an underlying highly reflecting surface (Proisy *et al.*, 2000). In this case, the backscattering coefficient for the co-polarizations HH and VV is enhanced by a factor lying between 3 and 10 dB, depending on the magnitude of canopy attenuation and thus on radar parameters and vegetation type (Hess *et al.*, 1990), depending on radar parameters and forest structure. Where the forest canopy is dense this enhancement is not observed due to greater canopy attenuation of the radar wave. Such observations are in concordance with theoretical studies that suggest that the enhancement backscattering observed in flooded forests originates from double-bounce returns or multiple scattering between the water surface and forest components (Engheta and Elachi, 1982; Richards *et al*., 1987; Wang and Imhoff, 1993, Wang *et.al*., 1995). In contrast the cross-polarization HV does not exhibit any particular enhancement, because it originates from multiple scattering within the canopy layer. In addition for dense flooded forests, no enhancement is observed, certainly owing to a strong canopy attenuation of the radar incident wave (Krohn *et al.,* 1983; Wu and Sader, 1987). The interaction between the microwave and the vegetation also depends on the frequency of the wave. At C band (~5cm), the penetration depth is of the order of a few meters within the crown and the radar wave interacts with the upper part of the canopy, mainly with leaves and twigs. Consequently, C band is sensitive to crown characteristics like the number density, size, permittivity and orientation of leaves, but

also to canopy structure, including crown architecture (leaves and branches) and canopy heterogeneity and backscatter at co-polarisations show high sensitivity to increasing biomass (Lucas *et al*., 2002) i.e. as leaf biomass increases, σ^o usually saturates rapidly. This is the case for HV polarization which results from multiple scattering between crown components. In contrast, HH and VV polarizations behave differently and continue to increase up to a biomass higher than the expected saturation threshold. This increase in σ^o may be related to variations in the canopy structure, which dramatically changes between the very homogeneous pioneer stage and the more heterogeneous mature stage. Overall, at C band, the best correlations with canopy parameters are obtained with VV polarization (Mougin, 1999). In contrast, at L band (~24cm), penetration into the canopy is deeper and may involve scattering from the trunks and ground surface. At this frequency there is high correlation between HV polarisation and some forest parameters (basal area, height, biomass). Finally, P-band penetration reaches the underlying water surface particularly in the pioneer stages, and polarisation differences are a direct result of the surface scattering and double-bounce effects. Mougin *et al*. (1999) reported experimental observations on the relations between mangrove parameters and backscattering coefficients for all frequencies. Results showed that, there is a positive relation between $\sigma 0$ and total biomass, with the largest sensitivity to biomass found at P-HV and L-HV.

There are several aspects of mangrove forest classification using remotely sensed data. The objectives of the study differ according to what can be expected from the different types of remote sensing data. Here an attempt was taken to classify and characterize mangrove forest depending on community, density and height of the wood using optical and SAR data. Though determination of mangrove height using remote sensing data is not a common approach, but during this study an attempt was taken with the support of strong ground survey data.

CHAPTER 6. *Study of mangrove Above-ground biomass and radar backscatter*

6.1 Introduction

Extension of optical remote sensing techniques to much larger, i.e., continental, scale can be frustrated by the inherent limitation of cloud.

The question of retrieving forest biomass from SAR data has been subject of numerous research works since the early 1990s. The first results using AIRSAR data showed that it was possible to invert P band SAR data into biomass maps. Using the currently available spaceborne SAR data, namely ERS, JERS and RADARSAT, ENVISAT, the biomass retrieval appears limited in terms of biomass range and, in certain cases, site specific.

To provide an overview on issues related to forest biomass retrieval, this paper will present a survey of the possibilities and limitations of SAR data at different frequencies, polarizations and incidence angles. First the definition of biomass and biomass parameters (age, height, stem volume, dbh) will be addressed, and the information requirements in forest management and in global environment studies for biomass information will be discussed.

6.2. Objective of the study

The main objective of this study is - Observing radar interactions with the mangrove community and also extracting information on mangrove biomass and other forest stand parameters from radar backscatter

6.3. Biomass Parameters

Measurements of biomass and related forest parameters (age class, height, basal area) are of prime importance in forestry applications and in environment and climate studies. However, the type of measurements and their required scale and accuracy differ in these applications. Forest management operations such as timber exploitation, forest thinning, aforestation monitoring requires quantitative, accurate information at a local level, on the timber volume and growth. At the regional level (or country level), requirements are mainly related to the mapping of forest resources and the identification of forest changes relevant to a forest resource inventory. In global environment and climate studies, biomass is a key variable in annual and long-term changes in the terrestrial carbon cycle, and needed in modeling carbon uptake and redistribution within the ecosystems. The amount and distribution of biomass over the earth's surface is one of the major uncertainties in our ability to understand the global carbon cycle. In forest resource

inventory and management the following main biomass and structural forest parameters are addressed: Timber volume, stem volume, DBH, mean height.

In forest management practices, biomass parameters are estimated in the following steps: sample plots or transects are selected in a forest region, for example plots of 0.5 ha or transects of 10x100 m; inside the plot, the species composition is established, diameter and height of all living trees down to a certain limit (e.g. 12 cm) are measured. Then the timber volume or stem volume, expressed in cubic metres per hectare, are estimated for each tree using existing allometric equations established for each species and age. For global change studies, the parameter of interest is the above ground dry weight (biomass, expressed in tonnes per hectare), estimated also using allometric equations, and a wood density value, varying typically from 0.5 g/cm3 to 0.7 g/cm3.

It can be understood that uncertainties in in-situ biomass estimates can be very important. Also, differences between measurements and estimation methods may cause large discrepancies between estimates. For example, the limit of recorded diameters of stem and branches can vary from 5 cm to 12 cm depending on the standard used. Also, for a given forest, discrepancies between values using different allometric equations can be very large . In an example of secondary forest, the differences between biomass estimates have been found as large as 50% for a 18 year stand, up to 400% for younger stands (Alves, 1997). In monospecific forests, the uncertainties are reduced. 20% is the figure generally given in biomass estimates for forest plantations.

Also, above all, biomass measurements on the ground are very time consuming, labor-intensive and often constrained by lack of access.

6.4 Radar remote sensing and forest Biomass

For the above reasons, the perspectives of using remote sensing techniques to estimate forest biomass presented an important interest. Remote sensing data available at different scales, from local to global, and from various sources, from optical to microwave, are expected to provide information that could be related indirectly, and in different manners, to biomass information. Numerous studies have demonstrated that approaches using optical remote sensing data do not work for most terrestrial biomass densities. In areas of low biomass, the NDVI has been used to derive LAI and biomass value. However, the relationship depends on the soil reflectance and NDVI saturates when the canopy reaches full coverage. Similar results have been obtained with mid-infrared channels. With their longer wavelength, microwaves are expected to penetrate into the canopy, to interact with different components of the trees, and to provide information about biomass up to a

higher saturation level compared to optical systems. The relationships between microwave backscatter and total above ground biomass have been studied extensively.

Experimental results have been obtained since early 1990's at different forest sites (Le Toan et. al., 1992, Dobson et al., 1992, Imhoff et al., 1995). The data were collected using multifrequency polarimetric SAR systems such as the AIRSAR and the Shuttle Imaging Radar SIR-C/X-SAR. These studies all showed that 1) biomass dependence of radar backscatter varies as a function of radar wavelength, polarization and incidence angle. Longer wavelength is the most sensitive, cross polarization HV is more sensitive than like polarizations HH and VV, 2) the sensitivity of radar backscatter intensity to variations of biomass saturates after a certain level of biomass is reached. The saturation level is higher for longer wavelengths. It was found that for C band HH or VV, the saturation is reached at 30 t/ha, whereas at P band HV, biomass as high as 200t/ha can be reached. More recently, ERS interferometric coherence has also been analyzed as a function of forest biomass. The coherence decreases as a function of forest biomass and saturates also at low biomass.

According to these results, the currently available space borne systems ERS, RADARSAT, operating at C band, HH or VV are not the most adapted to biomass retrieval. JERS 1, operated until October 1998 at L band HH, provided slightly better sensitivity and higher saturation point. Despite their limitations, the C-band SAR systems are and will be providing data on a regular basis with ERS, RADARSAT and ENVISAT ASAR. In terms of biomass retrieval, the possibilities of using the available data to get a low / high biomass class discrimination, or to go further and have more than one class in the low range of biomass, could be an advantage compared to optical systems, but only if the methods prove to be more robust, since both systems are sensitive only to biomass in a limited biomass range. The question to be addressed at present is to know how the radar measurements from ERS, RADARSAT, ENVISAT ASAR, and to a lesser extent JERS-1, are related to biomass parameters in different forests, and what is the possibility of inversion. An alternative to the use of existing space borne optical and radar remote sensing methods is to prospect other sensor types, either airborne systems which will be used as complementary to space borne operations, or new concepts which need to be considered for future space borne systems. Among the future systems that will be implemented in space in the next few years, polarimetric SAR at L band presents the best system for biomass retrieval, as shown by results obtained with SIR-C/X-SAR. Research and technical investigations aiming at developing a space borne P- band SAR are underway. Single pass interferometry, as in X-SAR/SRTM will be an alternative to have the information on the canopy height, in areas where precise DEM is available. From there, biomass information could be derived. High resolution airborne systems can be

developed to complement the spaceborne systems. Using a VHF airborne system, recent results demonstrated that the SAR intensity is still sensitive to biomass up to 300 tons/ha.

6.5 Envisat and forest Biomass.

RADARSAT provides data at different incidence angles. ENVISAT ASAR will have in addition the polarization diversity. For different incidence angles, the bare soil, when the surface is smooth in terms of the wavelength, will have a large angular variation of its backscatter compared to the canopy. In general, this will result in a reduced sensitivity of the signal with biomass for increasing incidence. The sensitivity to biomass is then higher at low incidence angles for RADARSAT and ENVISAT.

The two like polarizations of ENVISAT are not expected to bring additional information. It is not the case of the cross-polarization, where the backscatter results only from the canopy volume scattering, the ground surface contribution being negligible. The relationship with biomass can be expressed by the increase of the canopy backscatter with the increasing biomass. Thus, cross polarization is expected to provide more generalized direct - then inverse – relationships with biomass compared to like polarization.

For higher values of biomass, the signal saturates. To explain the signal saturation, the canopy may be assumed to be a homogenous medium with a single category of scatterers (here, needles). In the high biomass case, the attenuation of the incoming wave is important enough to cause the soil contribution to be negligible. In this case, the backscattering coefficient is found independent of the number of scatterers. The saturation level depends only on the distribution in size, orientation, and dielectric constant of the scatterers. As an example, the saturation level observed with SIR-C at C-band, 54°, HH is -11.5 dB and -13.5 dB for respectively Pinus Pinaster (maritime pine), and Pinus Nigra (corsican pine) for the Landes and the Lozère forest. The observations could be interpreted using the theoretical curve of backscattering coefficient at C-HH- 55° versus the cylinder radius of the main scatterer, of an homogeneous medium formed by cylindric needles with an uniform orientation distribution between 0 and 2p. The effective cylinder radius of the needles of pinus pinaster is actually larger than the needle radius of pinus nigra.

6.6. Site characteristics and Data Acquisition

6.6.1. Acquisition of ENVISAT ASAR Radar data.

Mangrove forest site of Lothian Island, belonging to Indian Sundarban region was imaged by the ENVISAT ASAR instrument on 26th June 2004 and 22nd May 2004. Full-polarimetric data were acquired at C- (5.3 GHz) band only at a incidence angle of 19.2° to 26.7° range. The data was in image mode. DN value of the raw image was the

amplitude value. From the data, the backscattering coefficients ó°HH, ó°VV and ó°HV (expressed in decibels, dB) were calculated using a model developed in ERDAS model maker tool. A detailed description of ENVISAT ASAR data is given in chapter – 4.

6.6.2. Characteristics of the study site.

The study site (21° 36′ 30″ N to 21° 42′ 30″ N and 88° 18′ 00″E to 88° 21′ 00″E) is located along the Saptamukhi estuarine region of Hoogly River at the confluence of saptamukhi and Bay of Bengal. The topography of the area is nearly flat, dissected with numerous tidal creeks. This site was mainly dominated by Avicennis species. For studying different biophysical parameters 19 sites of different mangrove communities were selected. At all of these sites the biophysical parameters like species composition, tree density, tree height and tree DBH were measured from 10*10 m plots.

6.7. Field data collection and analysis

Measurements were focused on 19 sites of different species composition. All the measurement sites are decided from the forest community map, prepared from the LISS III, 2004 and LISS IV, 2005 data in the previous study. Measurements related to forest structure and biomass like, species composition, Density, CBH, Tree height is collected from all the 19 plots of 10*10 m dimension. Measurements of all the 19 sites are given in the Table: 6-1.

6.7.1 Estimation of Mangrove Above Ground Biomass

Many workers have studied the structure and productivity of mangrove ecosystem, both in tropical and sub-tropical regions of the world (Tam et al. 1995: Steinke et al. 1995: Mackey :1993: Fromard et al: 1998 etc). A few studies on biomass productivity and utilization are confined to Sundarbans (Chakrabarti 1987, Roy Choudhuri 1991). Particularly there is no study on the community and biomass of the mangrove forest in this region. For this study the total above ground biomass is estimated from the tree volume formula used by Hema Joshi and Monoranjan Ghose, 2002.they used the two formula – one for herbs and small tress (Height ≤ 3.9 m)

Volume = $(\pi D^2/4).h$

Other for large trees (> 3.9m) – Volume = $(\pi D^2/12).h^3 / (h-b)^2$ where D = diameter (m) at 1.3m or half the height of the plant, b= 1.3m and h= height of the plant. Tree volume was then multiplied with the wood density of the different plants to calculate total biomass. For estimation of wood density, 10 to 25 wood sample from the individual trees of each species, approximately 30 cm long and 2.5 to 3.5cm diameter were cut and fresh and dry weight(oven dried at 105º till they attain constant weight) were taken. For herbaceous

Acanthus illicifolius, sample of whole plants were collected and diameter, length and fresh and dry weight was recorded. Dry weight value was calculated for each species separately in different sites. For different stands, the estimated biomass values, expressed in kg/100 m2, are given in Table: 6-1.

Moreover partitioned biomass only for Avicennia species were derieved form allometric relationships, developed from the data on Sundarban mangrove biomass study by Chakrabarti 1987, Roy Choudhuri 1991. The relationship between tree DBH (cm) and leaf, trunk, twigs and branches are shown below -

Trunk biomass = $1.9166*e^{0.0759*DBH}$ ($r^2 = 0.5357$)

Branch biomass = $0.0233*e^{0.3169*DBH}$ ($r^2 = 0.6042$)

Leaf biomass = $0.2513e^{0.1044*DBH}$ ($r^2 = 0.1044$)

All the mangrove stands are modeled as two-layered forest – the topmost canopy layer of m thick and the below canopy layer of m thick. Some stands are of three layered having the lowermost under story. In most of the stands the tree species are dominated by the *Avicennia alba, Avicennia marina, and Avicennia officinalis.* The conopy layer is composed of leaf and brunches of Avicennia species and the below canopy layer is composed of mainly trunk and understory of species like *Acanthus ilicifolius Linn, Aegialitis rotundifolia Roxb. Fl, Ceriops decandra (Griff.) Ding Hou, Excoecaria agallocha L* etc. the partitioned biomass of tow layers for all the stands are given the Table : 6-2.

Table 6-1 Estimated (Field measurements) Total Above ground Biomass and Total Basal area of different plots.

PLOT Nos	Dist form the north coast (m)	no of sps	total no of trees	COMMUNITY TYPE	Total Dry wt (kg/100 m^2)	total basal area (m^2/ha)
25	641.58	2	11	AVICENNIA DOMINATED (no acanthus)	77.088	11.95
16	1248.00	2	13	AVICENNIA DOMINATED (no acanthus)	91.243	15.01
14	1261.16	2	15	AVICENNIA DOMINATED (no acanthus)	107.784	15.81
17	1284.13	2	45	AVICENNIA DOMINATED (no acanthus)	76.630	10.88
15	1308.67	2	34	AVICENNIA DOMINATED (no acanthus)	131.501	11.91
3	1868.17	3	36	AVICENNIA DOMINATED (no acanthus)	60.555	9.65
1	2011.08	3	59	AVICENNIA DOMINATED (no acanthus)	107.957	18.36
45	36.00	2	211	AVICENNIA DOMINATED (with acanthus)	70.336	10.3
44	64.62	2	198	AVICENNIA DOMINATED (with acanthus)	104.326	16.07
47	387.22	3	242	AVICENNIA DOMINATED (with acanthus)	171.199	23.34
46	516.03	2	178	AVICENNIA DOMINATED (with acanthus)	153.537	22.58
19	617.74	2	739	AEGIALITIS DOMINATED	121.861	10.95
26	1754.98	3	79	AEGIALITIS DOMINATED	72.571	11.37
1	3023.08	3	20	AEGIALITIS DOMINATED	238.835	19.68
30	3087.44	4	109	AEGIALITIS DOMINATED	257.502	21.31
29	3192.89	3	65	AEGIALITIS DOMINATED	41.033	6.164
48	3218.87	3	96	CERIOPS DOMINATED	39.588	4.34
20	3274.62	5	95	CERIOPS DOMINATED	110.524	8.61
49	3507.46	3	80	CERIOPS DOMINATED	187.709	10.87

Table 6-2 Partitioned Above ground Biomass of different stands.

PLOT Nos	COMMUNITY TYPE	Total biomass at canopy layer (kg/100 m^2)	Total biomass at below canopy layer (kg/100 m^2)	Total Dry wt (kg/100 m^2)
25	AVICENNIA DOMINATED (no acanthus)	25.97	51.12	77.088
16	AVICENNIA DOMINATED (no acanthus)	28.74	62.50	91.243
14	AVICENNIA DOMINATED (no acanthus)	39.01	68.77	107.784
17	AVICENNIA DOMINATED (no acanthus)	22.81	53.82	76.630
15	AVICENNIA DOMINATED (no acanthus)	26.71	104.79	131.501
3	AVICENNIA DOMINATED (no acanthus)	15.48	45.08	60.555
1	AVICENNIA DOMINATED (no acanthus)	25.54	82.42	107.957
45	AVICENNIA DOMINATED (with acanthus)	15.39	54.95	70.336
44	AVICENNIA DOMINATED (with acanthus)	30.43	73.90	104.326
47	AVICENNIA DOMINATED (with acanthus)	43.03	128.17	171.199
46	AVICENNIA DOMINATED (with acanthus)	37.22	116.32	153.537
19	AEGIALITIS DOMINATED	18.61	103.25	121.861
26	AEGIALITIS DOMINATED	22.81	49.76	72.571
1	AEGIALITIS DOMINATED	16.08	222.75	238.835
30	AEGIALITIS DOMINATED	16.77	240.73	257.502
29	AEGIALITIS DOMINATED	9.24	31.80	41.033
48	CERIOPS DOMINATED	4.68	34.91	39.588
20	CERIOPS DOMINATED	5.31	105.21	110.524
49	CERIOPS DOMINATED	0.00	187.71	187.709

6.8 Estimation of Radar Backscatter

To perform a precise absolute image calibration and derive the radar backscattering coefficient for detected ground range products a detailed knowledge of the local slope (i.e. local incident angle) is required. Since this information is usually not available "flat terrain" is assumed during processing (based on the ellipsoid WGS84) and the final intensity image is therefore proportional to the radar brightness of the illuminated scene.

The relationship between the value of the image pixels ("DN") the radar brightness ($\beta°$)and the radar backscattering coefficient (σ°) can be written as ----

DN^2 = constant. $\beta°$ = constant. σ° / sin (α) = constant (α). σ°

The constant factor is hereafter referred as "absolute calibration constant" (K) – which is derived in the ASAR case from measurements over precision transponders. This factor is processor and product type dependent and might change between different beams for same product type. The constant (α) term is equal to the absolute calibration constant divided by the sine of the local incidence angle α.

Calibrated sigma nought (σ°) and gamma images for detected product was derived as:

$$\sigma^{\circ}_{i,j} = \frac{DN^2_{i,j}}{K} Sin(\alpha_{i,j}) \qquad \gamma_{i,j} = \frac{\sigma^{\circ}_{i,j}}{cos(\alpha_{i,j})}$$

$$for\ i = 1.....L\ and\ j = 1.....M$$

where

K = absolute calibration constant

$DN^2_{i,j}$ = Pixel intensity value at image line and column "*i,j*"

$\sigma^{\circ}_{i,j}$ = Sigma nought at image line and column "*i,j*"

$\alpha_{i,j}$ = Incidence angle at image line and column "*i,j*"

$\gamma_{i,j}$ = Gamma at image line and column "*i,j*"

Finally to convert sigma nought to dB:

$$\sigma^{\circ}[dB] = 10.\log_{10}(\sigma^{\circ})$$

Raw data of the ENVISAT, ASAR precision image was imported by the ENVI image processing software. This raw image is basically the intensity image. From the intensity image the following quantities were calculated for C (3.8 – 7.5 cm) frequency: the backscatter coefficient - $\sigma°_{VV,}$ $\sigma°_{HH}$, $\sigma°_{HV}$ (for VV, HH and HV polarization respectively). A backscattering model was developed in ERDAS module maker environment to prepare the Backscattering images of all the three polarization from the intensity value. Backscattering images of all three polarizations are shown in Figure: 6-1.

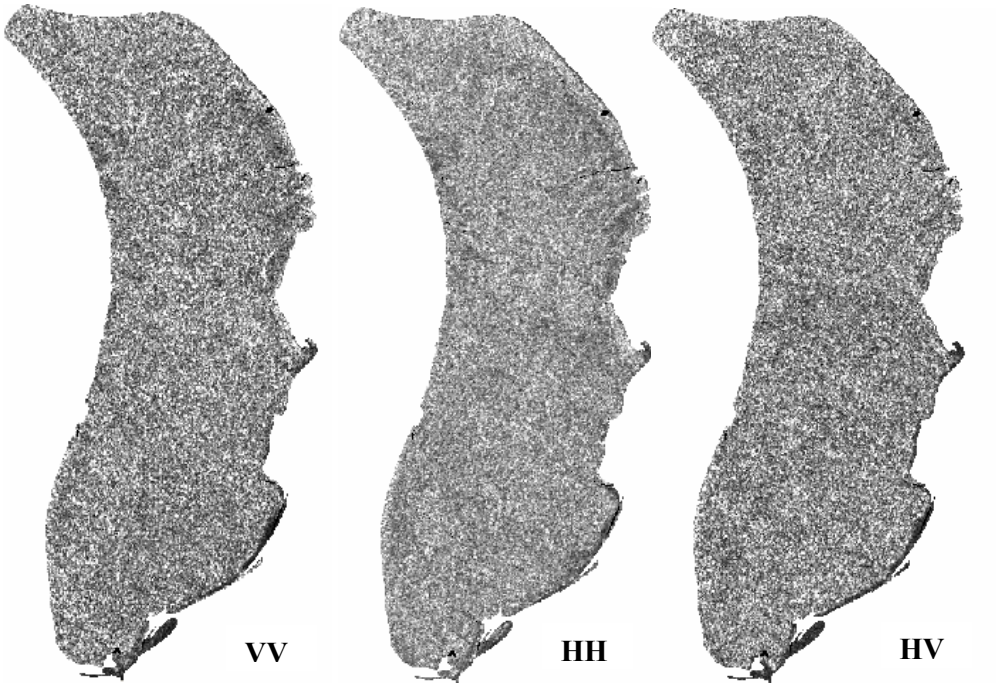

Figure 6-1 ENVISAT ASAR Backscattering images of different Polrization (VV, HH. HV) of the Lothian Island, Sundarban.

6.9 Polarimetric Radar response versus Mangrove Biomass

The calculated backscatter coefficients - σ°_{VV}, σ°_{HH}, σ°_{HV} were extracted from the backscattering images of respective polarization for the all plot locations. It was then compared with the total biomass of all the plots. Fig : shows the observed variation of the backscattering coefficient versus total biomass at C – band only. A logarithmic law was used to describe the overall behavior of the 19 closed canopies.

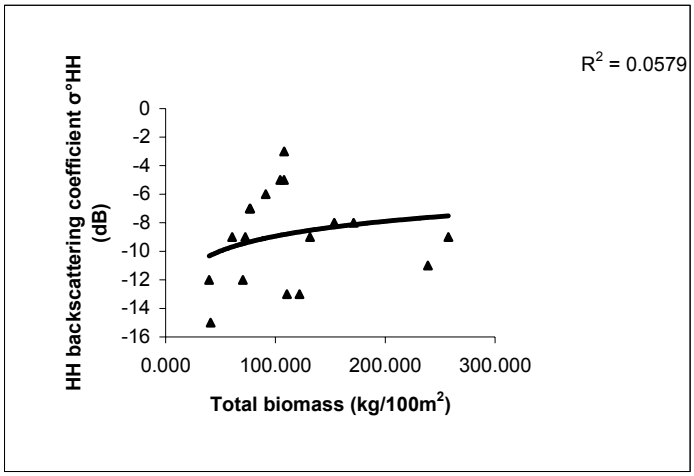

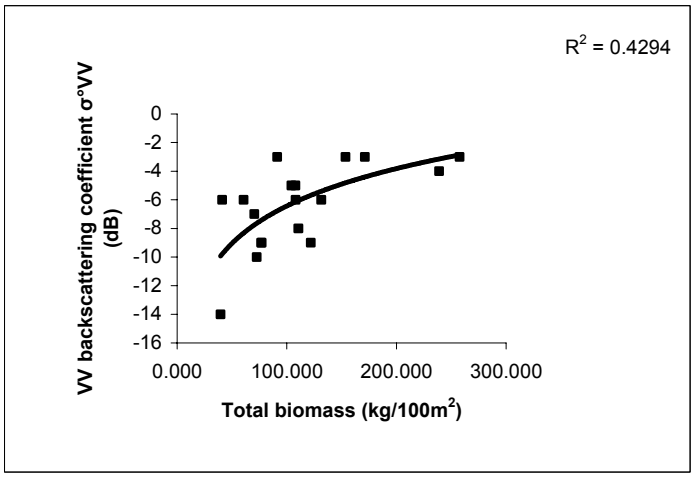

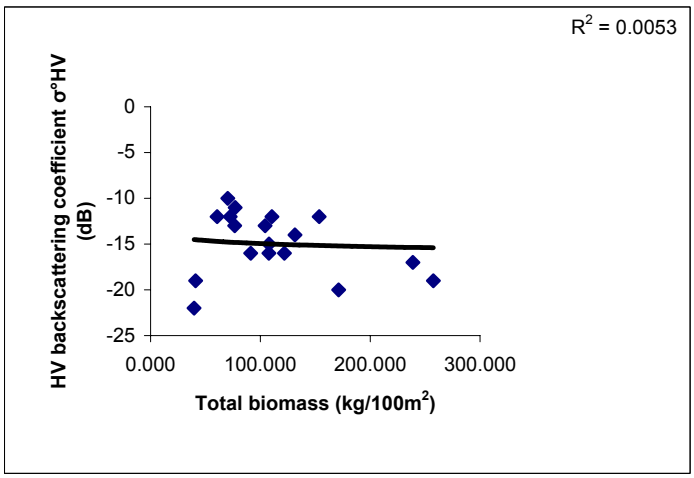

Figure 6-2 Measured Backscattering coefficient of different polarization (HH, VV, HV) versus total above ground Biomass.

Variation of Backscattering coefficients was also observed against the partitioned biomass of all the stands. It is shown in the Figure: 6-3 & 6-4.

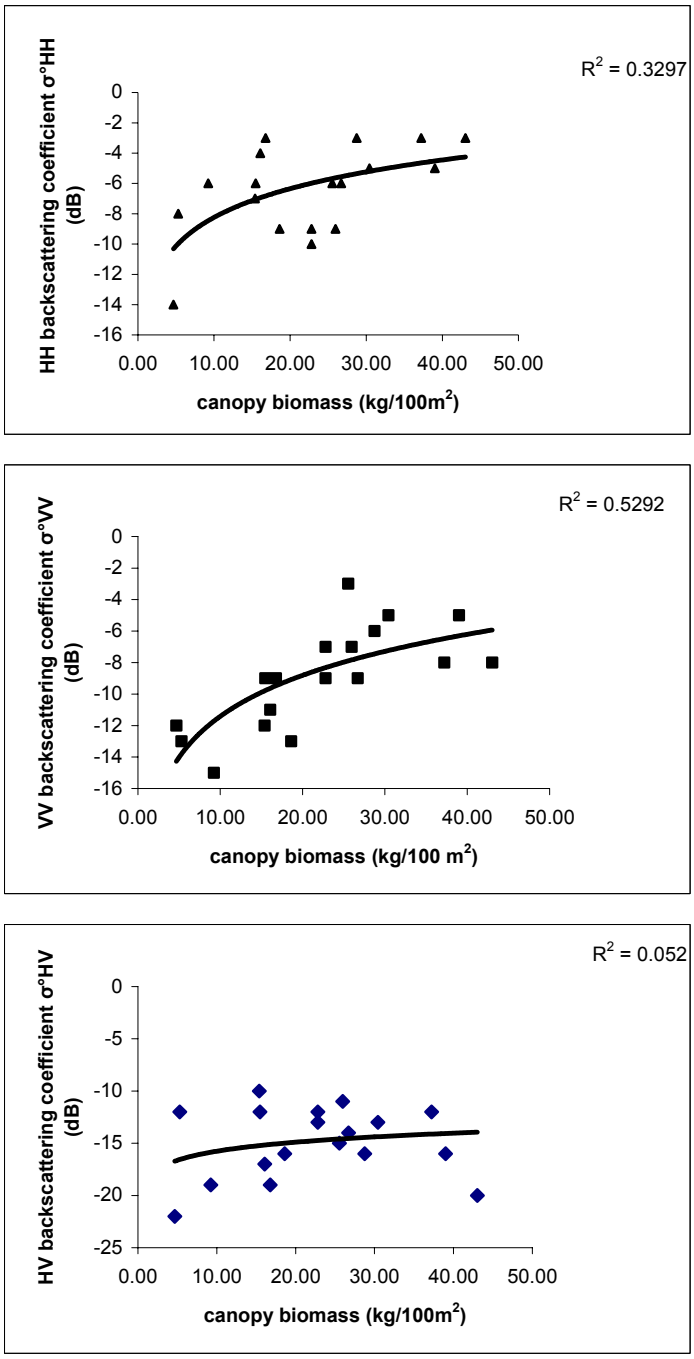

Figure 6-3 Measured Backscattering coefficient of different polarization (HH, VV, HV) versus total above ground Canopy Biomass.

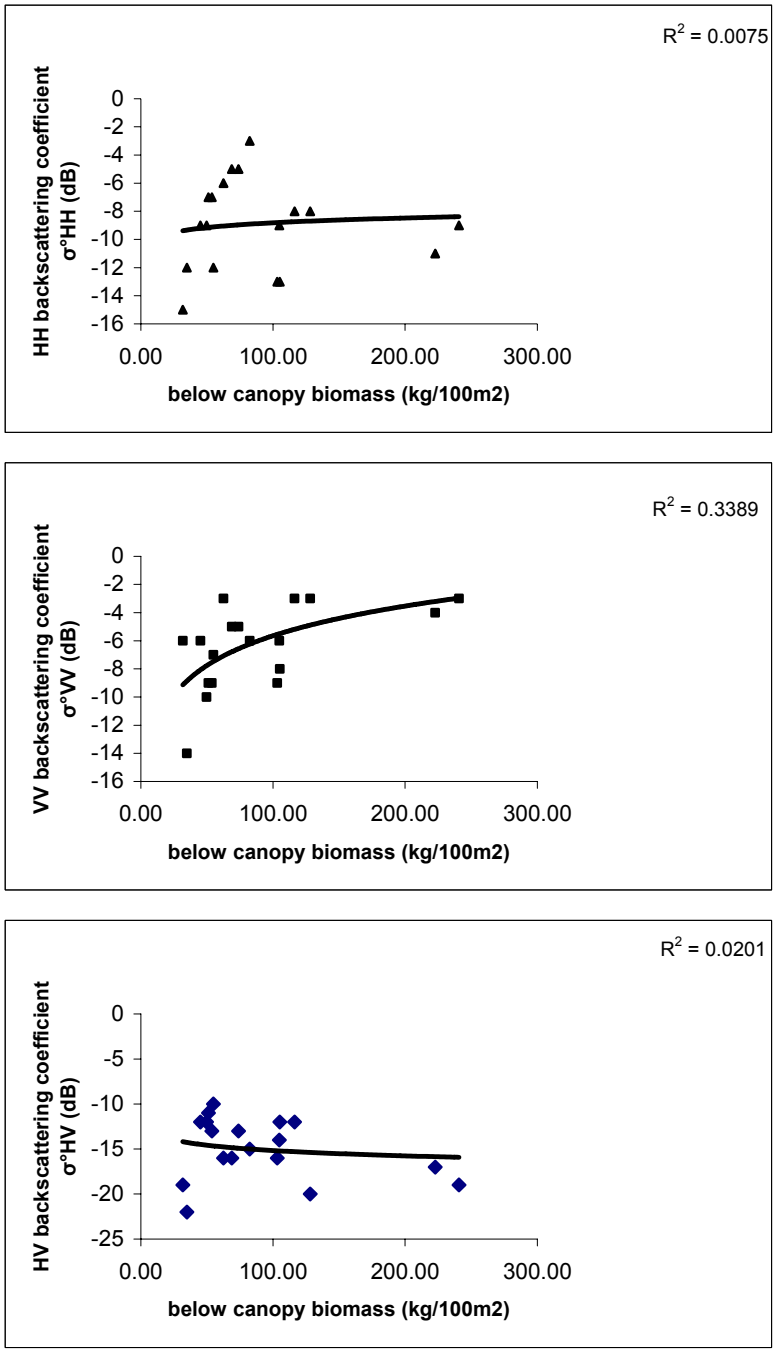

Figure 6-4 Measured Backscattering coefficient of different polarization (HH, VV, HV) versus total Above ground Below canopy Biomass.

6.9 Polarimetric radar response versus other stand parameters

The variation of same backscattering coefficients is again observed against the total basal area of each stands. Figure: 6-5 shows the correlation between backscattering coefficients and total basal area.

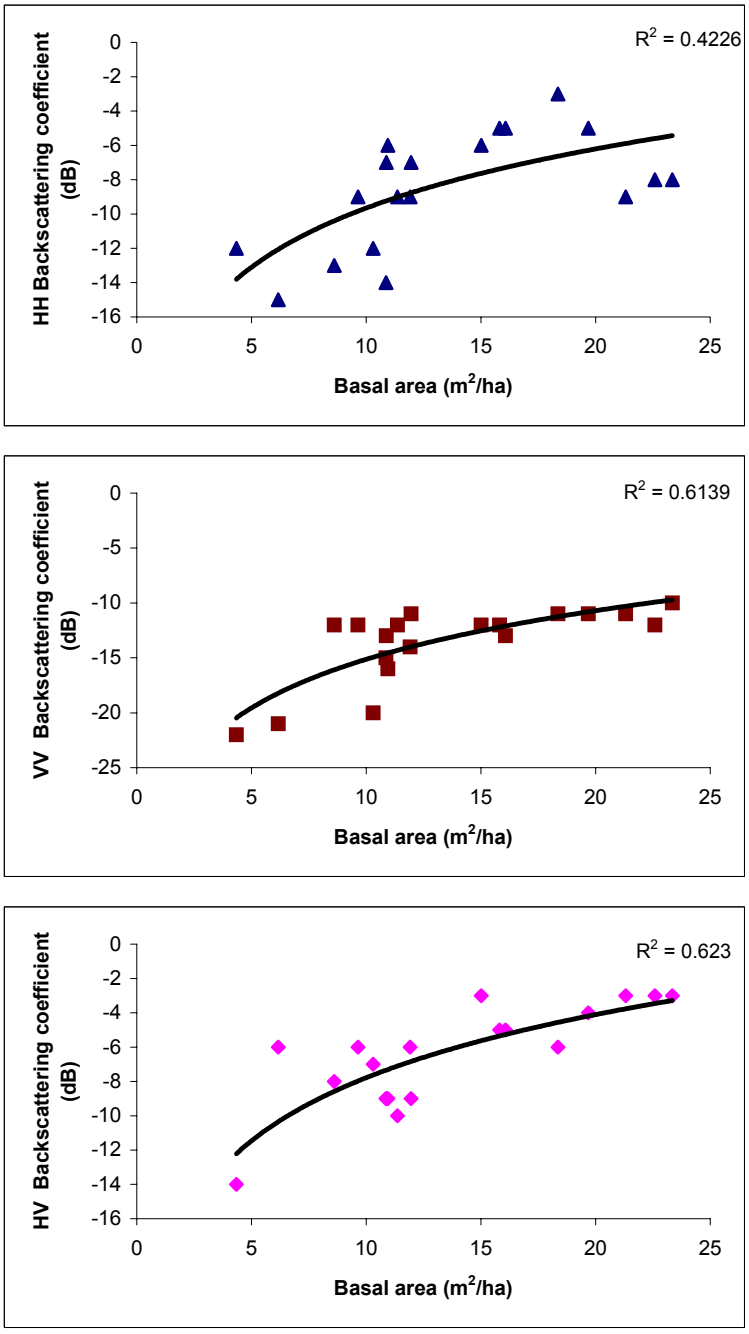

Figure 6-5 Measured Backscattering coefficient of different polarization (HH, VV, HV) versus total Basal area.

From the above study it has been found that degree of correlation between Backscattering coefficient and Total Basal area gradually increases from HH to HV polarization. HV polarization has highest correlation with total Basal area ($r^2 = 0.623$).

6.10. Exclusive conclusion and Recommendations

The capability of microwave energy to penetrate forest vegetation makes possible the extraction of information on both the foliar and woody components from radar data. Depth of penetration, and hence the type of derivable information, is dependent upon parameters relating to both the radar sensor and the target such as the wavelength, polarization and incidence angle used, as well as the geometric and dielectric properties of the target vegetation.

At C-band, the backscattered energy is correlated mainly with the crown constituents such as the leaves, twigs and small branches. Information on the other components beneath the canopy can be sensed through the use of bands with longer wavelengths such as the L-or P-band. The sensitivity of co-polarized and cross-polarized waves to the shapes and orientation of the different tree constituents provide an added advantage in the information extraction procedure.

The recent study shows the following linear correlation of Determination r^2 (Table: 6-3) between the Logarithm of partitioned biomass and Radar backscattering coefficient σ°(dB).

Table 6-3 Correlation coefficients (r^2) between the Logarithms of partitioned above ground biomass and Backscattering coefficient at different polarizations.

	Below canopy Biomass ($kg/100m^2$)	**Total Biomass ($kg/100m^2$)**	**canopy Biomass ($kg/100m^2$)**
C-VV	0.338	0.429	0.5292
C-HH	0.007	0.057	0.3297
C-HV	0.02	0.005	0.052

Note: for each forest parameters, the highest correlation is indicated with boldface characters.

It has been found from the above study that the level of correlation between polarized radar backscattering coefficient of C band wavelength and partitioned biomass of the mangrove forest gradually increases from below canopy biomass to canopy biomass for all the polarization. Again C-VV polarization shows the highest correlation for the all the partitioned biomass.

Backscatter at co-polarizations show high sensitivity to increasing biomass (Lucas *et al*., 2002). In case for HV polarization, which results from multiple scattering between crown components, as leaf biomass increases, σ^o usually saturates rapidly. In contrast, HH and VV polarizations behave differently and continue to increase up to a biomass higher than the expected saturation threshold. Overall, at C band, the best correlations with canopy parameters are obtained with VV polarization. The same observation was also reported by Mougin *et al*. (1999).

Given the relatively greater degree of penetration by horizontally polarized waves and the strong interaction of the vertically polarized energy with the vertically oriented canopy parts, different wavelength-polarization combinations can be used to suit the purpose of the study.

CHAPTER 7.

Effect of soil salinity on Mangrove distribution – A Remote Sensing and GIS approach.

7.1. Introduction

An estimated 1.27 to 1.67 billion tonnes of sediments are carried annually by the river systems of the Ganges-Brahmaputra-Meghna basin (MPO, 1986; Milliman and Meade, 1983). Before being deposited near the sea mouth, the freshly available alluvium from upstream comes in contact with seawater and becomes salty. Thereafter, it becomes more saline by interacting with the seawater that comes along the high tides and through creeks. More salt deposition occurs when capillary action takes place in the sub-surface and topsoil zones, compounded with high evapotranspiration during winter. However, the severity decreases during the onset of monsoon due to the fact that rainwater dilutes the salinity.

Mangroves are woody plants, which grow in loose wet soils of brackish to saline estuaries and shorelines in the tropics and subtropics. In India only 8 % coastline is occupies by mangals (Saenger et al, 1983). Mangrove community often exhibit distinct pattern of species distribution (Chapman 1976; Lugo & Snedaker 1974; Macnae 1968, Tomlinsorn 1986). Waring & Major (1964) reported that a complex of environmental factors determines the actual distribution of plant in nature, although each plant has a certain tolerance for each factor. Since the mangrove habitat is basically saline, several studies have attempted to correlate salinity with the standing crop of vegetation and productivity (Chen & Twilley 1998, 1999; Lugo 1980; Mall et al. 1987; Ukpong 1991). Local pattern of tidal inundation further influences soil characteristics that control species zonation of mangrove wetlands (Banerjee 1987; Naidoo 1980; Saha & Choudhury 1995; Walsh 1974; Watson 1982). Based on frequency of tidal inundation, mangrove forests have been classifies into five types viz over wash, fringe, riverine basin and swarf forests (Ludo and Snedaker 1974). Patches and zones of forest composition result from comoplex gradients of hydroperiodand soil conditions such as nutrient limitation (Boto & Wellington 1984; Feller 1995; Ukpong 1998) and abiotic stressor as salinity and sulfide (Cintron et al. 1978; Lugo 1978; Mackee1993; Nickerson & Thibodeau 1985). The distribution of mangrove species, in many cases can be explained primarily by salinity gradients (Ball 1998; Ukpong 1994). The pH of the soil significantly affects plant growth, primarily due to the change in availability of both essential elements such as phosphorus (P), as well as non essential elements such as alluminium (Al) that can be toxic to plants at elevated concentrations (Black,1993); Slattery et al. 1999; Wood ruff 1967). The importance of

both soil salinity and pH for the growth of mangroves has been emphasized by Wakushima et al, (1994a, 1994b). Sudarban shelters one of the most important mangrove communities of the world. A few published works deal with the community structure of this forest (Joshi & Ghosh 2002; Matilal et al.1986; Saha & Choudhury 1995).

In this study a Remote sensing and GIS approach is carried out on structure and species distribution of mangrove in Lothian island of Sundarban in relation to Salinity of substratum. The aim of this study is to specify the location of individual mangrove species (mainly three species of *Avicennia – A. marina, A. alba and A. officinalis*) along the gradients of soil salinity.

7.2. Methodology

In this study a community zonation map of the Lothian island was first prepared from the IRS LIV satellite imagery, acquired on july, 2005. in this map Avicennia dominated forest was identified easily but the species level distribution of the Avicennia was not identified. Generally three Avicvennia species are found in this Island – A. marina, A. alba, A officinalis. This has been done to retrieve the distribution of these species within the Avicennia dominated community. There are combination of abiotic factors such as frequency and duration of inundation, water logging of substrate, porewater salinity, nutrient availability, soil redox potential and pore water sulfide concentrations (McKee and others, 1988) determine mangrove species distribution (Odum and others, 1982; Woodroffe, 1992). Other environmental factors that account for mangrove distribution are climate, soil composition, wave energy, topography, and sedimentation (Chapman, 1976; Odum and others, 1982; Woodroffe, 1992). In this scope of study only soil salinity gradient was taken in consideration to retrieve the species level distribution three Avicennia species. Through out the study duration of one year from January'2005 to December'2005 soil and vegetation data were collected from the field and they were then analysed to retrieve the relation between importance value index (IVI) and soil salinity of these concerned species. A soil salinity map was prepared by interpolation technique from the field data in GIS environment. IVI maps of the concerned species are prepared from the soil salinity map using the developed relation between them. Then using these IVI maps species priority map was prepared and finally distribution of the three Avicennia species were extracted from the community zonation map and priority maps. A flow chart is shown in the Figure:7-1 for better understanding of the methodology.

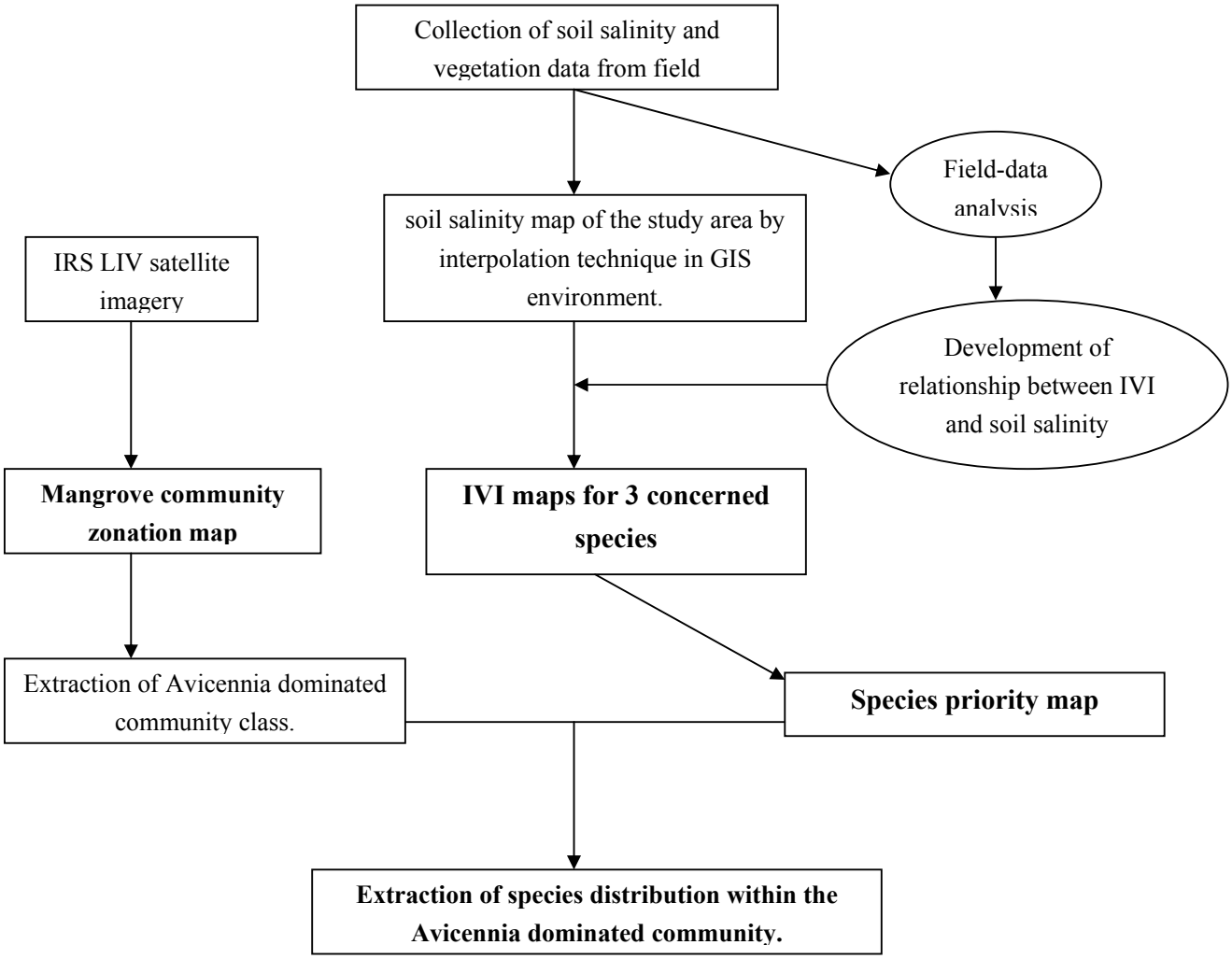

Figure 7-1 Methodology for extracting species distribution along the soil salinity gradient.

7.3. Vegetation and Soil sampling

vegetation was studied and soil samples were collected from 19 sites selected at different vegetation community. Sampling locations were designed with the help of community zonation maps, prepared from the IRS LIV satellite imagery. All the 19 sampling plots were 10*10 m^2 in dimension. In each 10*10 m quadrate, all the individual plants were identified and their number, diameter (at 1.3 m for trees and at half height for herbs and plants below 1.5m) and heights (using meter tape for short plants or setsquare technique) were recorded. The frequency of tidal inundation was also recorded in each site.

Three soil samples were collected from each site from a rooting depth of 15 cm in ploythene bags and brought to the laboratory. The soils were air-dried, crushed, using a pestle and mortar and then passed through a 10 mesh (2 nm) screen before analysis. The soil analysis was completed within two months after collection. pH was determined in 1:2.5 soil to water suspension using a pH meter (Jackson 1978). Electrical conductivity was determined in supernatant of 1:5 soil water mixture using a systronics conductivity meter and was converted into salinity (pH) following the equation:

Salinity (ppt) = 0.064 * EC*(% water in soil/100)*10 (where EC = Electrical conductivity (m mho cm^{-1}))

7.3. Mangrove Community-zonation using IRS P6 LISS VI data, 2005

7.3.1. Data used

For this study the following optical data have been used:

SATELLITE DATA:

OPTICAL DATA:

SATELLITE NAME - IRS P6.

Sensor Name	Path	Row	Date
LISS-IV	102	054	09.APR.05

OTHER DATA:

- ✓ TOPOGRAPHIC BASE MAP ON 1: 50,000 SCALE.
- ✓ MAPS OBTAINED FROM THE NATIONAL ATLAS AND THEMATIC MAPPING ORGANISATION (NATMO).
- ✓ MAPS PRESENT IN THE BOOK ENTITLED “COMMUNITY ZONATION OF SELECTED MANGROVE HABITATS OF INDIA USING SATELLITE DATA”, SAC, 2003.

7.3.2. Methodology for preparation of community zonation map from optical remote sensing data.

The different steps followed to prepare mangrove forest community zonation map is described in a flow chart below (Figure:7-2).

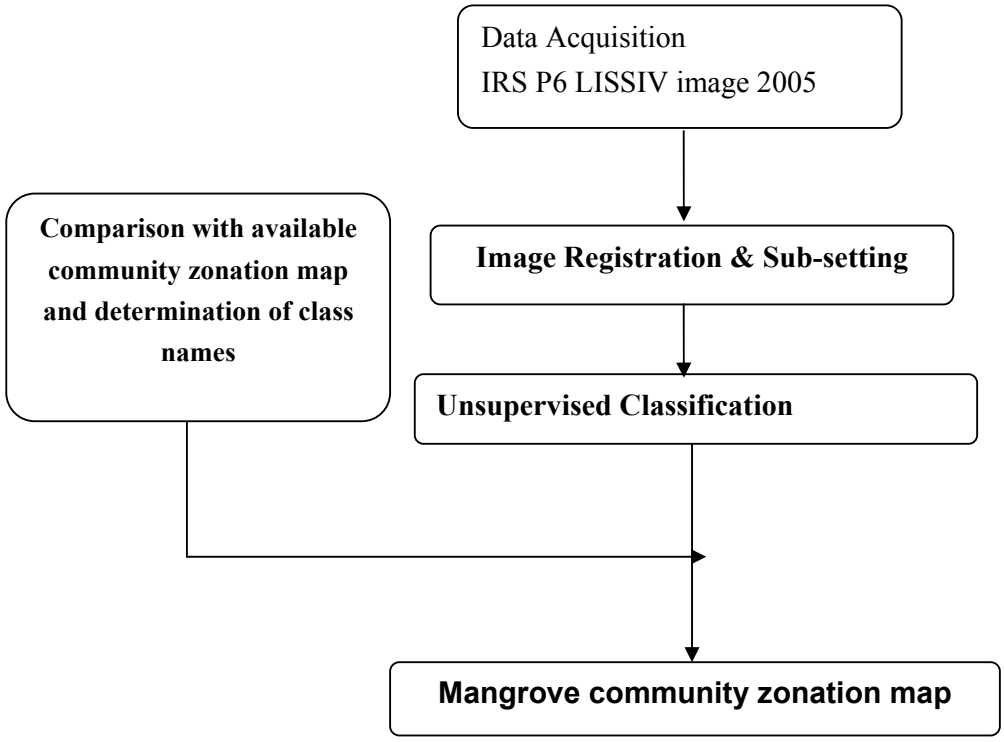

Figure 7-2 Flow chart showing steps for preparing community zonation map of the mangrove forest.

7.3.2.1. Georectification and subsetting of LIV data.

IRS P6 LISS IV data of the month of 9th April 2005 has been geo-referenced with the help of Geo-corrected data of P6 LISS III, 6th March, 2004. The polynomial order was kept First. The projection system is UTM with zone no. 45. Spheroid used is Everest and the datum is Indian Bangladesh. The root mean square error was 0.1481 of a pixel. The image has been resampled by nearest neighborhood method using pixel size 23.5m. Only Lothian Island has been sub set out from the whole image and classified taking help of the available community zonation map of Lothian Island (SAC, 2003).

7.3.2.2. Classification of data.

Unsupervised classification was applied to generate community map of Lothian Island. Merging of the clusters to actual community classes has been made based on the

community zonation map prepared by the previous workers (SAC, 2003). The out put map is shown in (Figure: 7-3.).

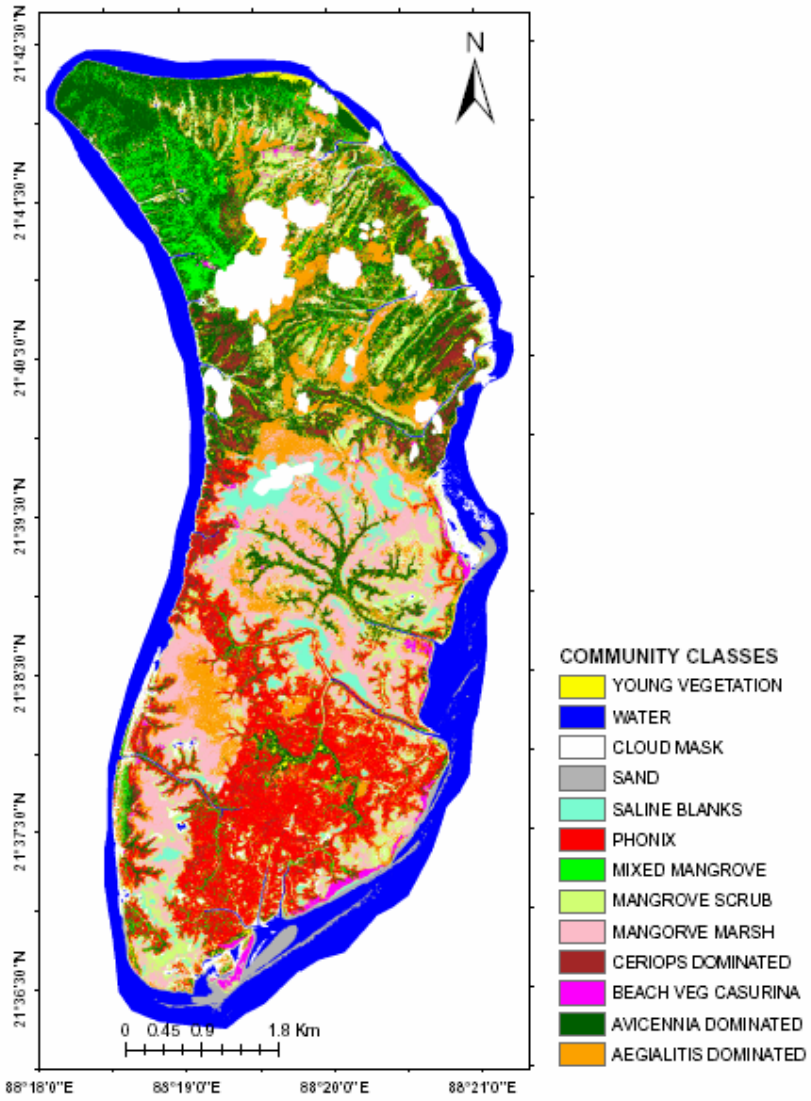

Figure 7-3 Community zonation map of Lothian Mangrove forest using IRS P6 LISS IV Data of April,2005

7.3.3. Accuracy Assessment

The output layer consists of 12 land Mangrove community classes. Classification accuracy assessment was performed by comparing the classified pixels with respect to

selective ground data or previous maps. For this purpose 128 well distributed user defined points were used.

Here, Error matrix has been created and figures for User's Accuracy, Producer's Accuracy, and Combined Accuracy (kappa statistic) have been compiled to evaluate the quality of each classification. User's Accuracy is a ratio statistic compiled by dividing the number of pixels correctly assigned to a category by the total number of pixels to the category. Producer's Accuracy has been calculated by dividing the number of accuracy pixels correctly assigned to a category by the number of accuracy pixels selected for that category. These two measures are useful in defining the type of classifications errors made and provide different perspectives of accuracy. Results showed lowest accuracy was obtained in the classification of Beach Vegetation (Casurina species) (54.55%), highest accuracy was obtained in classification of water, Phoenix(100.00%), Avicennia dominated forest, Aegialitis dominated forests and Sand (80.00%). For the other classes, estimated classification accuracy was in between (Table 7-1).

Table 7-1 Accuracy assessment table for Mangrove community Zonation, 2005 classification of Lothian Island.

CLASS NAME	REFERENCE TOTALS	CLASSIFIED TOTALS	NUMBER CORRECT	PRODUCERS ACCURACY	USERS ACCURACY
AVICENNIA DOMINATED	23	12	10	43.00%	83.33%
AEGIALITIS DOMINATED	12	10	8	66.67%	80.00%
MIXED MANGROVE	9	10	6	66.67%	60.00%
CERIOPS DOMINATED	7	10	7	100.00%	70.00%
MANGORVE MARSH	7	10	7	100.00%	70.00%
YOUNG MANGROVE VEGETATION	6	12	6	100.00%	50.00%
MANGROVE SCRUB	16	13	9	56.25 %	69.23%
BEACH VEGETAION (CASURIN SPECIES)	6	11	6	100.00%	54.55%
PHOENIX	15	10	10	66.67%	100.00%
SALINE BLANKS	9	10	7	77.78%	70.00%
SAND	8	10	8	100.00%	80.00%
WATER	10	10	10	100.00%	100.00%
Totals	128	128	94	73.44%	73.44%

Accuracy assessment - 128 user defined points were used, distributed throughout the layer.

Overall Classification Accuracy = 73.44%,

Overall Kappa Statistics (k^) = 0.7097

7.4. Analysis of Data

Differences in soil salinity among 19 sites were analysed by one-way ANOVA (SPSS 10) using data from three random samples of each site.

Various structural indices such as specific density (no.ha^{-1}) and IVI (importance value index) were calculated using the standard methodology (Cintron & Novelli 1984).

7.5. Preparation of soil salinity map at GIS environment.

for soil salinity mapping soil samples are collected randomly through the island in the GPS based field survey. The sample size is 50. All soil samples are analysed in laboratory for soil salinity. Then in GIS environment a vectorized point map of 50 locations whose salinity value are known, was prepared. Texture analysis of all the 50 soil samples is also done in the laboratory. It has been found by laboratory analysis the silt, clay and sand % of all the 50 samples are more or less same. So it can be conclude that the soil types of all the locations are same. From the soil type map of this island published in National Bureau of Soil Survey, Nagpur, it has been found that the whole Island more or less belongs to the same soil type except the southeren and south-western (‘Balir khal’ area) sandy region. The sandy area was identified in the community zonation map prepared from the IRS LIV’2005 satellite imagery. This sandy area is extracted from the community zonation map and excluded from the island boundary.

Soil salinity is generally controlled by frequency of tidal inundation. Naidoo & Rajman (1982) reported soil salinity to be related with extent of tidal inundation and seepage in the mangrove sils of sipingo and Mgendi,south Africa. The area, which is inundated by tidal water frequently, shows high salinity. The tidal water enters in to the island through the tidal creeks, which intersects the island into different fragments.

So the topography as well as tidal heights is the prime controller of soil salinity. As the flow of tidal water is responsible for soil salinity and a gradient of soil salinity was observed from low lying area to elevated area, so the magnitude of the soil salinity can be predicted for the un-sampled areas by using simple interpolation technique.

A IWD (Inverse weighted distance) method of interpolation was adopted in ARC GIS environment to interpolate the soil salinity from 50 known points with the areas of island having same soil type. Soil salinity value of 50 sample points were interpolated in the island boundary (excluding sandy area) to prepare a rasterized soil salinity map having same pixel size as IRS LIV imagery (6*6 m). The interpolated soil salinity map is shown in Figure: 7-3.

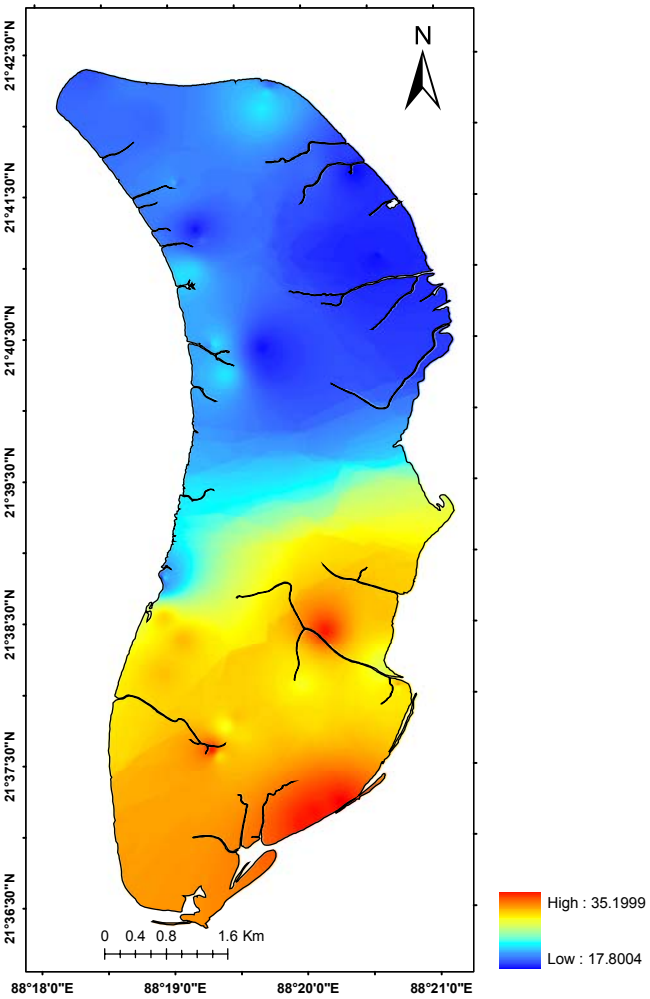

Figure 7-4 Soil Salinity map of the Lothian Island. (salinity unit is in ppt)

7.6. Preparation of IVI maps.

The importance of the contribution of each component species to thestand in terms of density, contribution to basal area (dominance) and probability of occurrence dthrough out the plot (frequency) are described by the following parameters:

$$\textit{Relative density} = \frac{\textit{no.of individuals of a species}}{\textit{Total of no.individual (all species)}} \textit{ X 100}$$

$$\textit{Relative frequency} = \frac{\textit{frequency of a species}}{\Sigma\textit{frequency of all species}} \textit{ X 100}$$

$$\textit{Relative dominance} = \frac{\textit{Total basal area of species}}{\textit{basal area of all species}} \textit{ X 100}$$

frequency is defined as the probability of finding the species in any one plot and can only be compared between plots of equal size.

The importance value (IVI) (curtis 1959) is the sum of the relative density, relative frequency and relative dominance.

IVI values of three Avicennia species – A. marina, A. alba and A. officinalis were calculated for all the 19 plots. IVI value for Avicennia marina species varies from 6.82 – 171.49, for Avicennia alba species from 0.25 to 96.94 and for Avicennia officinalis from 36.82 – 65.08.

A correlation analysis was done between IVI & soil salinity for all the Avicennia species separately. From the correlation analysis the following equations and correlation coefficient (r^2) values were obtained for 3 different Avicennia species. –

Avicennia marina – ($r^2 = 0.439$), (IVI = -12.484*salinity + 159.13)

Avicennia alba – ($r^2 = 0.602$), (IVI = 9.302*salinity + 1.4017)

Avicennia officinalis – ($r^2 = 0.741$),(IVI = 6.3561*(salinity)^2-25.893*(salinity)+64.542)

All of these equations were then used to create a map of IVI for three Avicennia species from the soil salinity map. IVI maps of different Avicennia species are shown in (Figure:7-5, 7-6 and 7-7).

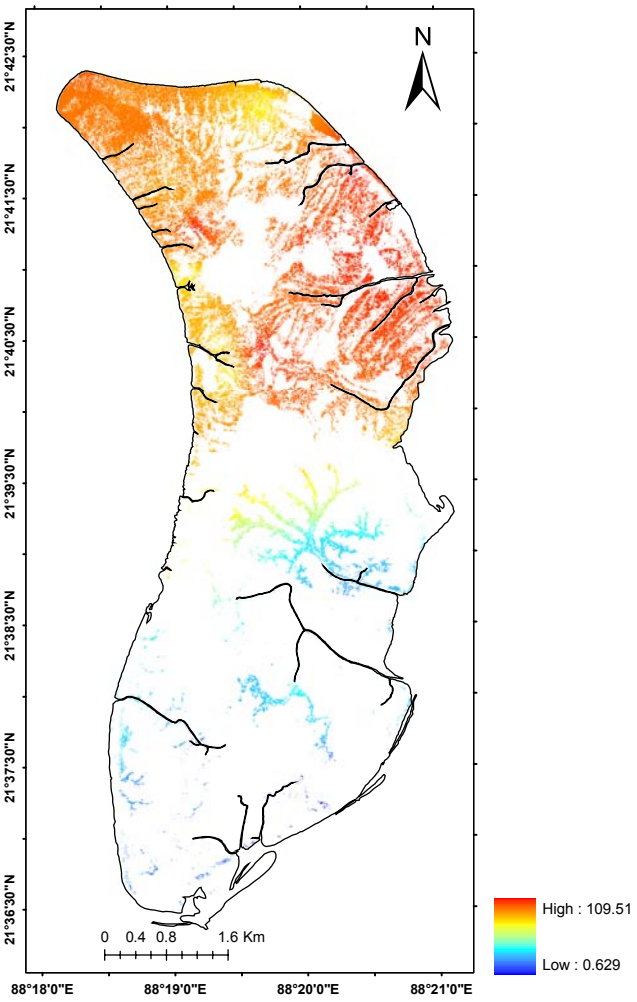

Figure 7-5 IVI map of Avicennia marina species

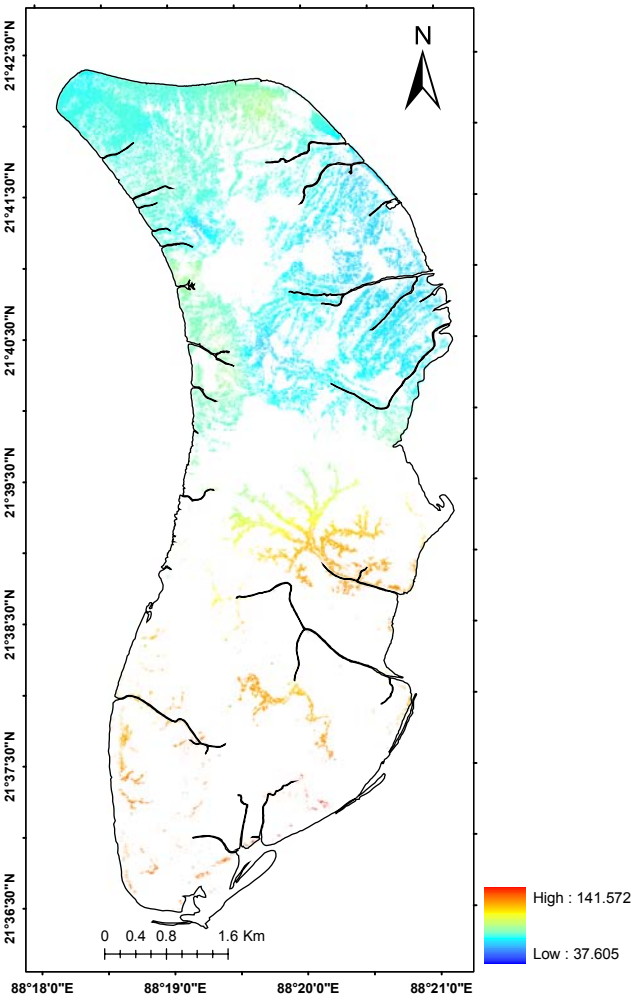

Figure 7-6 IVI map of Avicennia alba species.

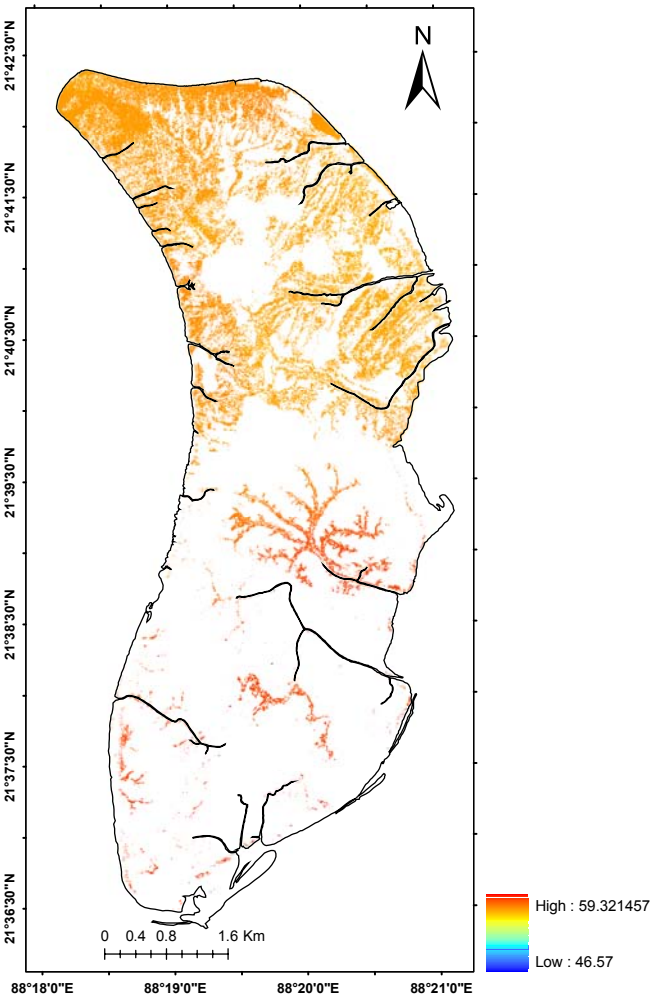

Figure 7-7 IVI map of Avicennia officinalis species.

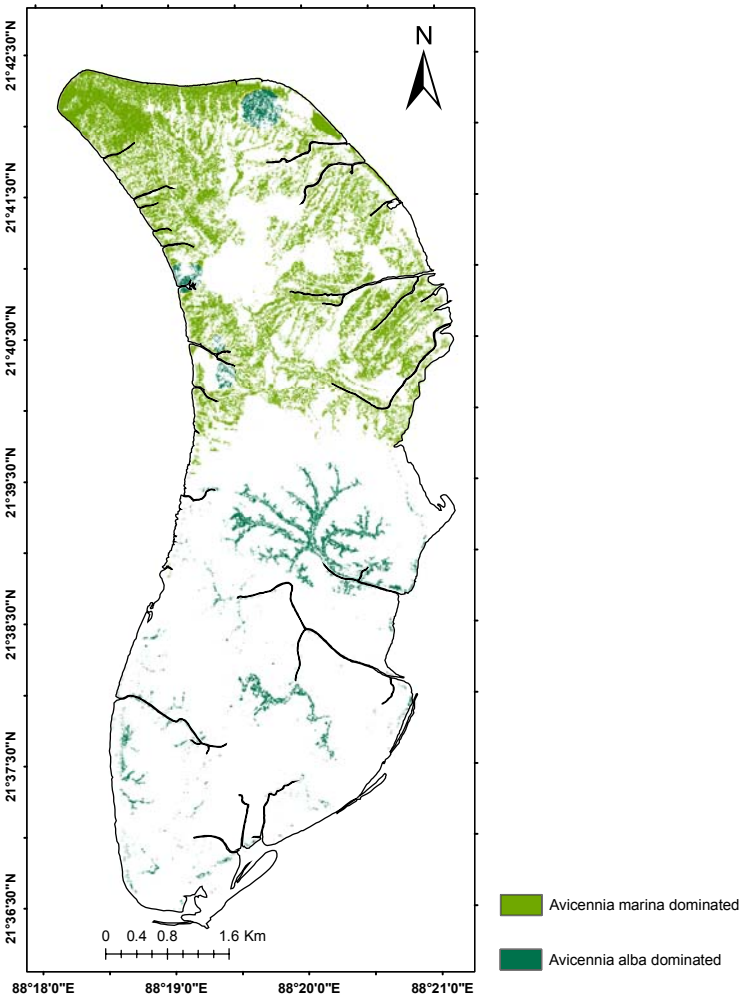

Figure 7-8 Distribution of two Avicennia species in the Avicennia dominated community

7.7. Extracting Species distribution within the Avicennia dominated community.

Avicennia dominated community class was extracted from community zonation map. IVI maps of all the three Avicennia species were subsetted to this Avicennia dominated community area. Then a spatial analysis was done between these subsetted IVI maps to retrieve the three Avicennia species distribution within this community class and thus updating the mangrove vegetation classification. The spatial distribution of the Avicinnia species within the Avicennia dominated class is shown in the Figure: 7-8.

7.8. Result and Discussion.

A total of ten species (8 obligate mangroves and 2 mangrove associates) were found in 19 sites (table -). However Banerjee et al. (1989) and Naskar & Guha Baksi (1987) reported 37 obligate mangroves and 32 mangrove associates in the whole Indian sundarbans. With the exception of *Acanthus ilicifolius* (herb), *Aegialitis rotundifolia* (shrub), all are trees. *Avicennia alba* is more concentrated near the coast where as *A. officinalis* at land ward side. Considerable density of A. marina occurs in almost all the sites. *Avicennia alba* and *A. officinalis* occur dominantly in soils with high salinities.

Among the three Avicennia species A. marina got the high importance value for most of the Avicennia dominated community followed by A. alba. The forest is largely dominated by Avicennia marina which pointing to its wide adaptability in different environments.

The modalities of three Avicennia species on the soil salinity gradient are presented in Figure: 7-9.They provide information on the ecological optimum and amplitude for each Avicennia species relative to other.

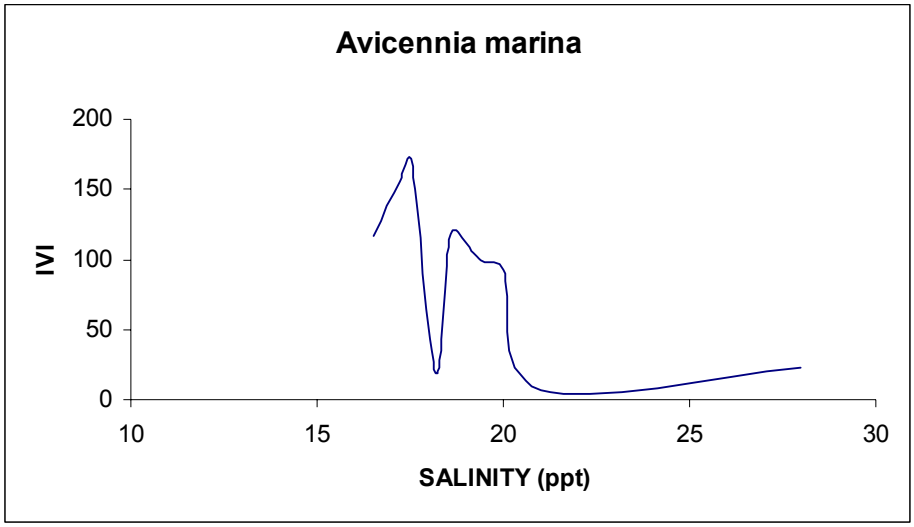

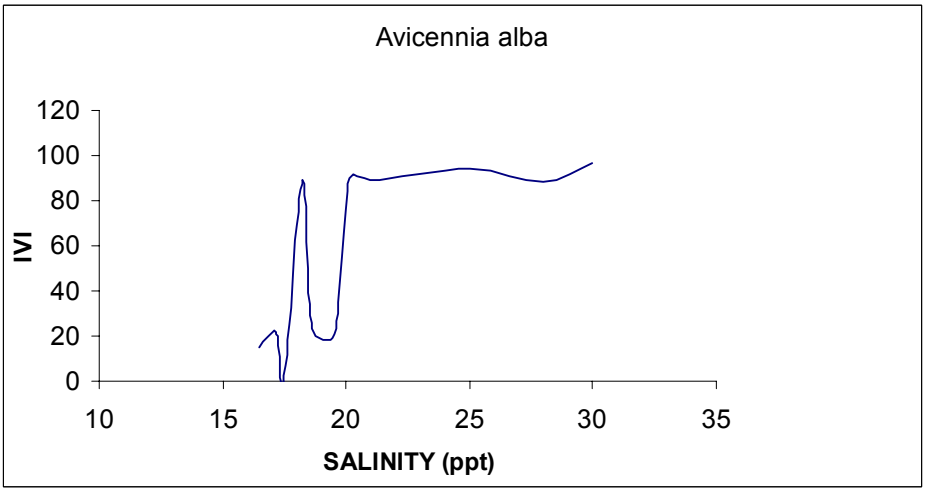

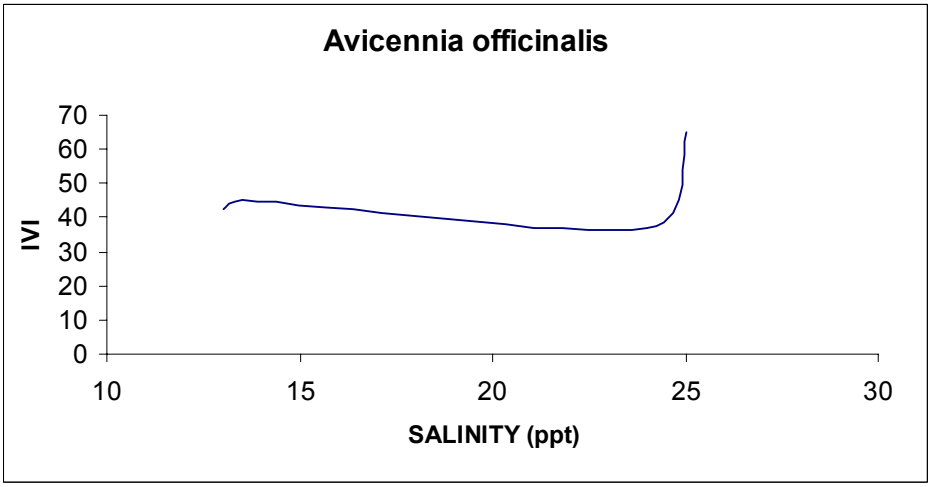

Figure 7-9 Performance of Three Avicennia species along the soil salinity gradient.

Figure:7.9 shows Avicennia alba is bimodal with ecological optima at salinity values of 18.2 and 20.1ppt Avicennia marina has ecological optima at salinity 17.5 and 18.6 ppt

Avicennia officinalis is also bimodal having ecological optima at salinity 13.02 and 25.00ppt.

The inter specific differences in salt tolerance reflect a physiological continuum ranging from moderately salt tolerant glycophytes to highly salt tolerant and apparently obligate halophytes (Ball 1996)

it has been stated that mangroves are naturally stressed ecosystems (kennealy 1982). An ecological factor, which may be present in excessiveor insufficient quantities, could be limiting to the distribution and composition of species. The species distribution may further be narrowed by competition or interaction with other species to a zone within its physiological tolerance of the factor (waring & Manjor 1964). Wakushima et al. (1994a, 1994b) suggested that soil pH and salinity in dry season are the important factors governing the zonal distribution of Japan and Thai mangroves. From the present observations, it is revealed that most of the species occupy a zone to which it is best adapted; however, there are overlapping occurrences of different species although with varying ecological optima along salinity gradients. The mangroves obviously share a niche attribute for these two factors in soil.

CHAPTER 8. *Mapping of Mangrove Primary Productivity – A Remote sensing approach.*

8.1. Introduction

Mangrove primary productivity can be divided into three components: 1) Benthic productivity of inter-tidal zone, 2) Aquatic productivity of plankton, Community and 3) Mangrove tree productivity. In this study only mangrove tree primary productivity is studied with the aid of remote sensing and ground data.

8.2. Aim of the study

The aim of the study is to map the species wise mangrove GPP scenario of the Lothian Island, belonging Indian Sundarban region using remote sensing and GIS approach.

8.3. Methodology

In this study a "community indices" approach was used to map the mangrove Gross primary productivity, both from detailed field survey and remote sensing aspect. Mangrove leaf area index was mapped community-wise. The leaf area index (LAI) map is the base map of GPP mapping. The LAI map reflects the total amount of one sided leaf surface over one m^2 ground area.

The approximate NPP of the whole mangrove canopy per m² of ground area over a day can be described by the following equation:

$P_N = A \times d \times LAI$

Where A = average rate of photosynthesis (g C m^{-2} leaf area hr^{-1}) for all leaves in the canopy, d = day length (hr), and LAI is the leaf area index already estimated for each pixel. For different concerned mangrove species of Sundarban, the photosynthetic rate was reported by Paramita Nandi and M. Ghosh.2001. Day length in the Sundarban region is on average about 12 hours. So Community wise LAI map was used to map this NPP (Net Photosynthetic Production) spatially through out the mangrove community. The overall methodology is graphically represented in the Figure: 8-1

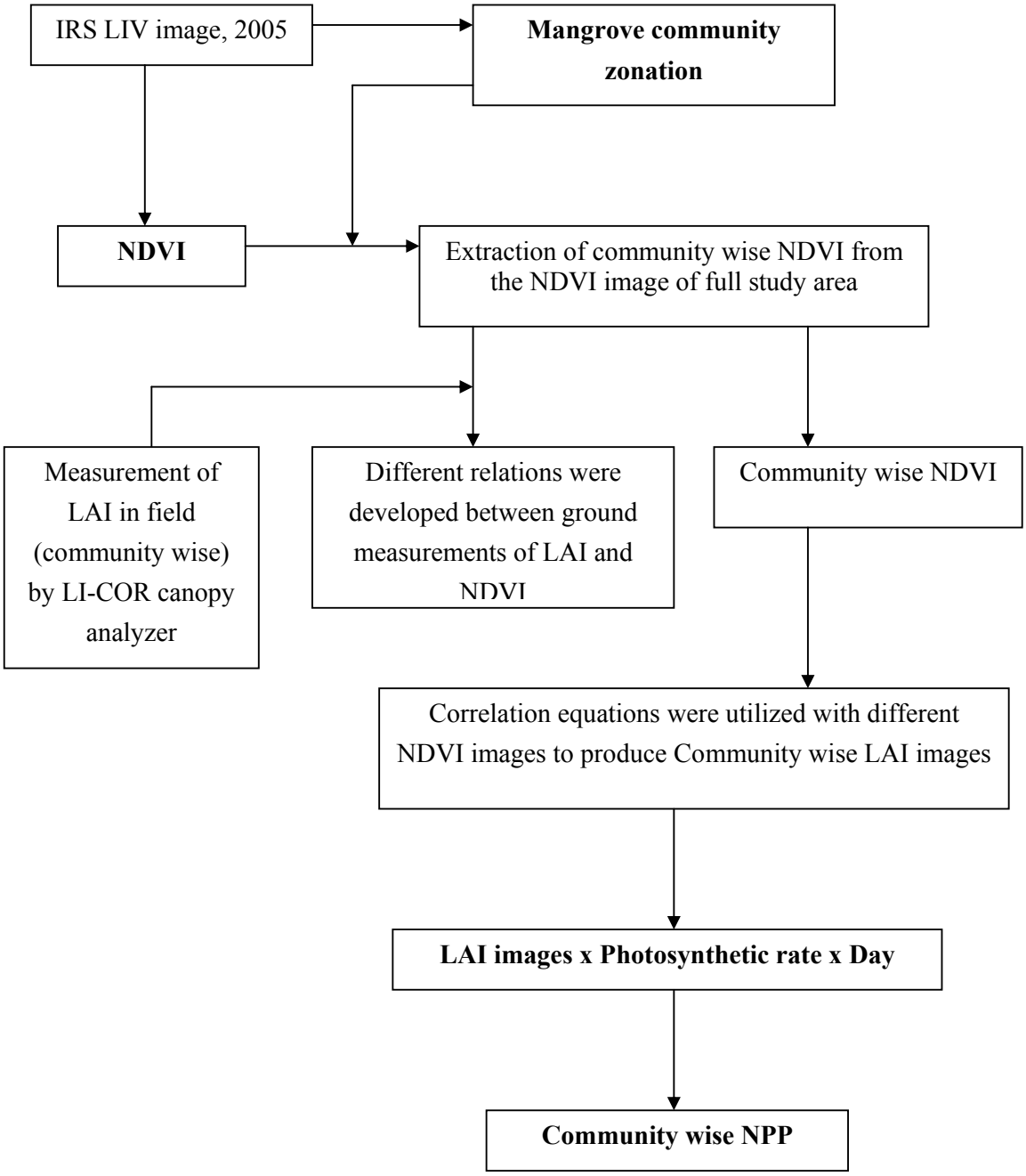

Figure 8-1 Methodology used for extracting spatial distribution of mangrove NPP from remote sensing and GIS approach.

8.4. Mangrove LAI (Leaf area index)

8.4.1. Introduction

The plant canopy is a locus of physical and biogeochemical process in an ecosystem. The functional and structural attributes of plant canopy are affected by microclimatic conditions, nutrient dynamics, herbivore activities, and many other factors. The amount of foliage contained in plant canopies is one basic ecological characteristic indicating the integrated effect of these factors. In turn canopy leaf serves as the dominant control over primary production (photosynthesis), transpiration, energy exchange and other physiological attribute pertinent to a range of ecosystem processes. Subsequently canopy leaf area is often treated as a core element of ecological field and modeling studies (e.g. Sellers et al., 1998, 1997; Bondeau et al., 1999).

8.4.2. Different Measurement strategies LAI in the field

Many methods have been developed to quantify LAI from the ground. There are some direct and indirect methods discussed below.

Direct methods

Direct or semi-direct methods involve a measurement of leaf area, using either a leaf area meter or a specific relationship of dimension to area via a shape coefficient. In coniferous species, projected leaf area differs from the developed one by a coefficient depending on a needle cross-sectional area (Grace, 1987; Barclay, 1998; Sellin, 2000). Leaf area is measured on a sub-sample of leaves and related to dry mass (e.g. via specific leaf area, SLA, $cm^2\ g^{-1}$). Finally, the total dry mass of leaves collected within a known ground-surface area is converted into LAI by multiplying by the SLA. As the direct methods only relate to foliage, they are the only ones giving real access to leaf area index. They allow separate computation of the shape, size and number of leaves. Direct methods provide the reference for the calibration or evaluation of indirect methods. It is crucial to sample leaves correctly for establishing leaf area to dry mass ratio, as it changes among species and among sites for a given species. Direct methods include harvesting, allometry and litter collection.

Harvesting the vegetation and measuring the area of all the leaves within a delimited area is the first method, widely used for crops and pastures. This method is well adapted for

vegetation of small structure, but is destructive. Such an exhaustive approach cannot be applied to large areas or to large trees, but it is suitable for measuring LAI in the space of a gas exchange chamber.

Foresters have developed a less destructive method that relates foliage area to the diameter of the sapwood area at breast height or at crown base (Grier and Waring, 1974; Albrekston, 1984; Makela et al., 1995). The leaf area per unit sapwood area varies from 0.15-0.75 m^2 cm^{-2} in conifers (Waring et al., 1982). It has been suggested that the product of sapwood area and sapwood permeability should improve the relationship with leaf area (Whitehead et al., 1984; Shelbrune et al., 1993). The underlying hypothesis is that leaf area is in balance with conducting tissues, hence such allometric relationships are site and species dependent, and, in some cases, also year dependent. Any changes in the leaf versus sapwood area ratios due to management, health, fertility (Brix and Mitchell, 1983) or ageing are not reflected in a single allometric relationship. For broad-leaved species, most of the diffuse porous species exhibit dispersed sapwood and, in ring porous species like oaks, the efficiently conducting sapwood is limited to the most recent rings (Rogers and Hinckley, 1979). Because of the difficulties of measuring the conducting area, the sapwood area should be replaced by more readily measured variables, such as diameter at breast height (Vertessy et al., 1995). Finally, if the establishment of allometric relationships with leaf area is conducted in individual trees by taking into account the height of branches, the vertical distribution of LAI may be estimated (Bidlake and Black, 1989; Maguire and Bennett, 1996). According to these authors, estimating allometric relationships through destructive sampling is a reliable method of deriving LAI for a given experimental site, but remains year-dependent. Hence such an approach cannot be used to describe a time-course of LAI recovery after any change in canopy opening.

In deciduous stands, a non-destructive method consists of collecting leaves in traps distributed below the canopy during leaf fall. Litter collection has been widely used in forest ecology. Litter has to be collected in a number of traps with a known collecting area every second week at least to avoid losses and decomposition. Collected litter is dried (at 60-80 °C for 48 h) and weighed to compute the dry mass of litter as g m^{-2}. Leaf dry mass at each collection date is converted into leaf area by multiplying the collected biomass by the specific leaf area (SLA, expressed in m^2 g^{-1}). Finally, the leaf area index is the accumulated leaf area over the period of leaf fall. The estimating of specific leaf area is the most critical point in this procedure. It varies with species (Chason et al., 1991; Niinemets and Kull, 1994), site fertility (Vanseveren and Herbauts, 1977; Jurick, 1986; Burton et al., 1991), date and year, duration of remaining in the traps, weather and even within stands (Bouriaud et al., 2003). Sorting leaves by species for weighing and establishing specific area ratio is of importance: litter collection is the only method giving

access to the contribution of each species to total leaf area index. Once again, this method is a reference one and is suitable for deciduous species: it can give a decrease of LAI during leaf fall and the contribution of each species to total leaf area index.

First proposed by Guittet (J Guittet, personal communication), the needle technique is derived from the inclined point quadrat method (Warren Wilson, 1959, 1960, 1963). It is an alternative for sampling litter in deciduous stands without traps. A fine needle of 1 mm in diameter is plunged vertically into the litter lying on the soil, as soon as all the leaves have fallen to avoid any decomposition of the leaves. With a vertical probe and horizontal leaves, the number of leaves collected on the needle corresponds to the contact number and equals the leaf area index. This method needs an intensive sampling (from 100 to 300 points) to quantify an average contact number and LAI properly (Nizinski and Saugier, 1988; DufreÃne and Breda, 1995). The method is well suited for oak and beech forests with their large leaves and is easiest to apply in sites where litter is completely decomposed every year to avoid mixing with litter from previous years. Recently, this line-intercept method was adapted to an old Douglas-fir canopy in a spectacular way (Thomas and Winner, 2000): a vertical line (one edge of a fiberglass measuring tape, <0.10 mm thickness) was lowered from a crane from above the canopy and each intercept point was checked.

Indirect methods

Consequently, many indirect methods of measuring LAI have been developed. Indirect methods infer leaf area index from measurements of the transmission of radiation through the canopy, making use of the radiative transfer theory (Anderson, 1971; Ross, 1981). These methods are non-destructive and are based on a statistical and probabilistic approach to foliar element (or its complement, gap fraction) distribution and arrangement in the canopy (Jones, 1992). LAI is calculated by inversion of the exponential expression of the gap fraction:

$$P(\theta) = e^{-G(\theta, \alpha)LAI / \cos(\theta)}$$

Where θ is the zenith angle of view, α is the leaf angle, $P(\theta)$ is the gap fraction, $G(\theta, \alpha)$ is named the G-function and corresponds to the fraction of foliage projected on the plane normal to the zenith direction. $G(\theta, \alpha)$ depends on leaf-angle distribution α. The latter is generally not known, and the LAI calculation requires gap fraction measurements for a range of θ angles of view. Another alternative is to work at an angle of elevation of about 32°, which is quite insensitive to distribution of leaf inclination (Warren Wilson, 1963; Jones, 1992).

Radiation measurement and `gap fraction'-based methods must be distinguished. The radiation measurement method uses the turbid medium analogy, which makes the assumptions that (1) leaves are randomly distributed within the canopy, and (2) individual leaf size is small when compared with the canopy. With these assumptions, gap fraction is equivalent to transmittance. The gap fraction-based methods are dependent on leaf-angle distribution (Campbell, 1986). By inverting equation (1), the expression for LAI is:

$$LAI = \ln(P(\theta))\cos(\theta) / G(\theta)$$

as the G-function here is independent of the leaf-angle distribution, a. The `gap fraction'-based methods (canopy analyser systems and hemispherical images) use several ways to solve this equation as described in theory papers (Miller, 1967; Nilson, 1971; Norman and Jarvis, 1974; Ross, 1981; Norman and Welles, 1983; Lang, 1986, 1987; Norman and Campbell, 1989; Breda et al., 2002).

In fact, the indirect methods do not measure leaf area index, as all canopy elements intercepting radiation are included. Therefore, the terms of plant area index (PAI) or surface area index (SAI) are preferred if no correction to remove branches and stems is made.

Radiation measurement method:

Monsi and Saeki (1953) expanded the Beer-Lambert extinction law to plant canopies. The law of Beer-Lambert expresses the attenuation of the radiation in a homogenous turbid medium. In such a medium, the flux is absorbed proportionately to the optical distance. The method of LAI evaluation by the inversion of the Beer-Lambert equation requires the measurement of both incident (Io) and below-canopy radiation (I). Following Monsi and Saeki (1953) and with a random distribution of leaves within the canopy:

$$I = I_o e^{(-k \times LAI)} \text{ hence } LAI = -1/k \ln(I/I_o)$$

where Io is the incident radiation, I is the radiation transmitted below-canopy, k is the extinction coefficient and LAI is the leaf area index. From equation (2), the expression for k is:

$$k(\theta, \alpha) = G(\theta, \alpha)/\cos(\theta)$$

i.e. k is a function of leaf angle distribution, a, and leaf-azimuth angle q (Jones, 1992). The incident radiation can be measured above the canopy or in a nearby open area in the

case of tall stands. Beer-Lambert's equation is inverted to compute k, based on an independent direct measurement of LAI (by allometry or litter fall) and on the measured transmittance (Vose and Swank, 1990; Smith et al., 1991; Burton et al., 1991). Then, seasonal transmittance and k are used to derive LAI . Several authors have discussed how to determine k (Ledent, 1977; Smith, 1993; Vose et al., 1995; Hassika et al., 1997) and the accuracy of the method (Nel and Wessman, 1993). Pierce and Running (1988) proposed the use of a constant k value of 0.52 for coniferous species based on measurements by Jarvis and Leverenz (1983). The extinction coefficient also depends on stand structure and canopy architecture (Turton, 1985; Smith et al., 1991; DufreÃne and Breda, 1995). Campbell (1986) and Thomas and Winner (2000) ascribed 10% of the variation in LAI to the effects of alternative assumptions of distribution of foliage inclination. Comeau et al. (1998) have discussed integration over time and effects on LAI calculation. The canopy extinction coefficient is a function of wavelength (Jones, 1992), radiation type and direction (Berbigier and Bonnefond, 1995). It is also important to maximize spatial integration by the use of large sensors, linear sensors or mobile sensors. The variation is such that the k coefficient would better be estimated for every stand (Johansson, 1989; Cannell et al., 1989; Smith et al., 1991).

In conclusion, the monitoring of seasonal transmittance remains one of the most efficient ways of daily monitoring both LAI increases and decreases. These two highly dynamic phases are difficult to survey with manual measurements, but are essential for the calculation of the seasonal time-course of energy fluxes. As an example, the progression of transpiration as LAI expands during spring in an oak stand has to be monitored with a daily resolution. Other smaller LAI fluctuations, induced by successive flushing or by pest damage, could also be detected, dated and quantified by this method. Such measurements, nevertheless, often remain spatially limited by the number of below-canopy sensors used. An interesting answer may be to use a mobile sensor allowing both continuous and spatially integrated light measurements.

Mangroves are intertidal, often grow in dense stands and have complex aerial root systems which make the sampling regimes described so far difficult to carry out. However, Clough *et al.* (1997) estimated LAI from a ground area of 900 m^2, their objective being a comparison between an estimation of mangrove LAI based on gap-fraction analysis with a direct collection method. To measure the LAI of mangroves over large areas would require measurements at many different locations, an extremely time-consuming process. The difficulty of moving through dense mangrove stands and the general inaccessibility of many mangrove areas would clearly pose a further problem.

The interception, scattering and emission of radiation is closely related to the canopy structure of vegetation. Spatial aspects of LAI can be indirectly measured from the

spectra of mangrove forests, and so many of the problems associated with obtaining LAI values for entire mangrove forests are avoided. A semi-empirical model described in this section provides an indirect estimation of mangrove LAI with gap-fraction analysis being used as ground-truthing information to calibrate remotely sensed data. Thematic maps of LAI for the entire area covered by mangroves are derived to a high level of accuracy, without the need for large numbers of ground measurements.

8.4.3. Development of relations between community wise LAI and NDVI

8.4.3.1. Ground survey of LAI measurement

From the mangrove community zonation map (Figure: 7-2) a base-map was prepared for field study. Community structure of the study area reveals that only Avicennia dominated, Aegialitis dominated and Phoenix communities are more or less homogeneous through out the study area. Other mangrove communities are not considered for LAI estimation, as they are not homogeneous in species composition. So only these three community patches, well marked in the base map were accessed and LAI measurements of these different communities were done using the Li-Cor LAI 2000 canopy analyzer. The fieldwork is done at the month of April 2005 – the same time as of IRS L4 image acquisition.

For each community patches 10 well-distributed sample points were measured for developing relation between LAI and NDVI and another 10 points for each were measured for accuracy assessment.

8.4.3.2. Preparation of NDVI (Normalized difference Vegetation Index) surface of the study area

NDVI was calculated from the reflectance (ρ) values of the georectified IRS L4 satellite imagery of the study area as follows:

$$NDVI = \frac{\rho NIR - \rho Red}{\rho NIR + \rho Red}$$

Resolution of the image is 5.8m. NDVI image of the total study area is given in the Figure: 8-2. NDVI patches of three community type viz - Avicennia dominated community, Aegialitis dominated community and Phoenix community were extracted from the full NDVI image of study area by using different community masks, prepared from the community zonation map (Figure: 7-2). NDVI values of each sampling point locations were extracted from the different community NDVI images. These NDVI

values were tabulated against the LAI measurements of the same locations in the each community type. Then different regression models were developed between these Ground measurements of LAI and the NDVI values extracted from the remote sensing values for different mangrove communities.

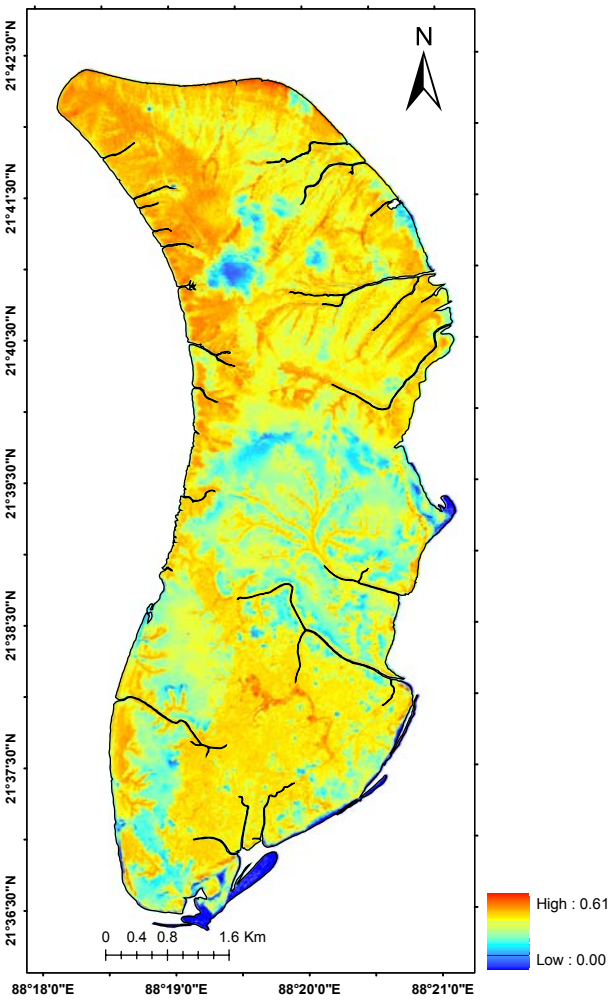

Figure 8-2 NDVI image of Total Lothian Island.

8.4.3.3. Development of Correlations between LAI and NDVI

NDVI values of each sampling point locations were extracted from the different community NDVI images. These NDVI values were tabulated against the LAI measurements of the same locations in the each community type. Then different regression models (Figure: 8-3) were developed between these Ground measurements of LAI and the NDVI values extracted from the remote sensing values for different

mangrove communities. The relations developed between them from three different mangrove communities are shown below –

For Avicennia dominated community – LAI = 16.243*NDVI - 3.2043

For Aegialitis dominated community – LAI = 11.173*NDVI - 1.2457

For Phoenix community – LAI = 13.911*NDVI - 1.9247

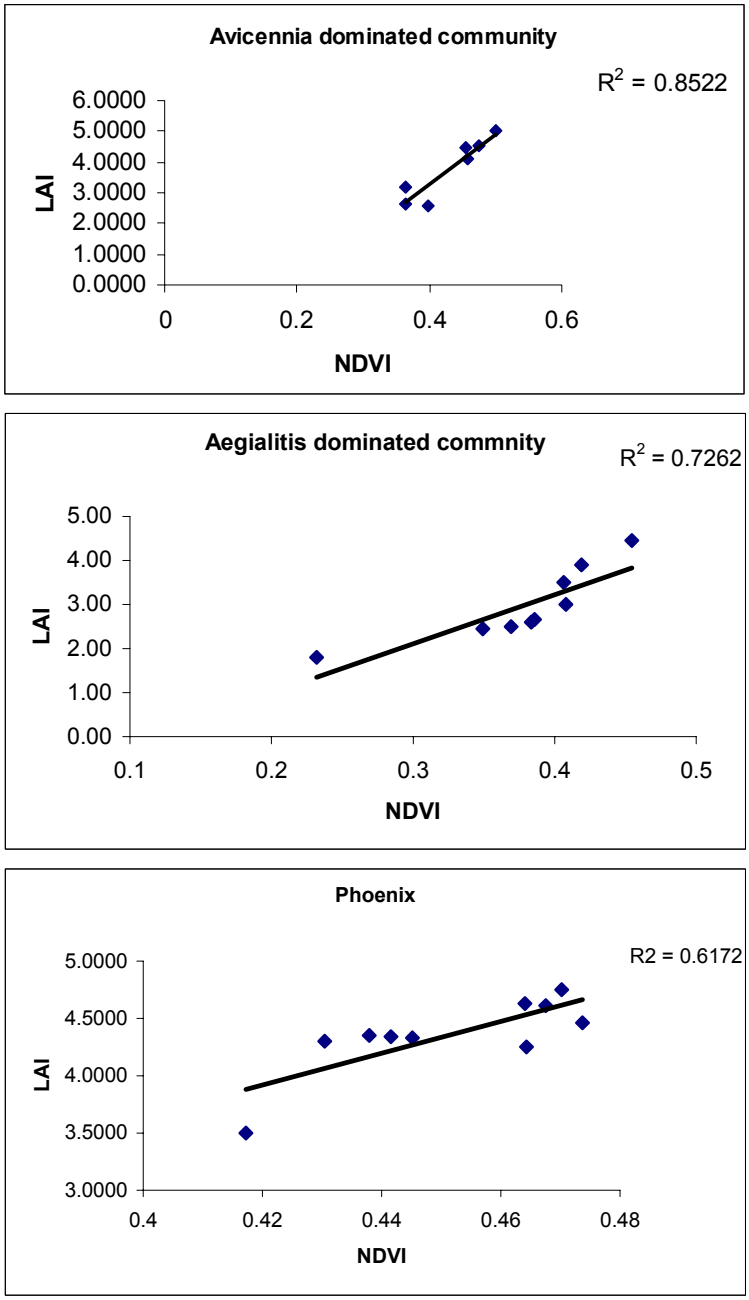

Figure 8-3 Ground measurements of LAI versus NDVI of different Mangrove communities.

8.4.4. Preparation of LAI images of different mangrove community

Relations developed between NDVI of different mangrove community and ground measurements of (LAI community wise) were used to develop the LAI map of three different mangorve communities – Avicinnia dominated (Figure: 8-4), Aegialitis dominated (Figure: 8-5) and phoenix (Figure: 8-6) from the NDVI images of these respective communities.

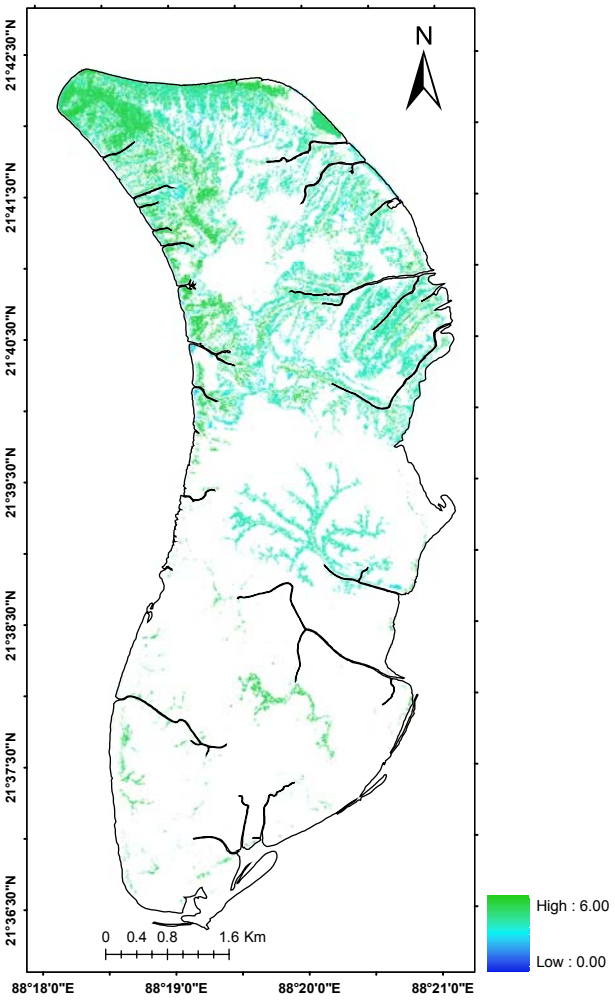

Figure 8-4 LAI map of Avicennia dominated Community.

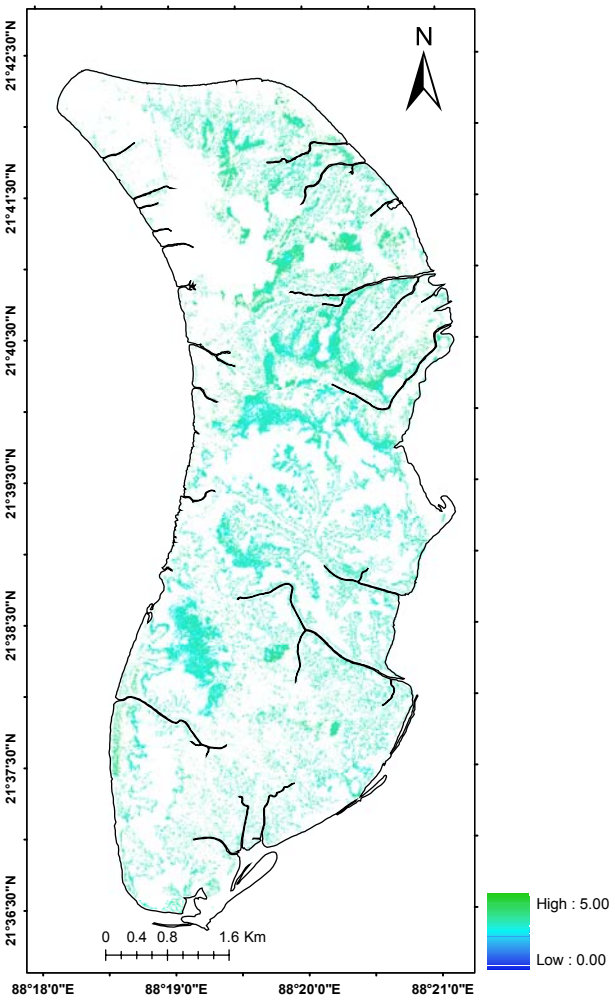

Figure 8-5 LAI map of Aegialitis dominated community.

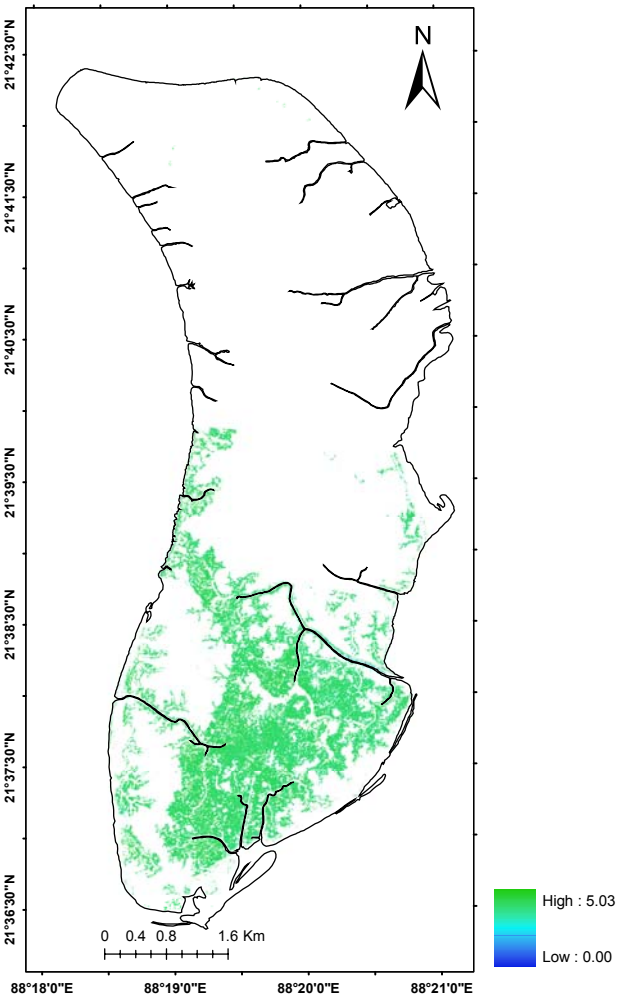

Figure 8-6 LAI map of Phoenix community.

8.4.5. Accuracy assessment

For Accuracy assessments of the above predicted LAI surfaces of the three different Mangrove community – The Predicted values of LAI for the 10 accuracy sites of each community was extracted from the LAI layers of different communities and a Regression analysis was done between these predicted values and the LAI measured in the field for

the accuracy sites. Figure:8-7 shows the regressions of the predicted and observed values of LAI for different communities. From this analysis it has been found that the accuracy of LAI – NDVI model for Avicennia dominated community is 70.11%, for Aegialitis community it is 87.53% and for Phoenix community it is 85.28%.

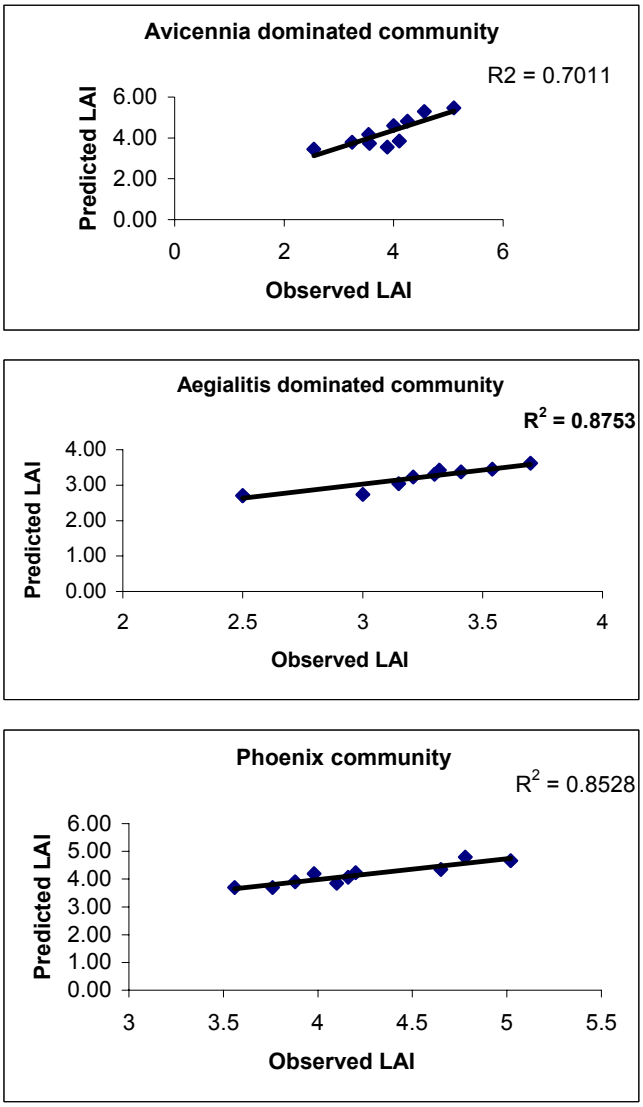

Figure 8-7 Linear Regressions between Observed and Predicted values of LAI for different Mangrove Community.

8.5. Mangrove Net Primary Production (NPP)

The approximate net photosynthesis of the whole plant canopy above a unit area (1 m x 1m) of ground can be described by:

$P_N = A \times d \times LAI$

Where A = average rate of photosynthesis (g C m^{-2} leaf area hr^{-1}) for all leaves in the canopy, d = day length (hr), and LAI is the leaf area index already estimated for each pixel.

Average rate of photosynthesis of the concerned mangrove species are given in the table: 8-1

Table 8-1 Photosynthesis rate of some mangrove species of indian sundarban region.

species	season	PAR ($mmolm^{-1}s^{-1}$) (±SE)	Air Temp (°C)(±SE)	Leaf Temp (°C)(±SE)	Photosynthesis rate ($\mu molm^{-1}s^{-1}$) (±SE)	Salinity (ppt)(±SE)	Soil pH (±SE)
Aegialitis rotundifolia	summer	1.50 (0.47)	37.43 (0.07)	39.77 (0.64)	8.97 (0.19)	18 (0.20)	7.45 (0.01)
	winter	0.90 (0.19)	33.38(0.30)	36.68 (0.49)	6.06(1.95)	19.00(0.03)	7.50(0.16)
Avicennia alba	summer	1.78(0.41)	37.05(0.78)	37.20(2.69)	9.58(4.09)	15(0.06)	6.80(0.18)
	winter	1.18(0.19)	25.25(0.28)	38.10(1.72)	11.11(3.38)	15(0.06)	6.80(0.18)
Avicennia marina	summer	0.98 (0.36)	37.13(0.98)	37.63(3.87)	8.98(3.18)	16.00(1.21)	6.80(0.18)
	winter	1.43(0.20)	32.27(0.95)	37.37(1.87)	11.80(3.18)	24(1.76)	7.73(1.35)
Avicennia officinalis	summer	1.46(0.89)	37.53(0.49)	38.93(2.89)	8.22(1.42)	15.00(0.06)	6.80(0.18)
	winter	0.65(0.33)	30.00(0.87)	31.45(1.39)	8.56(3.94)	24(1.76)	7.76(0.19)
Phonerix paludosa	summer	2.02(0.09)	38.43(0.74)	45.80(2.32)	3.69(2.12)	16(1.21)	7.40(0.07)
	winter	-	-	-	-	-	-

The above data on photosynthetic rate of concerned mangrove species of Indian Sundarban was reported by Paramita Nandy (Datta) and M. Ghosh, 2001. For each parameters listed in the above table they collected the data from three individual leaves at the upper, middle and lower portions of each plant.

A model was designed in the ERDAS module maker to generate the Net photosynthetic production (NPP) images of the concerned community type by using the community specific LAI images. The NPP images of the three different communities are shown in the following Figures – for Avicennia dominated community NPP image of 2004 in summer and in winter season are shown in Figures: 8-8 and 8-9 respectively. For Aegialitis dominated community NPP image of 2004 in summer and in winter season are shown in Figures: 8-10 and 8-11 respectively. For Phoenix community NPP image of 2004 in summer season is shown in Figures: 8-12 and finally Total NPP image for three communities in both summer and winter seasons are shown in Figure:8-13 & 8-14 respectively.

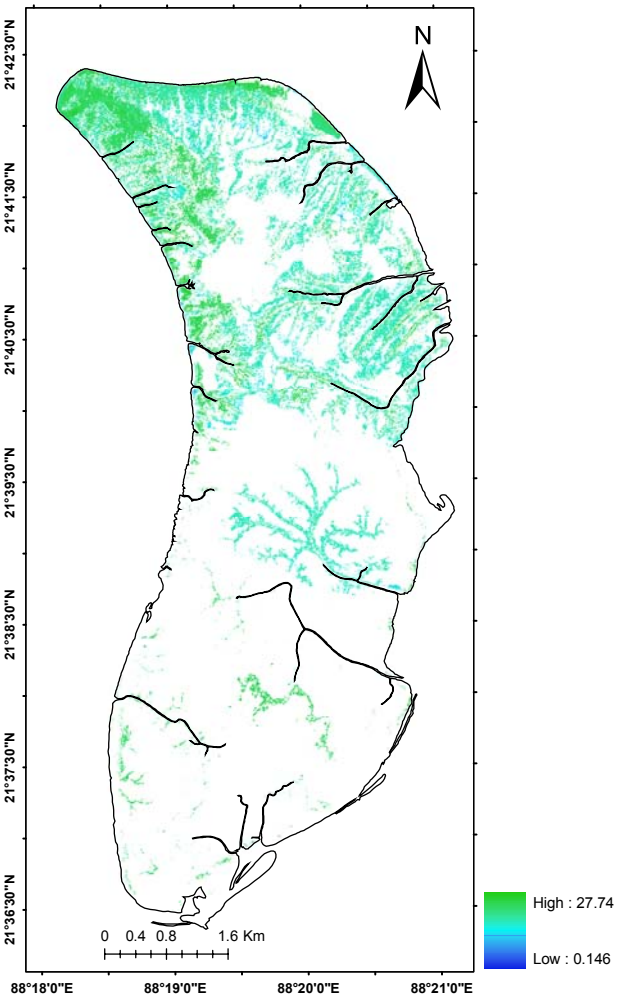

Figure 8-8 NPP map of Avicennia dominated community in summer (gCm-2d-1)

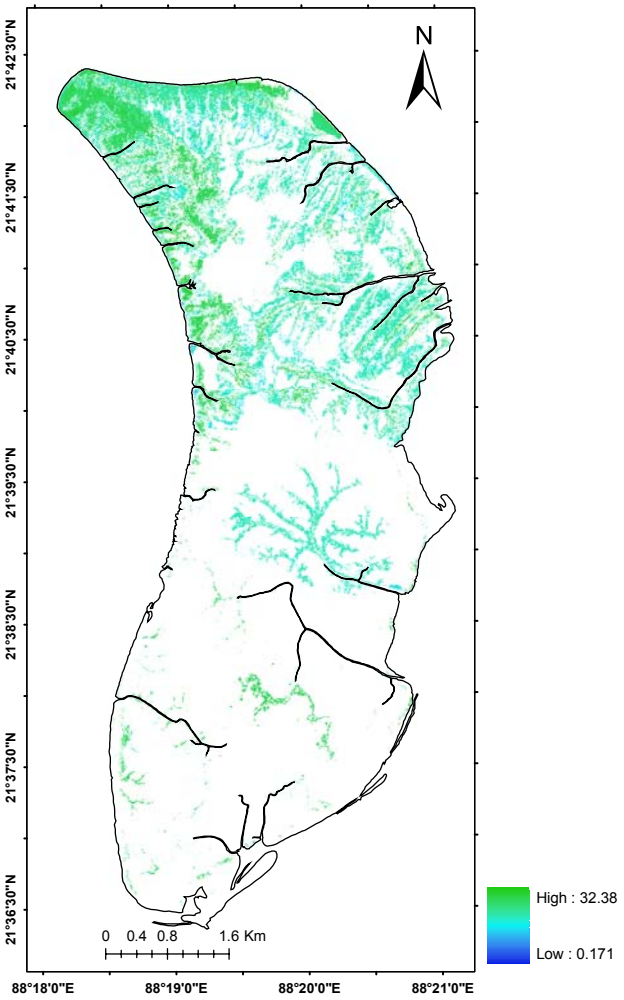

Figure 8-9 NPP map of Avicennia dominated community in Winter (gCm-2d-1)

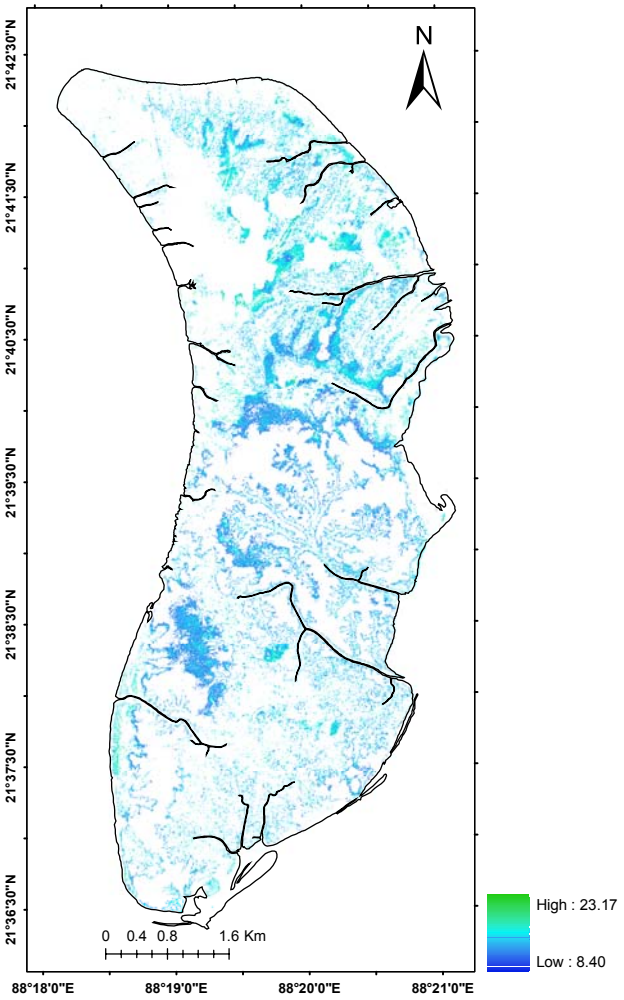

Figure 8-10 NPP map of Aegialitis dominated community in summer (gCm-2d-1)

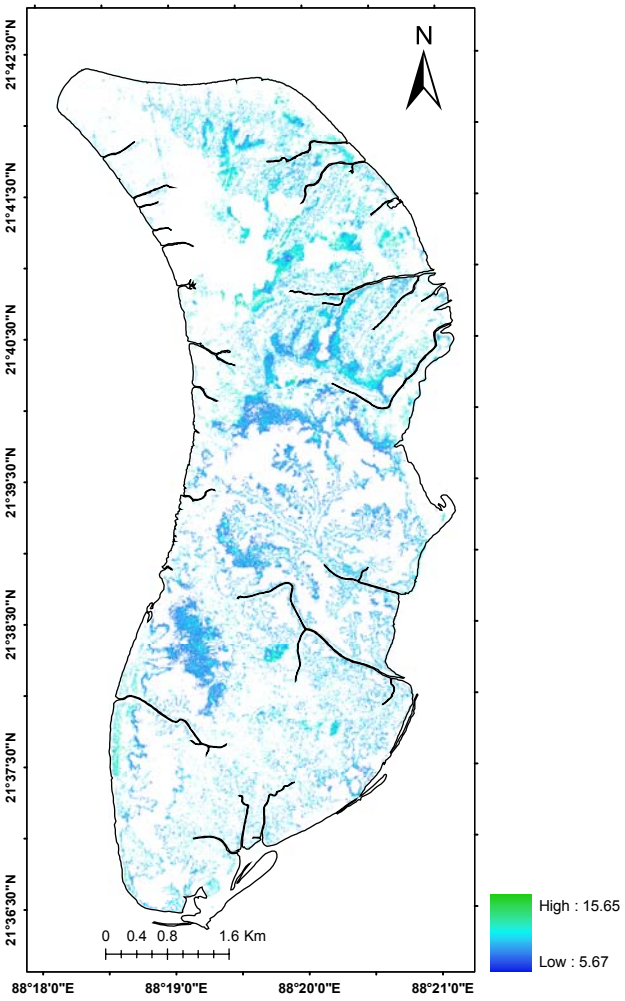

Figure 8-11 NPP map of Aegialitis dominated community in winter (gCm-2d-1)

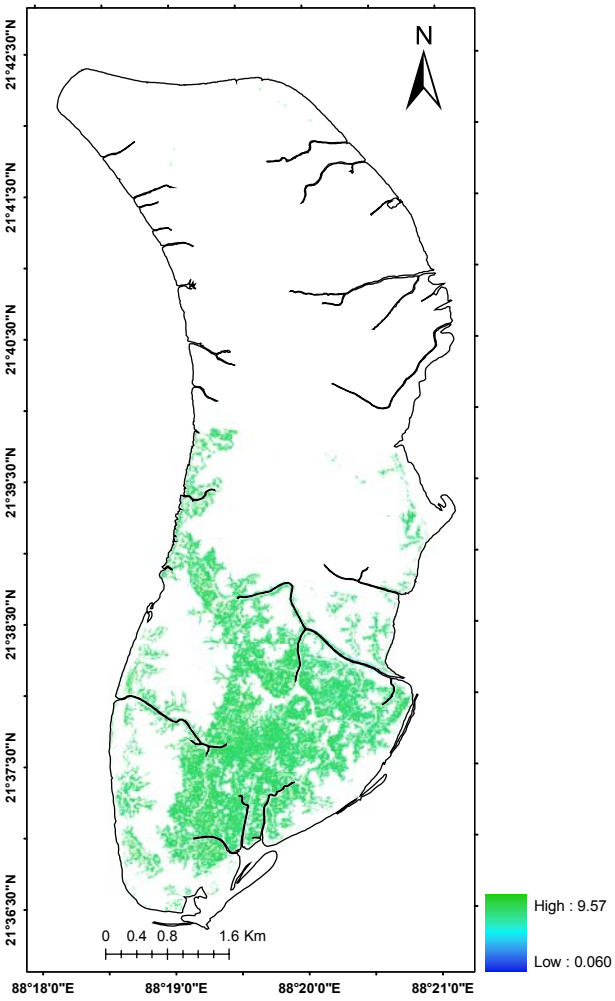

Figure 8-12 NPP map of Phoenix dominated community in summer (gCm-2d-1)

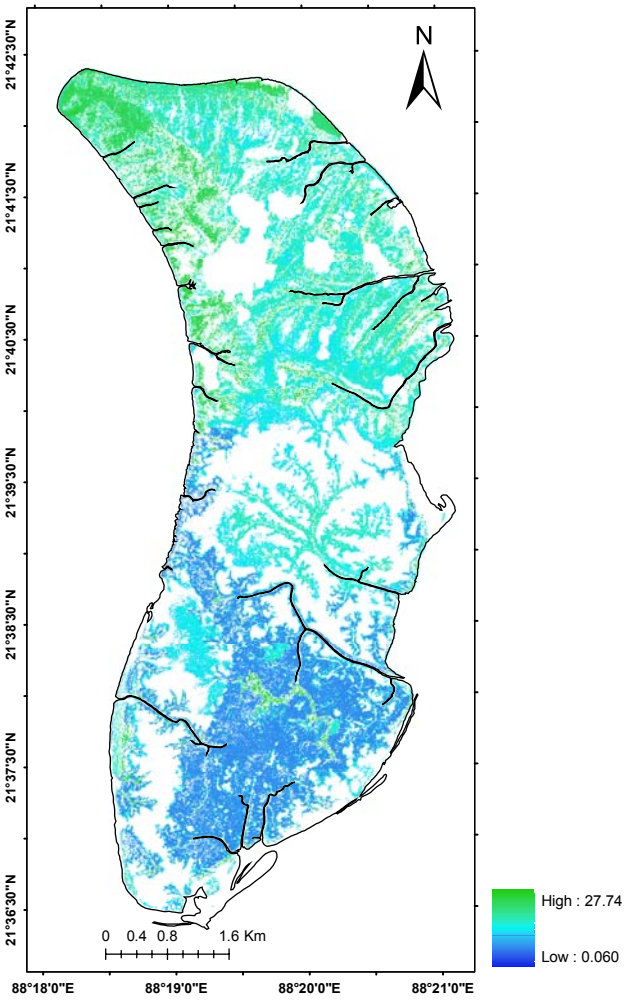

Figure 8-13 Total NPP of three mangrove community in summer (gCm-2d-1)

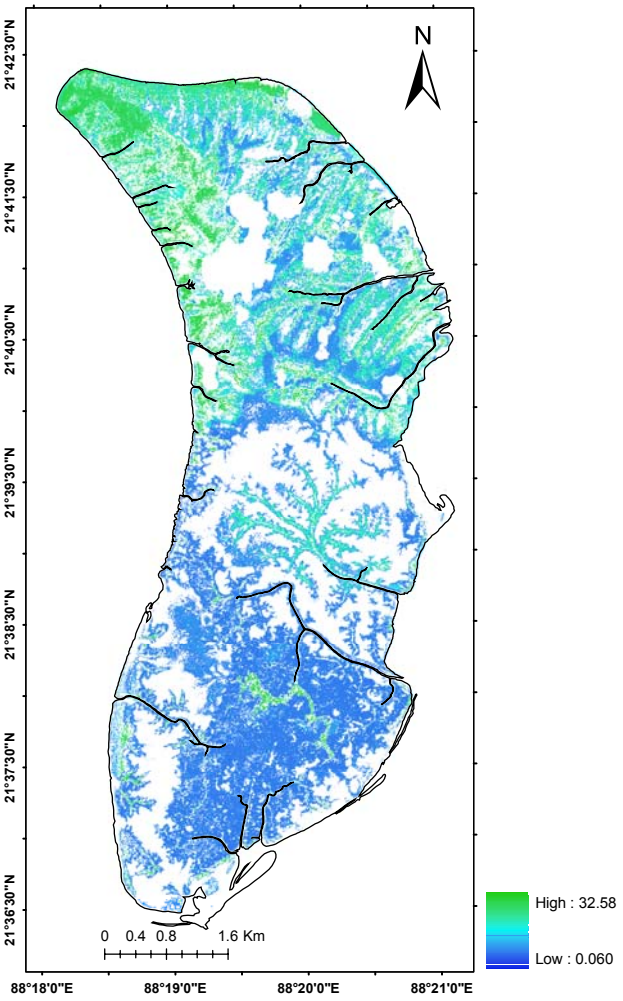

Figure 8-14 Total NPP of three mangrove community in winter (gCm-2d-1)

8.6. Result and Discussion

The NPP image of different mangrove community shows that for Avicennia dominated forest NPP ranges from 0.1461-27.57$gCm^{-2}d^{-1}$ in summer and in winter it is from 0.1716 – 32.385 $gCm^{-2}d^{-1}$, for Aegialitis dominated community in summer it is from 8.407 – 23.175 $gCm^{-2}d^{-1}$ and in winter from 5.677 – 15.651 $gCm^{-2}d^{-1}$. For Phoenix it is from 0.060 – 9.570 $gCm^{-2}d^{-1}$. For estimation of Avicennia dominated community the Average photosynthetic rate of all available Avicinnia species (A.marina, A.alba and A. officinalis) was considered. In this study only this three-mangrove community were considered, because these communities are more or less homogeneous from the species variation point of view. Both the summer and winter NPP images were generated from this study.

8.7. Conclusion and Recommendations

The above study of NPP image generation of different mangrove communities shows as Remotesensing and GIS approach in mapping variation of NPP through out the whole study area. Here the photosynthetic rated used for different community for two different seasons are constant to each community type. But the real scenario is that the photosynthetic rate of a particular species is controlled by some physicochemical and climatic factors like - soil salinity, PAR (Photosynthetic Active radiation), Air temperature etc. in this short duration of study it was not possible to generate the species specific relations of photosynthetic rates and all of these controlling factors.

Temporal variation of PAR can get from remote sensing data, Soil salinity surfaces of different seasons can be generated from detailed multitemporal ground survey and tidal zonation maps in GIS environment. The temperature surfaces also can be created from interpolating weather station data. So it is highly recommended that if all these species specific relations can be developed then a more realistic NPP scenario of the concerned study area can be generated.

Again another limitation for mapping LAI from Remotesensing aspect is that – the relation between LAI and image NDVI differs community wise. Rather it can be told that the relations are species specific. So LAI estimation for mixed canopies using this technique is not recommended.

References

Albrekston A. 1984. Sapwood basal area and needle mass of Scots Pine (Pinus sylvestris L.) trees in Central Sweden. Forestry 57, 35-43.

Anderson MC. 1971. Radiation and crop structure. In: Sestak Z, Catsky J, Jarvis PG, eds. Plant photosynthetic production: manual of methods. The Hague, The Netherlands: Junk.

Baker, J.R., Mitchell, P.L., Cordey, R.A., Groom, G.B., Settle, J. J., Stileman, M. R.1994. Relationship between physical characteristics and polarimetric radar backscatter for Corsican pine stands in Thetford Forest, UK. Int. J. Remote Sens. 15 (14): 2827 – 2849

Bamler, R., Schättler, B. (1993): SAR Data Acquisition and Image Formation. In: Schreier, G. (Ed.): SAR Geocoding – Data and Systems. pp. 53-102. Wichmann: Karlsruhe.

Banerjee, L. K., 2002. Sundarbans Biosphere Reserve. In Singh NP (Ed) and Singh K.P. (Ed), Floristic diversity and conservation Strategies in India, Vol. V – In-situ and ex-situ conservation, BSI, Ministry of Environment and Fores, pp. 2801 - 2830.

Banerjee, L.K. 1987. Comparative study of the mangroves of the Sundarbans and that of the Mahanadi delta. J. Econ. Tax. Bot. 9(1): 119-131.

Banerjee,L.K.1987. Ecological studies on the mangals in Mahanadi estuarine-delta orissa:India tropical ecology 28:117-125

Barclay HJ. 1998. Conversion of total leaf area to projected leaf area in lodge pole and Douglas-fir. Tree Physiology 18, 185-193.

Berbigier P, Bonnefond JM. 1995. Measurements and modeling of radiation transmission within a stand of maritime pine (Pinus pinaster Ait). Annales des Sciences Forestie¡res 52, 23-42.

Bidlake WR, Black RA. 1989. Vertical distribution of leaf area in Larix occidentalis: a comparison of two estimation methods. Canadian Journal of Forest Research 19, 1131-1136.

Black,C.A1993.Soil fertility evolution and control .Lewish publishers,BocaRaton,FL.

Bondeau, A., Kicklighter, D.W., & Kaduk, J.,1999 Comparing Global Models of terrestrial net Primary Productivity (NPP) : importance of Vegetation structure on Seasonal NPP estimaties. Global Change Biology, 5, 35 – 45.

Boto,K.G & J.T Wellington.1984.Soil characteristics and nutrient status in northern Australian mangrove forest.estuaries7:61-69.

Bouriaud O, Soudani K, Breda N. 2003. Leaf area index from litter collection: impact of specific leaf area variability within a beech stand. Canadian Journal of Remote Sensing (in press).

Breda N, Soudani K, Bergonzini JC. 2002. Mesure de l'indice foliaire en forest. Paris: ECOFOR.

Brix H, Mitchell AK. 1983. Thinning and nitrogen fertilization effects on sapwood development and relationships of foliage quantity to sapwood area and basal area in Douglas-fir. Canadian Journal of Forest Research 13, 384-389.

Burton AJ, Pregitzer KS, Reed DD. 1991. Leaf area and foliar biomass relationships in northern hardwood forests located along an 800 km acid deposition gradient. Forest Science 37, 1041-1059.

Burton AJ, Pregitzer KS, Reed DD. 1991. Leaf area and foliar biomass relationships in northern hardwood forests located along an 800 km acid deposition gradient. Forest Science 37, 1041-1059.

Campbell GS. 1986. Extinction coefficients for radiation in plant canopies calculated using an ellipsoidal inclination angle distribution. Agricultural and Forest Meteorology 36, 317-321.

Cannell MGR, Milne LJ, Sheppard LJ, Unsworth MH. 1989. Radiation interception and productivity of willow. Journal of Applied Ecology 24, 261-278.

Chakrabarti K. (1987) Sundarbans mangroves – biomass productivity and resources utilization: an indepth study . Indian Forester 113:622-628.

Chapman V.J., 1976. Mangrove Vegetation.J. Cramer, Vaduz, Germany.

Chason J, Baldocchi D, Hutson M. 1991. A comparison of direct and indirect methods for estimating forest leaf area. Agricultural and Forest Meteorology 57, 107-128.

Chen,R & R.R.Twilley.1998.A gap dynamic model of mangrove forest development along gradients of soil salinity and nutrients resource.journal of ecology 86:37-52

Chen,R & R.R.Twilley.1999.Paterns of Mangrove forest structure and soil nutrients dynamics along the shark river estuary,Florida ,Estuaries22:955-970

Cintron,G.,A.eLugo,D.J.pool& G.Mories .1978.Mangrove and arid environment in Puerto Ricoand adjacent islands.biotropica 10:110-121

Clough, B.F., Ong, J.E., and Gong, G.W., 1997, Estimating leaf area index and photosynthetic production in canopies of the mangrove *Rhizophora apiculata. Marine Ecology Progress Series*, 159, 285–292.

Comeau P, Gendron F, Letchford T. 1998. A comparison of several methods for estimating light under a paper birch mixedwood stand. Canadian Journal of Forest Research 28, 1843-1850.

COPOCOS, 00-01. Status of Coastal Sea, West Bengal, Coastal Pollution Control Series, COPOCS / 21 / 2000 – 2001

Costa, M. P. F., 2000. Net Primary Productivity of Aquatic Vegetation of the Amazon Floodplain: A multi-SAR satellite approach. PhD thesis, University of Victoria, Victoria, Canada.

Curlander, J.C., McDonough, R.N. (1991): Synthetic aperture radar : systems and signal processing. Wiley Series in Remote Sensing.

Dobson, M. C., Pierce, L. E., and Ulaby, F. T., 1996. Knowledge-based land-cover classification using ERS-1/JERS-1 SAR composites. IEEE Transactions on Geoscienceand Remote Sensing, 34, 83–99.

Dobson, M. C., Ulaby, F. T., Le Toan, T., Kasische, E. S. and Christensen, N., 1992. Dependence of radar backscatter on coniferous forest biomass. IEEE Trans. Geosci. Remote Sensing. 30(2): 412 – 415.

Dobson, M.C., Ulaby, F.T., Le Toan T., Kasische, E.S., Christensen, N., 1992. Dependence of radar backscatter on coniferous forest biomass. IEEE Transactions on Geoscience and Remote Sensing, 30(2), pp 412-415.

DufreÃne E, Bre¬da N. 1995. Estimation of deciduous forest leaf area index using direct and indirect methods. Oecologia 104, 156-162.
DufreÃne E, Breda N. 1995. Estimation of deciduous forest leaf area index using direct and indirect methods. Oecologia 104, 156-162.

Dwivedi, R. S., Rao B. R. M., Bhattacharya S., 1999. Mapping wetlands of the Sundaban Delta and it's environs using ERS-1 SAR data, Int. J. Remote Sensing, vol. 20, no. 11, 2235 – 2247

Engheta, N., and Elachi, C., 1982. Radar scattering from diffuse vegetation layer over a smooth surface. IEEE Trans. Geosci. Remote Sens. 20:212–216.

Estes, J., 2001. "The History of Remote Sensing". http://pollux.geog.ucsb.edu/~jeff/ 115a/remotesensinghistory.html.

Fromard F., Puig H., Mougin E., Marty G., Betoulle J.L., and Cadamuro L.,1998 structure, above ground biomass and dynamics of mangrove ecosystems: new data from French Guiana. Oceologia 115:39-53.

Gao, J., 1998, A hybrid method toward accurate mapping of mangroves in a marginal habitat from SPOT multispectral data. International Journal of Remote Sensing, 19, 1887–1899.

Grace J. 1987. Theoretical ratio between `one-sided' and total surface area for pine needles. Forest Science 17, 292-296.

Graham, L.C., "Synthetic interferometer radar for topographic mapping", 1974, Proc. Inst. Electron. Eng., Vol 62, p. 763.

Green E., Clark C., Assessing Mangrove Leaf area index and canopy closure.,The remote sensing handbook for tropical coastal management., www.unesco.org/csi/pub/source/rs13.html.

Green, E. P., Clark C. D., Mumby P. J., Edwards A. J. and Ellis, A. C., 1998a. Remote Sensing techniques for mangrove mapping. International Journal of Remote Sensing, 19, 935–956.

Green, E. P., Mumby P. J., Edwards A. J., Clark, C. D., and Ellis, A. C., 1998b, The assessment of mangrove areas using high resolution multispectral airborne imagery. Journal of Coastal Research, 14, 433–443.

Grier CC, Waring RH. 1974. Conifer foliage mass related to sapwood area. Forest Science 20, 205-206.

Hanssen, R.F., Weckwerth, T.M., Zebeker, H.A., Klees, R. (1999): High-Resolution Water Vapor Mapping from Interferometric Radar Measurements. Science. Vol. 283 (5406). pp. 1297-1299.

Hashim, M. and Kadir W. H. W., 1999. Comparison of Jers-1 and Radarsat synthetic aperture Radar data for mapping mangrove and its biomass. http://www.gisdevelopment.net/aars/acrs/1999/ps1/ps1017b. shtml

Hassika P, Berbigier P, Bonnefond JM. 1997. Measurements and modelling of the photosynthetically active radiation transmitted in a canopy of maritime pine. Annales des Sciences Forestie¡res 54, 715-730.

Hess, L. L., Melack, J. M. and Simonett, D. S., 1990. Radar detection of flooding beneath the forest canopy: a review. Int. J. Remote Sens. 14:1313–1325.

Hess, L.L., Melack,J.M., and Simonett, D.S., 1990, Radar detection of flooding beneath the forest canopy : a review. International journal of Remote Sensing, 14, 1313 – 1325. http://www.gisdevelopment.net/aars/acrs/1998/ts8/ts8003a.shtml

Hutching,P.A., and Saenger,P., 1987, Ecology of Mangroves (Queensland, Australia: University of Queensland press).

Imhoff, M .L., 1995a, A theoretical analysis of the effect of forest structure on synthetic aperture radar backscatter and the remote sensing of biomass. IEEE Trans. Geosci. Remote Sensing. 33 (2): 341 – 352

Imhoff, M .L., 1995b, radar backscatter and biomass saturation: ramifications for global biomass inventory. IEEE Trans. Geosci. Remote Sensing. 33 (2): 511 – 518.

Imhoff, M., Story, M., Vermillion, C., Khan, F., and Polcyn, F., 1986. Forest canopy characterization and vegetation penetration assessment with space-borne radar. IEEE Trans.forest biomass IEEE Trans. Geosci. Remote Sens. 33: Geosci. Remote Sens. 24:535–542.

Imhoff, M.L., 1995. Radar backscatter and biomass saturation: ramifications for global biomass inventory. IEEE Transaction on Geoscience and Remote Sensing, 33 (2), pp 511-518.

Jarvis PG, Leverenz JW. 1983. Productivity of temperate, deciduous and evergreen forests. In: Lange OL et al., eds. Physiological plant ecology. IV. Encyclopedia of plant physiology, Vol. 12D. New York: Springer-Verlag, 233-280.

Jensen, J. R.,Lin, H., Yang, X., Ramsey III, E. W., Davis, B. A., and Thoemke, C. W., 1991. The measurement of mangrove characteristics in southwest Florida using SPOT multispectral data. Geocarto International, 2, 13–21.

Johansson T. 1989. Irradiance within the canopies of young trees of European aspen (Populus tremula) and European birch in stands of different spacings. Forest Ecology and Management 28, 217-236.

Jones HG. 1992. Plant and microclimate, 2nd edn. Cambridge, UK: Cambridge University Press.

Joshi H and Ghose M., 2001, Structural variability and Biomass Production of Mangroves in Lothian Island of Sundrbans. India., Proceedings of the International Symposium on Mangrove and Salt marsh ecosystem, Arid Zona Environments.

Joshi H and Ghose M., 2003, Forest structure and species distribution along soil salinity and pH gradient in Mangrove swamps of the Sundarbans., Tropical Ecology 44(2): 195-204.
July 2003, Toulouse., Vol. 6, pp. 3995-3997.

Jurick TW. 1986. Temporal and spatial patterns of specific leaf weight in successional northern hardwood tree species. American Journal of Botany 78, 1083-1092.

Karam, M. A., Amar, F., Fung, A. K., Mougin, E., Lopes, A., Le Vine, D. M., and Beaudoin, A. (1995), A microwave polarimetric scattering model for forest canopies based on vector radiative transfer theory. Remote Sens. Environ. 53: 16–30.

Kasischke E. S., Melack J.M. and Dobson M C, 1997, The Use of Imaging Radars For Ecological Applications – A Review. Remote Sensing of Environment, 59, 141 – 156.

Kasischke E. S., Melack J.M. and Dobson M C, 1997, The Use of Imaging Radars For Ecological Applications – A Review. Remote Sensing of Environment, 59, 141 – 156.

Klausing, H., Holpp, W. (2000): Radar mit realer und synthetischer Apertur. Verlag Oldenburg: Oldenburg.

Krohn, D., Milton, N. M., and Segal, D. B. (1983), SEASAT synthetic aperture radar (SAR) response to lowland vegetation types in eastern Maryland and Virginia. J. Geophys. Res. 88(C3):1937–1952.

Lang ARG, Yueqin X. 1986. Estimation of leaf area index from transmission of direct sunlight in discontinuous canopies. Agricultural and Forest Meteorology 37, 229-243.

Lang ARG. 1987. Simplified estimate of leaf area index from transmittance of the sun's beam. Agricultural and Forest Meteorology 41, 179-186.

Laur, H., Bally, P., Meadows, P., Sanchez, J., Schättler, B., Lopinto, E., Esteban, D. (1998): Derivation of the backscattering coefficient □0 in ERS SAR PRI products. ESA Technical Document. ES-TN-RS-PM-HL09. Iss. 2.5b, 7. September. 1998.

Le Toan, T., A. Beaudoin, J. Riom, D. Guyon, 1992. Relating forest biomass to SAR data. IEEE Transactions on Geoscience and Remote Sensing, 30(2), pp 403-411.

Le Toan, T., Beaudoin, A., and guyon, D., 1992. Relating forest biomass to SAR data, IEEE Trans. Geosci. Remote Sensing. 30(2): 403 – 411.

Ledent JF. 1977. Sur le calcul du coefficient d'extinction durayonnement solaire incident direct dans un couvert vegetal. Oecologia Plantarum 12, 291-300.

Lewis, A., Henderson, F.M. (1998): Radar fundamentals: The geoscience perspective. In: Henderson and Lewis (Ed.): Principles and applications of imaging radar. Manual of Rem. Sensing. Vol. 2, pp. 131-181.

Löw, A., Mauser, W. (2003): Generation of geometrically and radiometrically terrain corrected ScanSAR images. Proc. IEEE Int. Geos. RS Symposium, 21-25

Luckman, A., Baker, J., Kuplich, T., Yanasse, C., and Frery, A., 1997. A study of the relationship between radar backscatter and regenerating tropical biomass for spaceborne (SAR) instruments. Remote Sensing of Environment, 60, 1–13.

Lugo, A.E. & S.C.Snedaker 1974. the Ecology of Mangroves.,Annual review of Ecology and Systematics 5: 39-64.

Lugo,A.E.1978.Stress and ecosystems:pp.62-101.In:J.HThorp&J.W.Gibons(eds) Energy and environmental stress. DOE 771114.Dept.

Macnae, W. 1968, Ageneral account of the fauna and flora of Mangrove swamps and forest in the Indo – west Pacific Region. Advances in Marine Biology. 6:72-270.

Maguire DA, Bennett WS. 1996. Patterns in vertical distribution of foliage in young coastal Douglas-Fir. Canadian Journal of Forest Research 26, 1991-2005.

Makela A, Virtanen K, Nikinmaa E. 1995. The effects of ring width, stem position and density on the relationship between foliage biomass and sapwood area in Scots Pine (Pinus sylvestris L.). Canadian Journal of Forest Research 25, 970-977.

Makey A.P. (1993) Biomass of the Mangrove Avicennia marina (Forsk) Vierh. Near Brisbane, south-eastern Queensland. Aust, J.Mar. Freshwater Res.44 : 721-725.

Matilal , S.,B.B.mukherjee, N.Chatterjee & M.D.Gupta.1986.Studies on soil & vegetation of Mangrove forests of Sunderbans.indian Jurnal of Marine Science 15:181-184.

McDonald, H. C., Waite, W. P., and Demarche, J. S., 1980. Use of Seasat satellite radar imagery for the detection of standing water beneath forest vegetation. Proceedings of American Society of Photogrammetry Annual Technical Meeting, Niagara Falls (New York: American Society of Photogrammetry), pp. RS-3-B-1-RS-3-B-13.

Mckee, K.L.1993,soil physicochemical properties and mangrove spices distribution-reciprocal effects ? Journal of ecology 81:477-487

Meier, E., Frei, U., Nüesch, D. (1993): Precise terrain corrected geocoded images. In: Schreier, G. (Ed.): SAR Geocoding – Data and Systems. pp. 173-186. Wichmann: Karlsruhe.

Miller JB. 1967. A formula for average foliage density. Australian Journal of Botany 15, 141-144.

Mitra, A. and Pal S. 2002. The oscillating mangrove ecosystem and the Indian Sundarbans,(Eds Shakti Banerjee),WWF, W.B. State Office. Barna Prakashani, Kolkata.

Monsi M, Saeki T. 1953. Uber den Lichtfaktor in den Pflanzengesellschaften und seine Bedeutung fur die Stoffproduktion. Japanese Journal of Botany 14, 22-52.

Moreira, J.R. (1992): Bewegungsextraktionsverfahren für Radar mit synthetischer Apertur. = DLR Forschungsberichte. DLR-FB-92-31.

Mougin, E., Proisy, C., Marty, G., Fromard, F., Puig, H., Betoulle, J. L., and Rudant, J. P., 1999. Multifrequency and multipolarization radar backscattering from mangrove forests. IEEE Trans. Geosci. Remote Sens. 37:94–102.

Mumby, P. J., Green, E. P. Edwards, A. J., and Clark, C. D., 1999. The cost-effectiveness of remote sensing for tropical coastal resources assessment and management. Journal of Environmental Management, 55, 157–166.

Murray M. R., Zisman S. A., Furley P. A., Munro D.M., Gibson J., Ratter J., Bridgewater S., Minty C.D., Place C.J., 2003, The mangroves of Belize Part 1. distribution, composition and classification, Forest Ecology and Management 174, 265–279.

Naidoo ,G& F.Raiman.1980. Mangrove soils of Beachwood area,Durban. Journal of South African Botany 46:293-304

Nandy P. and Ghosh M., 2001, Photosynthesis and water – use efficiency of some mangrove from sundarbans, India.Journal of Plant Biology, Dec 2001, 44(4): 213-219.

Nel EM, Wessman CA. 1993. Canopy transmittance models for estimating forest leaf area index. Canadian Journal of Forest Research 23, 2579-2586.

Niinemets U, Kull K. 1994. Leaf weight per area and leaf size of 85 Estonian woody species in relation to shade tolerance and light availability. Forest Ecology and Management 70, 1-10.

Nilson T. 1971. A theoretical analysis of the frequency of gaps in plant stands. Agricultural Meteorology 8, 25-38.

Nizinski JJ, Saugier B. 1988. A model of leaf budding and development for a mature Quercus forest. Journal of Applied Ecology 25, 643-655.

Norman JM, Campbell GS. 1989. Canopy structure. In: Pearcy RW, Ehleringer JR, Mooney HA, Rundel PW, eds. Plant physiological ecology: field methods and instrumentation. London: Chapman and Hall, 301-325.

Norman JM, Jarvis PG. 1974. Photosynthesis in Sitka Spruce (Picea sitchensis (Bong.) Carr.) III. Measurements of canopy structure and interception of radiation. Journal of Applied Ecology 11, 375-398.

Norman JM, Welles JM. 1983. Radiative transfer in an array of canopies. Agronomy Journal 75, 481-488.

Olmsted, C. (1993): Scientific SAR User's guide. Alaska SAR facility. Technical Document. ASF-SD-003.

Peng Gong, Ruiliang Pu, Greg S. Biging, and Mirta Rosa Larrieu, 2003, Estimation of forest leaf area index using vegetation indices derived from Hyperion Hyperspectral data., IEEE Transactions on Geoscience and remote sensing, Vol. 41, no.6, june, 2003.

Peter N. Tiangco and Bruce C. Forester, 2000, Development of Trunk-Canopy Biomass and Morphology Indices from Quadpolarized Radar Data., ACRS, 2000,GIS Development http://www.gisdevelopment.net/aars/acrs/2000/ts12/ts1203d.asp

Pierce LL, Running SW. 1988. Rapid estimation of coniferous forest leaf area using a portable integrating radiometer. Ecology 67, 1762-1767.

Proisy C., Mougin E, Fromard F., and Karam M. A., 2000. Interpretation of Polarimetric Radar Signatures of Mangrove Forests, Remote Sens. Environ. 71:56–66

Proisy C., Mougin E, Fromard F., and Karam M. A., 2000. Interpretation of Polarimetric Radar Signatures of Mangrove Forests, Remote Sens. Environ. 71:56–66

Proisy C., Mougin E., Fromard F, Trichon V., Karam M.A., 2002, On the influence of canopy structure on the radar backscattering of mangrove forests., International Journal of Remote Sensing, vol.23, no 20, 4197-4210.

Ramsey, E., and Jensen, J.R. 1996. Remote sensing of mangrove wetlands: relating canopy spectra to site-specific data. Photogramatic Engineering & Remote Sensing, Vol.62, pp.939-948.

Rasolofoharinoro, M., Blasco, F., Bellan, M. F., Aizpuru, M., Gauquelin, T., and Denis, J., 1998. A remote sensing based methodology for mangrove studies in Madagascar. International Journal of Remote Sensing, 19, 1873–1886.

Richards, J. A., 1990. Radar backscatter modeling of forests: a review of current trends. International Journal of Remote Sensing. 11(7):1299 - 1312.

Richards, J.A., Woodgate, P. W., and Skidmore,A. K., 1987. An explanation of enhanced radar backscattering from flooded forests. Int. J. Remote Sens.18:1319–1332.

Rogers R, Hinckley TM. 1979. Foliar weight and area related to current sapwood area in oak. Forest Science 25, 298-303.

Rosich, B., Meadows, P. (2004): Absolute calibration of ASAR Level 1 products generated with PF-ASAR. ESA technical note. ENVI-CLVL-EOPG-TN-03- 0010. version 1.4, 23.01.2004.

Ross J. 1981. The radiation regime and architecture of plant stands. The Hague, The Netherlands: Dr Junk W.

Roy Choudhuri P.K., 1991, Biomass Production of Mangrove plantation in sundarban, West Bengal (India) – A case study, Indian Forester 177: 3-12.

Saha,S.& A choudhury. 1995. Vegatation analysis of restored and natural mangrove forests in sagar island,sunderban east coast of India .Indian journal of marine science 24: 133-136.

Satyanarayana B., Thierry B., Seen D. L., Raman A.V., Muthusankar G., 2001. Remote sensing in mangrove research – Relationship between dendrometric parameters: a case for coringa, East coast of India, paper presented in 22 nd Asian conference on remote Sensing, 5 – 9 November, 2001, Singapur.

Sellers, P. J., Hall, F.G., Asar, G., Strebel, D.E., & Murphy, R.E. (1988) the first ISLSCP field experiment (FIFE). Bulletin of the American Meteorological Society, 69, 22-27.
Sellin A. 2000. Estimating the needle area from geometric measurements: application of different calculation methods to Norway spruce. Trees 14, 215-222.

Shafiee M., Surip N., lbrahim N. and Saedin I, 1998. Suitability of Landsat TM and JERS1 Data in Land Cover/Use Mapping Application.

Shelbrune VB, Hedden RL, Allen RM. 1993. The effects of site, density and sapwood permeability on the relationship between leaf area and sapwood area in loblolly pine (Pinus taeda L.). Forest Ecology and Management 58, 193-209.

Shepard, N. (2000): Extraction of Beta Nought and Sigma Nought from RADARSAT CDPF products. Canadian Space Agency Technical Document. Rev. 4, 28. April 2000.

Smith FW, Sampson AD, Long NJ. 1991. Comparison of leaf area index estimates from tree allometrics and measured light interception. Forest Science 37, 1682-1688.

Smith FW, Sampson AD, Long NJ. 1991. Comparison of leaf area index estimates from tree allometrics and measured light interception. Forest Science 37, 1682-1688.

Smith NJ. 1993. Estimating plant area index and light extinction coefficients in stands of Douglas-fir (Pseudotsuga Menziesii). Canadian Journal of Forest Research 23, 317-321.

Steinke T.D., Ward C.J., and Rajh A. (1995) forest structure and biomass of mangroves in Mgeni estuary, South Africa. Hydrobiologia, 295: 159-166.

Tam N.F.Y., Wong Y.S., Lan C.Y., and Chen G.Z.(1995) community structure and standing crop biomass of Mangrove forest in Futian Nature Reserve, Shenzhen, China. Hydrobiomogia 295: 193 – 201.

Thomas SC, Winner WE. 2000. Leaf area Index of an old-growth Douglas-Ær forest estimated from direct structural measurements in the canopy. Canadian Journal of Forest Research 23, 1922-1930.

Thomas SC, Winner WE. 2000. Leaf area Index of an old-growth Douglas-fir forest estimated from direct structural measurements in the canopy. Canadian Journal of Forest Research 23, 1922-1930.

Tomlinsorn, P.B.1986. Botany of Mangroves. Cambridge Univresity press; Cambridge.

Turton SM. 1985. The relative distribution of photosynthetic active radiation within four tree canopies, Cragieburn Range, New Zealand. Australian Forest Research 15, 383-394.

Ulaby, F.T., Moore, R., Fung, A.K. (1982): Microwave remote sensing: Active and Passive: Vol. 2 – Radar Remote Sensing and surface scattering and emission theory. Addison-Wesley.

Upkong, I.E. 1998. the composition and distribution of species in relasion to soil soil nutrients gradients in mangrove swamps in south eastern Nigeria . Tropical Ecology 39:55-67.

Vanseveren JP, Herbauts J. 1977. Index foliaire, parame¡tres foliaires et caracte¬ristiques edaphiques stationnelles dansquelques peuplements forestiers de Lorraine belge. Annales des Sciences Forestie¡res 34, 215229.

Vertessy RA, Benyon RG, O'Sullivan SK, Gribben PR. 1995. Relationships between stem diameter, sapwood area, leaf area and transpiration in a young mountain ash forest. Tree Physiology 15, 559-567.

Vose JM, Sullivan NH, Clinton BD, Bolstad PV. 1995. Vertical leaf area distribution, light transmittance, and the application of the Beer±Lambert Law in four mature hardwood stands in the southern Appalachians. Canadian Journal of Forest Research 25, 1036-1043.

Vose JM, Swank WT. 1990. Assessing seasonal leaf area dynamics and vertical leaf distribution in eastern white pine (Pinus strobes L.) with a portable light meter. Tree Physiology 7, 125-134.

Walsh,G.E. 1974Mangroves:A review ,pp.51174in:R.Reimold & W.Queen (eds) Ecology of halophytes .Academic Press,New York.

Wang Y., Hess L. L., Filoso S., and Melack J. M., 1995. Understanding the radar backscattering from flooded and non- flooded Amazonian forests: results from canopy backscatter modeling. Remote Sens. Environ. 54:324–332.

Wang, Y., and Imhoff, M. L., 1993. Simulated and observed L-HH radar backscatter from tropical mangrove forests. Int. J. Remote Sens. 14:2819–2828.

Waring RH, Schroeder PE, Oren R. 1982. Application of the pipe model theory to predict canopy leaf area. Canadian Journal of Forest Research 12, 556-560.

Waring, R.H., & J. Major. 1964. Some vegetation of California redwood region in relation to gradient of moisture, nutrients, light and temparature. Ecological Monographs 34:167-215.

Warren Wilson J. 1959. Analysis of the spatial distribution of foliage by two-dimensional point quadrats. New phytologist 58, 92-101.

Warren Wilson J. 1963. Estimation of foliage densness and foliage angle by inclined point quadrats. Australian Journal of Botany 11,95-105.

Watson, J.1928.mangrove forest of the Malay peninsula. Malayan Forest records 6.Fraser & Neave, Ltd,.Singapore.

Whitehead D, Edwards WRN, Jarvis PG. 1984. Conducting sapwood area, foliage area and permeability in mature trees of Picea sitchensis and Pinus contorta. Canadian Journal of Forest Research 14, 940-947.

Wright, L.D., Coleman, J.M., 1973. Variations in morphology of major river deltas as a function of ocean wave and river discharge regimes. American Association of Petroleum Geologists Bulletin 57, 370 – 398.

Wu, S. T., and Sader, S. A., 1987. Multipolarization SAR data for surface feature delineation and forest vegetation characterization. IEEE Trans. Geosci. Remote Sens. 25:67–76.